5-2024

Real-Time Degradation Abatement Framework for Energy Storage System in Automotive Application using Data-Driven Approaches

Laxman Timilsina
ltimils@clemson.edu

Real-Time Degradation Abatement Framework for Energy Storage System in Automotive Application using Data-Driven Approaches

---

A Dissertation
Presented to
the Graduate School of
Clemson University

In Partial Fulfillment
of the Requirements for the Degree
Doctor of Philosophy
Electrical Engineering

---

by
Laxman Timilsina
May 2024

Accepted by:
Dr. Christopher S. Edrington, Committee Chair
Dr. Johan H. Enslin
Dr. Yingjie Lao
Dr. Behnaz Papari
Dr. Gokhan Ozkan

Abstract

The increasing popularity of electric vehicles (EVs) is driven by their compatibility with sustainable energy goals. However, the decline in the performance of energy storage systems, such as batteries, due to their degradation puts EVs and hybrid electric vehicles (HEVs) at a disadvantage compared to traditional internal combustion engine (ICE) vehicles. The batteries used in these vehicles have limited life. The degradation of the battery is accelerated by the operating conditions of the vehicle, which further reduces its life and increases the reliability and economic concerns for the vehicle's operation.

The aging mechanism inside a battery cannot be eliminated but can be minimized depending on the vehicle's operating conditions and different control mechanisms that can alter the operating conditions. Different operating conditions affect the aging mechanism differently. Knowing the factors and how they impact battery capacity is crucial for minimizing degradation. This dissertation presents the detailed degradation mechanism inside the battery and the major factors responsible for the degradation, along with their effects on the battery during the operation of EVs. Then, to abate the degradation mechanism, a prognostic-based control framework (PBCF) for HEVs is proposed. Also, this framework reduces the overall cost of operating HEVs by taking into account the degradation of the energy storage systems. The strategy utilizes a degradation forecasting model of energy storage systems to predict their degradation paths. Analytical and data-driven approaches are used to find the degradation path of the energy storage systems as follows:

- Markov Chain Model
- Neural Network Model

These two models employ distinct datasets to validate the feasibility of the proposed strategy. The predicted degradation rate is then used to control the HEV via its energy management

(EM) system in order to reduce the degradation of energy storage systems. During the simulation, three distinct operating scenarios are developed to observe their effects on battery degradation and the response of the proposed control strategy PBCF.

Dedication

I dedicate this work to my parents, who never had the opportunity to attend university themselves but worked tirelessly throughout their lives to provide the best education for their two children. My endeavors are overshadowed by the immense sacrifices they undertook to secure us a quality education. Their unwavering support and dedication have been my inspiration.

- Laxman

Acknowledgment

I extend my heartfelt gratitude to my academic advisor and mentor, Dr. Christopher S. Edrington. His exceptional expertise and unwavering guidance have been pivotal in shaping my Ph.D. journey and culminating in the completion of this dissertation. Dr. Edrington's inventive approach of providing guidance while allowing me the freedom to conduct my research has been instrumental in making my Ph.D. journey significantly enjoyable and less stressful. This unique approach played a crucial role in enabling me to successfully complete my Ph.D. with a sense of fulfillment and satisfaction.

I would like to thank Dr. Gokhan Ozkan for his unwavering support and invaluable assistance throughout my academic journey. Dr. Ozkan's consistent presence and willingness to help whenever technical issues arose or matters needed attention have been truly invaluable.

I would also like to extend my gratitude to the exceptional individuals at RT-COOL with whom I had the privilege of collaborating on different projects. Their constant encouragement has inspired me to pursue further publications. I would like to thank Dr. Phuong H. Hoang, for actively contributing and guiding me on several topics. His consistent support, even after departing from RT-COOL, will always hold a lasting place in my memory.

Finally, I would like to express heartfelt gratitude to my Ram Timilsina and Shraddha Prasai for their unwavering support throughout my Ph.D. journey. Their consistent encouragement during challenging moments has been priceless. Their steadfast belief in me and continual presence have served as a motivating force, adding deeper meaning to this academic pursuit.

This work was supported by Clemson University's Virtual Prototyping of Autonomy Enabled Ground Systems (VIPR-GS) under Cooperative Agreement W56HZV-21-2-0001 with the US Army DEVCOM Ground Vehicle Systems Center (GVSC). DISTRIBUTION STATEMENT A. Approved for public release; distribution is unlimited. (OPSEC 8288)

Contents

List of Figures

List of Tables

Publications Directly Related to this Dissertation.

Journals:

1. **L. Timilsina**, O. Ciftci, A.Moghassemi, G. Ozkan, B. Papari, C. S. Edrington, A Real-time Implementation of Dual Energy Management for Hybrid Electric Vehicles, *IEEE Transactions on Transportation Electrification*, In Preparation.
2. **L. Timilsina**, O. Ciftci, A.Moghassemi, Gokhan Ozkan, Behnaz Papari, Christopher S. Edrington, A Real-time Analysis of Impact of Vehicle-to-Grid connection on Degradation of Battery used in EVs/HEVs, *eTransportation*, In Preparation.
3. **L. Timilsina**, P. H. Hoang, G. Ozkan, B. Papari, C. S. Edrington, A Real-time Degradation Abatement Technique in Hybrid Electric Vehicle using Data-Driven Methods, *IEEE Transactions on Vehicular Technology*, Under Review.
4. **L. Timilsina**, P. H. Hoang, G. Ozkan, B. Papari, C. S. Edrington, A Real-time Prognostic-based Control Framework for Series Hybrid Electric Vehicles, *IEEE Access*, 2023.
5. **L. Timilsina**, Payam R. Badr, P. H. Hoang, G. Ozkan, B. Papari, C. S. Edrington, Battery Degradation in Electric and Hybrid Electric Vehicles: A Survey Study, *IEEE Access*, 2023.

Conferences:

1. **L. Timilsina**, P. H. Hoang, A.Moghassemi, A. Arsalan, P. K. Chamarthi, G. Ozkan, B. Papari, C. S. Edrington, Impact of Vehicle-to-Grid (V2G) on Battery Degradation in a Plug-in Hybrid Electric Vehicle, *SAE WCX*, to appear.
2. **L. Timilsina**, A.Moghassemi, E. Buraimoh, A. Arsalan, G. Ozkan, B. Papari, C. S. Edrington, Power Quality Improvement of a Microgrid System using Shunt Active Power Filter, *International Conference on DC Microgrids (ICDCM)*, to appear.
3. **L. Timilsina**, A.Moghassemi, E. Buraimoh, A. Arsalan, S M Imrat Rahman, G. Ozkan, B. Papari, C. S. Edrington, Degradation and State of Health Prediction of a Battery used in a Microgrid in Real-time, *International Conference on DC Microgrids (ICDCM)*, to appear.
4. **L. Timilsina**, O. Ciftci, A.Moghassemi, G. Ozkan, B. Papari, C. S. Edrington, A Dual Energy Management for Hybrid Electric Vehicles, *IEEE Transportation Electrification Conference*, to appear.
5. **L. Timilsina**, P.R. Badr, A. Arsalan, G. Ozkan, B. Papari, C. S. Edrington, Reliable Fault-tolerant Distributed Control for Traction IPMSM in EV/HEV, *IEEE Transportation Electrification Conference*, to appear.

6. **L. Timilsina**, P. H. Hoang, A. Arsalan, B. R. Badr, G. Ozkan, B. Papari, C. S. Edrington, Degradation Abatement in Hybrid Electric Vehicles using Data-Driven Technique, *Transportation Research Procedia, Elsevier*, 2023

7. P. H. Hoang, G. Ozkan, **L. Timilsina**, C. S. Edrington, A Prognostic Based Control Framework for Hybrid Electric Vehicles, *SAE International*, 2022.

Other Publications.

Journals:

1. G. Muriithi, **L. Timilsina**, A. Arsalan, G. Ozkan, B. Papari, C. S. Edrington, Detection of Cyber Attack in Plug-in Hybrid Electric Vehicle, *IEEE Transactions on Transportation Electrification*, In Preparation

2. A.Moghassemi, **L. Timilsina**, S M Imrat Rahman, A. Arsalan, P. K. Charmathi, G. Ozkan, C. S. Edrington, Z. Zhang, Nearest Level Control Based Modular Multi-level Converters For Power Electronics Building Blocks Concept In Electric Ship System, *IEEE Transactions on Transportation Electrification*, In Preparation

3. E. Buraimoh, G. Ozkan, **L. Timilsina**, C.S. Edrington, B. Papari, Advanced Power Management in Military-Based Vehicle-to-Grid and Vehicle-to-Vehicle Microgrid— Distributed Real-Time Co-Simulation, *IEEE Transactions on Transportation Electrification*, In Preparation

4. E. Buraimoh, G. Ozkan, **L. Timilsina**, C.S. Edrington, B. Papari, Adaptive Multi-Parameter Model Free Delay Compensation in Real-Time Co-Simulation, *IEEE Transactions on Transportation Electrification*, In Preparation

5. A. Arsalan, B. Papari, G. Muriithi, S M I. Rahman **L. Timilsina**, G. Ozkan, P. K. Chamarthi, C. S. Edrington, Enhanced Real-Time ATM-based MPC for Electric Vehicles with Cyber-Physical Security Consideration, *IEEE Transactions on Transportation Electrification*, Under Review

6. P.R. Badr, G. Ozkan, B. Papari, C.S. Edrington, V. A. Phillips, **L. Timilsina**, Evolutionary Multi-objective Current Magnitude Optimization for Traction IPMSM in Electric/Hybrid-Electric Vehicles, *IEEE Transactions on Transportation Electrification*, Under Review

7. B. Papari, P.R. Badr, D. Scruggs, A. Arsalan, P.K. Chamarthi, A. Moghassemi, **L. Timilsina**, G. Ozkan, C.S. Edrington, V. A. Phillips, **L. Timilsina**, Evolutionary Multi-objective Current Magnitude Optimization for Traction IPMSM in Electric/Hybrid-Electric Vehicles, *IEEE Transactions on Transportation Electrification*, Under Review

8. S M I. Rahman, A. Moghassemi, A. Arsalan, **L. Timilsina**, P. K. Chamarthi, G. Ozkan, B. Papari, C. S. Edrington, Emerging Trends and Challenges in Thermal Management of Power Electronic Converters: A State of The Art Review, *IEEE Access*, 2023, Under Review
9. E. Buraimoh, G. Ozkan, **L. Timilsina**, P. K. Chamarthi, C.S. Edrington, B. Papari, Overview of Interface Algorithms, Interface Signals, Communication and Delay in Distributed Power Systems Real-Time Co-Simulation, *IEEE Access*, 2023
10. P. H. Hoang, G. Ozkan, P. R. Badr, **L. Timilsina**, C. S. Edrington, Integrating Degradation Forecasting Into Distribution Grids' Advanced Distribution Management Systems, *International Journal of Electrical Power and Energy Systems*, 2023.

Conferences:

1. A.Moghassemi, **L. Timilsina**, A. Arsalan, G. Ozkan, C. S. Edrington, Z. Zhang, Nearest Level Control Based Modular Multi-level Converters For Power Electronics Building Blocks Concept In Electric Ship System, *IEEE Transportation Electrification Conference*, Accepted.
2. P. K. Chamarthi, A.Moghassemi, S M I. Rahman, **L. Timilsina**, G.Ozkan, C.S. Edrington, B. Papari, A Proposed Cuk Converter based Dual Input Hybrid Converter Topology as EV Charging Station, *IEEE Transportation Electrification Conference and Expo*, In Preparation.
3. P. K. Chamarthi, S M I. Rahman, A.Moghassemi, **L. Timilsina**, G.Ozkan, C.S. Edrington, B. Papari, A Novel Four Switch Transformerless Inverter with Step Up/Down Capability for PV Fed Grid Connected Systems, *IEEE Transportation Electrification Conference and Expo*, In Preparation.
4. S M I. Rahman, A.Moghassemi, **L. Timilsina**, P.R. Badr, Q.Zhu, R. Prucka, G.Ozkan, C.S. Edrington, B. Papari, Model-based Active Thermal Management for Neutral-point Clamped Power Converter with Adaptive Weight, *IEEE Transportation Electrification Conference and Expo*, In Preparation.
5. A.Moghassemi, **L. Timilsina**, A. Arsalan, G. Ozkan, C. S. Edrington, Z. Zhang, Power Electronics Building Blocks: State-of-Health and End-of-Life, In Preparation.
6. G. Ozkan, S M I. Rahman, A. Moghessemi, **L. Timilsina**, P.H. Hoang, P.R. Badr, C.S. Edrington, Q. Zhu, R. Prucka, Model-based Active Thermal Management for Neutral-point Clamped Power Converter with Adaptive Weight, IEEE Transportation Electrification Conference, 2024, Accepted.
7. A. Arsalan, B. Papari, G. Muriithi, **L. Timilsina**, G. Ozkan, P. K. Chamarthi, C. S. Edrington, Machine Learning Approach for Open Circuit Fault Localization in EV Motor Drive Systems, *SAE International*, 2024, Accepted.
8. E. Buraimoh, **L. Timilsina**, A. Arsalan, G. Ozkan, C. S. Edrington, B. Papari, Model Free Time Delay Compensation for Damped Impedance Method Interfaced Power System Co-Simulation Testing,

SAE International, 2023.

9. A. Arsalan, **L. Timilsina**, B. Papari, G. Muriithi, G. Ozkan, P. K. Chamarthi, C. S. Edrington, Cyber Attack Detection and Classification for Integrated On-board Electric Vehicle Chargers subject to Stochastic Charging Coordination, *Transportation Research Procedia, Elsevier*, 2023.

Nomenclature

BEV	Battery Electric Vehicle
BMS	Battery Management System
CAN	Controller Area Network
CAN-H	CAN High
CHIL	Controller-Hardware-In-the-Loop
CAN-L	CAN Low
DF	Degradation Forecasting
DLC	Device Level Control
DoD	Depth of Discharge
DoE	Department of Energy
DNN	Deep Neural Network
DP	Dynamic Programming
DRTS	Digital Real-time Simulator
ECU	Electronic Control Unit
EM	Energy Management
EoL	End of Life
ESS	Energy Storage System
EV	Electric Vehicle
FEV	Full Electric Vehicle
FL	Forecasting Layer
FNN	Feedforward Neural Network
HEV	Hybrid Electric Vehicle
HF	Hybridization Factor
HIL	Hardware-in-the-Loop
HMI	Human-Machine Interface

ICE Internal Combustion Engine

Li-ion Lithium ion

LSTM Long Short Term Memory

NN Neural Network

NiMH Nickel-Metal Hydride

NS Numerical Simulation

PBCF Prognostic-based Control Framework

PHEV Plug-in Hybrid Electric Vehicle

PM Power Management

PMP Pontryagin's Minimum Principle

RT-COOL Real-Time Control and Optimization Laboratory

RNN Recurrent Neural Network

RUL Remaining Useful Life

SNL Sandia National Laboratory

SoC State of Charge

SoH State of Health

V2G Vehicle-to-Grid

V2V Vehicle-to-Vehicle

Chapter 1

Introduction

The fluctuating cost of non-renewable energy resources, concern over global greenhouse gas emissions, and rigorous rules and regulations for vehicle emissions have prompted research toward clean and green transportation systems [1]. [2] provides data that shows the transportation sector accounts for a larger share of overall energy consumption (i.e., 26%). This consumption is attributable to the millions of conventional automobiles that use internal combustion engine (ICE), which run on fossil fuels (petroleum products) and emit carbon dioxide, hydrocarbon, sulphur oxides, and carbon monoxide as a byproduct. These gases give rise to the pollution that is hazardous to both the environment and living organisms and contributes to the production of greenhouse gases (GHG), which have a significant impact on global warming. In 2020, CO_2 emission from energy consumption in the United States was found to be 4.6 billion metric tons (Bmt) (decreased by 11% from 2019 due to the impact of COVID-19) [3]. Petroleum consumption accounted for 45% of CO_2 emissions and about 77% of petroleum CO_2 emissions occurred in the transportation sector [3]. Also, light and medium vehicles (weighing up to 26,000 pounds) contribute heavily to GHG emissions (more than 80%) as per the report provided by the United States Environmental Protection Agency (EPA) [4]. The extensive depletion of fossil fuels, issues related to global warming, and erratic rise in the price of these fossil fuels have given rise to the development of distributed energy resources [5], along with the Electric Vehicles (EVs). Such vehicles have a positive effect on the environment by reducing gas emissions and deviating toward clean and green technology as demanded by modern society [6]. As a result, more EVs, hybrid electric vehicles (HEVs), and plug-in hybrid electric vehicles (PHEVs) are being produced and used day-by-day as alternatives to conventional vehicles powered by ICEs. [7, 8, 9].

The EVs, whether battery electric vehicles (BEVs) or other kinds of EVs, are considered next-generation transportation that uses alternative energy storage systems (ESSs) to replace or in conjunction

with ICE. For this transportation to gain popularity and replace conventional ICE vehicles, the ESS must maintain high capacity and power capabilities along with safe operation for more than ten years [10].

The selection of an appropriate ESS for an HEV or full electric vehicle (FEV) is influenced by several factors. Figure 1.1 provides an overview of critical considerations while choosing an ESS. The cost of the ESS has a direct impact on the overall vehicle cost, constituting around 30% of the total vehicle cost [11]. Thus, a lower cost for the selected ESS results in a more economical vehicle. The size of the chosen ESS directly influences the vehicle's design. It is essential to consider the size of the ESS, as the overall size of the HEV depends on it. Given the weight and volume constraints within the vehicle, an ESS with a smaller size and weight is the most suitable option. Another crucial criterion is the lifecycle of the ESS. Different ESS technologies have varying lifecycles, and selecting a system with a longer lifetime is advantageous for HEV/FEV applications. As the vehicle operates under high speeds and extreme conditions, it is crucial for the selected ESS to withstand these demanding operating conditions and operate safely. Power density and energy density are critical metrics determining the selection of an ESS. Higher power and energy densities make a particular ESS more suitable for EV applications. These metrics measure the ability of the system to deliver power and store energy efficiently.

It is important to note that finding an ESS that meets all of these criteria is challenging. Therefore, trade-offs are inevitable, and a specific ESS is chosen to fulfill the majority of these criteria, considering the specific requirements of the vehicle.

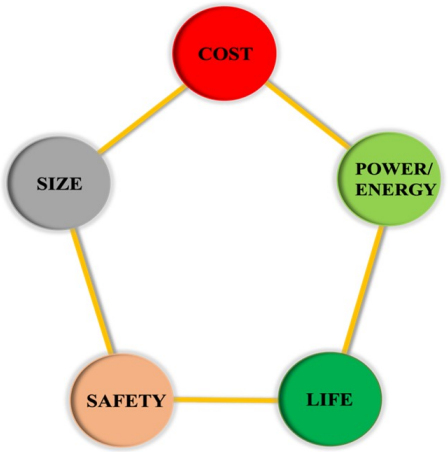

Figure 1.1: Important metrics for a ESS in HEV/FEV.

There are several ESSs available in the market. Flywheel, fuel cell, supercapacitor (SC), and battery are the most common ESS, which have their own inherent properties. Figure 1.2 compares these ESS in terms of energy density and power density, whereas Figure 1.3 compares with broad parameters based on

the data provided by [12] and [13], respectively. Fuel cells exhibit higher energy density compared to other ESS; however, they are seldom used in HEVs. This is primarily due to the expensive manufacturing cost of fuel cells, which surpasses that of internal combustion engines [14]. Additionally, storing hydrogen gas at room temperature and pressure in vehicles poses challenges, as hydrogen is flammable and necessitates a continuous fuel supply. Supercapacitors excel in power density but fall short in terms of energy density for EV applications. Among the available ESS options, batteries currently dominate as the preferred choice for energy storage in EVs. This is attributed to their high energy density, compact size, and reliability [12].

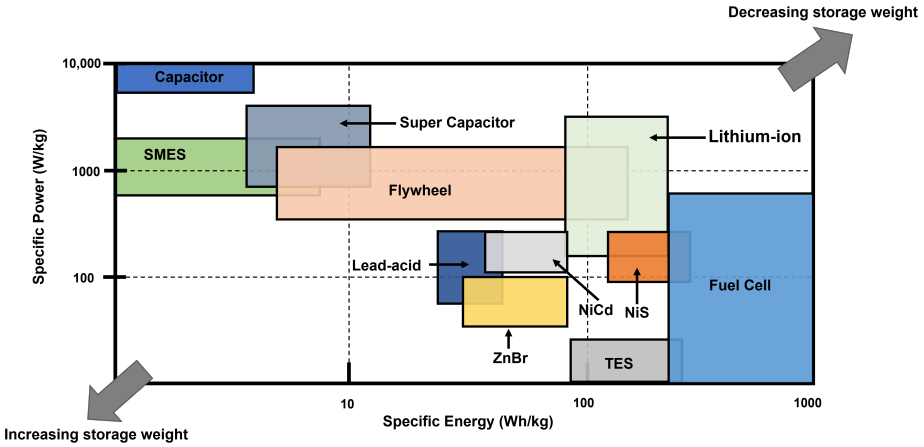

Figure 1.2: Comparison between various ESS in terms of energy density and power density [15].

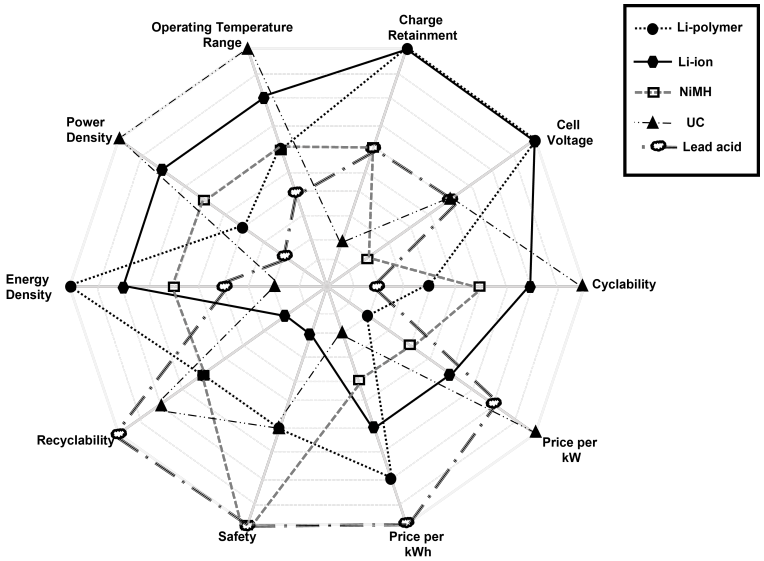

Figure 1.3: Comparison of attributes of various ESS [15].

There are different types of batteries with different specifications. Lead acid batteries have been in

use since the 1900s due to their durability, affordability, inherent safety features, and tolerance to temperature variations [16]. However, overcharging of these batteries leads to water loss as hydrogen is produced at the positive electrode [17]. The use of lead as current collectors in these batteries results in low energy density and susceptibility to corrosion when exposed to a sulfuric acid electrolyte. As a result, lead-acid batteries are not commonly employed in automotive applications due to their extended charging time and heavy weight, in addition to these concerns. Nevertheless, lead-acid batteries still find wide usage in cost-sensitive applications where low energy density and limited cycle life are not significant factors. These applications prioritize ruggedness and tolerance to abuse. Examples of such applications include automotive starting systems, lighting applications, and battery-powered uninterruptible power supplies (UPS).

NiMH (Nickel-metal hydride) batteries replaced lead-acid batteries in EV applications due to their higher energy density, which is twice that of lead-acid batteries. Additionally, the components of NiMH batteries are environmentally benign and can be recycled [12]. NiMH batteries offer improved safety features compared to lead-acid batteries, as they can operate at higher voltages, have a wide operating temperature range, and are resistant to overcharging and discharging. However, one drawback of NiMH chemistry is its relatively high self-discharge rate. When overcharged, NiMH batteries utilize excess energy to split and recombine water, making them maintenance-free [17]. Nevertheless, if these batteries are charged at excessively high rates, hydrogen buildup may occur, leading to cell rupture due to the generation of excessive heat. Over-discharging can also result in reverse polarization of the cell, causing a reduction in capacity. Furthermore, NiMH batteries exhibit unsatisfactory performance at low temperatures [17].

The most promising choice among existing battery technologies applicable to EVs is lithium-ion (Li-ion) batteries, which are also now regarded as the best option for developing future-generation EVs. Li-ion batteries are emerging as the best fit for EVs as they have a higher energy density than any other battery technologies, higher power density, good high-temperature performance, and, most importantly, are lighter and smaller than other batteries, which can also be seen in Figures 1.2 and 1.3, respectively. These batteries have high energy-to-weight ratios, no memory effect, and a low self-discharge, due to which they are replacing NiMH batteries. They can operate in a wide range of state of charge (SoC) while maintaining a long cycle life [18]. Also, the operating voltage of Li-ion batteries is high (3.7V on average). The only disadvantage compared with NiMH batteries is that they require a protection circuit or battery management system (BMS) and are expensive [13, 17]. However, the cost of Li-ion battery production for a large number of HEVs is less than that of NiMH battery which is shown by Figure 1.4 [13].

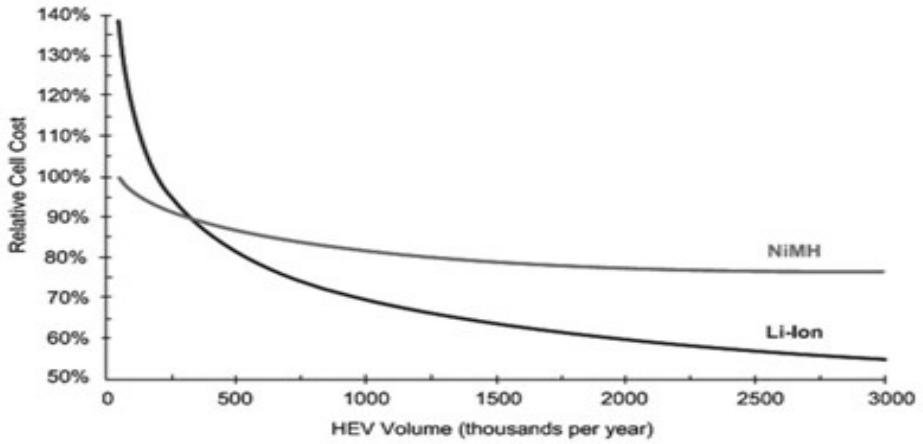

Figure 1.4: NiMH and Li-ion HEV cell cost as a function of vehicle production volume [13].

1.1 Need of HEV

HEVs are those vehicles that utilize multiple energy sources to provide propulsion power. There are various types of HEVs based on this concept, including engine and fuel cell, battery and fuel cell, engine battery and capacitor, battery and flywheel, and battery and battery hybrids [19]. HEVs, powered by alternative sources and enabled by high-efficiency electric motors and controllers, offer a clean, efficient, and environmentally friendly transportation solution. They create a clean environment and reduce operating costs compared to gas-powered vehicles. Significant advancements in power electronics technology have enhanced the reliability and efficiency of HEVs [20, 21, 22].

The most common type of HEV combines an ICE and an electric motor to propel the vehicle. Depending on the way the ICE and motor contribute to the vehicle's transmission, HEVs can be classified into different architectures, such as series hybrids, parallel hybrids, series-parallel hybrids, and complex hybrids.

The Series HEV is a straightforward hybrid vehicle design where the ICE is not directly connected to the drivetrain. Instead, the engine's output is converted into electricity through a generator. This generated electricity is then used either to charge a battery or to power an electric motor that drives the vehicle's wheels. In this configuration, three propulsion devices are employed: the engine, the motor, and the generator [20]. One of the main advantages of this design is the flexibility it offers due to the absence of a direct connection between the wheels and the ICE. This allows for easy control of power distribution to each wheel and simplifies traction control. However, a drawback of this type of HEV is the requirement for separate motor-generator sets. The combined efficiency of these sets is generally lower than that of a conventional transmission [23]. In this dissertation series HEV is used to verify the proposed strategy.

In addition to the vehicle architecture, HEVs can be categorized based on the desired level of hybridization. The cost of an HEV under these categories is influenced by the capacity of ESS utilized in the vehicle. The concept of hybridization factor (HF), as introduced in [23], allows for the classification of HEVs on a spectrum between HF=0 (representing an ICE vehicle) and HF=1 (representing an FEV). The hybridization factor (HF) can be expressed as a measure of power supplied by the ICE and motor as

$$HF = \frac{P_{EM}}{P_{EM} + P_{ICE}} \tag{1.1}$$

where, P_{EM} = Peak power of electric motor and P_{ICE}= is the peak power of ICE.

According to this hybridization factor, that determines the amount of electric power fed by an electric motor, HEV can be classified into the following categories:

- Micro Hybrid
- Mild Hybrid
- Full Hybrid

PHEVs (Plug-in Hybrid Electric Vehicles) share similarities with conventional hybrid vehicles, incorporating both an engine and an electric motor. These vehicles can recharge their batteries through regenerative braking or using the engine. However, there are key distinctions that set PHEVs apart from regular HEVs. The primary difference lies in the presence of an additional charging port on the PHEV. This port allows the battery to be charged from an external power supply, granting the vehicle the ability to be plugged in. Furthermore, PHEVs typically possess higher-capacity batteries compared to their HEV counterparts. This larger battery capacity enables PHEVs to travel significantly longer distances using the electric motor alone, providing enhanced electric-only driving capabilities.

FEVs or HEVs are considered viable solutions to reduce petroleum consumption and GHG emissions. While FEVs may be the preferred option over HEVs for this purpose, their adoption can face challenges for three primary reasons: infrastructure support, battery supply, and public assurance during the transition from ICE vehicles to FEVs. The lack of infrastructure support for FEVs poses a significant hurdle. The establishment of numerous charging stations in various locations is necessary, requiring the expansion and modernization of electrical grids to ensure a reliable power supply to these stations. Additionally, the shift to FEVs necessitates extensive supply chains for ESSs, particularly batteries. The mining and transportation of minerals for these batteries can be a logistical challenge, especially considering the dominance of China in lithium battery supply chains. Public confidence in shifting from ICE to FEVs is another important consideration. Range anxiety, stemming from concerns about the limited range of FEVs due to battery degradation, often raises apprehension among consumers. Overcoming this anxiety and assuring the public about the reliability and convenience of FEVs is crucial for their widespread adoption.

Considering these factors, the transition to FEVs will require time and effort. In the meantime, HEVs emerge as a favorable solution. Current data support this notion, as shown in Figure 1.5, illustrating the different types of EV sales in the US from 2000 to 2021. According to the US Department of Energy (DOE) [24], more than 65% of the total EVs sold in 2021 were HEVs. Presently, around 74% of registered EVs in the US are HEVs, while PHEVs and FEVs make up 9% and 17%, respectively [24]. A notable observation from Figure 1.5 is that the number of EV sales has doubled from 2020 to 2021.

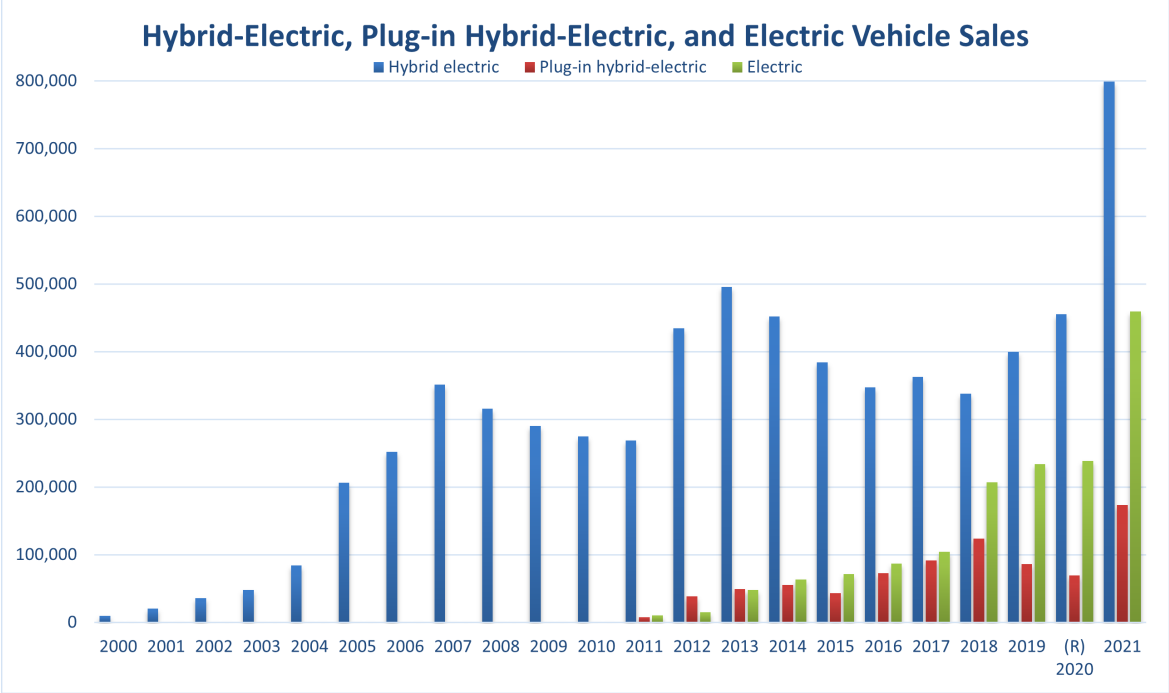

Figure 1.5: EV sales over the years [24].

1.2 Challenges in EVs/HEVs

The components used in a vehicle degrade with time due to the vehicle's operation. As a result, these components' output is compromised, which could make the vehicle's operation unreliable. One of these components is the ESS utilized in EVs and HEVs. Compared to a gasoline-powered car, the initial cost of an electrified vehicle is typically higher. Nearly 30% of the overall cost of the vehicle goes toward ESS [25]. The ESS degradation raises concerns regarding electrified vehicles' system dependability and viability. As a result, there will be a significant impact on economic goals from ESS deterioration.

The degradation of the battery results in a decrease in its capacity, and when the capacity drops

below 80%, the reliability of the vehicle operation becomes questionable. This implies that for the vehicle to operate reliably, the battery's operational range should fall within 80% to 100% of its initial capacity. After the battery's capacity reaches 80%, the battery needs to be replaced [26]. However, replacing the battery would lead to a significant increase in the vehicle's operational costs, making it an uneconomical.

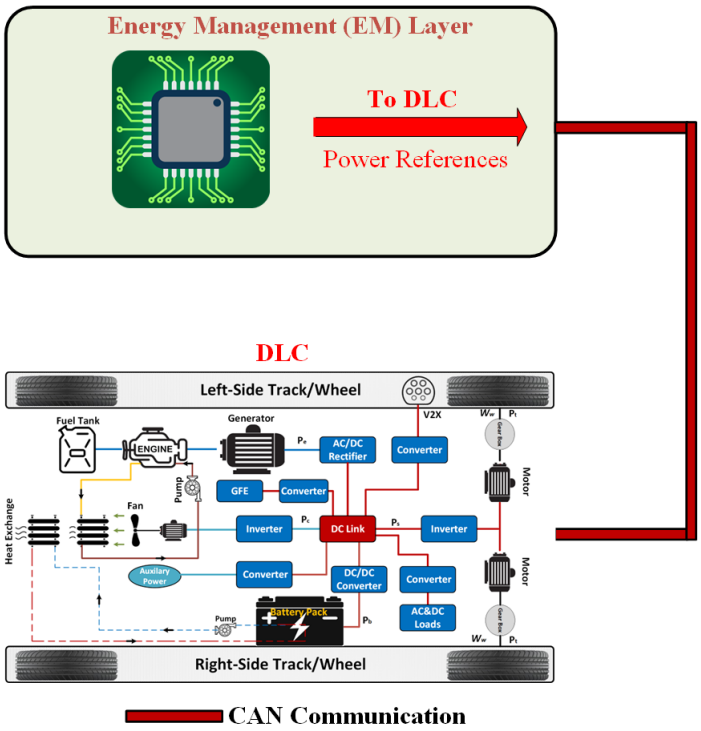

Figure 1.6: Control architecture in existing HEVs.

The degradation of the battery used in HEV can be minimized by controlling the vehicle's operation scenario. The presence of multiple sources in the vehicle demands energy management (EM), as shown in Figure 1.6. The techniques used by the EM have an impact on the rate at which the battery of an HEV degrades [27]. This observation supports the idea that EM plays a crucial role in controlling the power from multiple power-generating sources in the vehicle. Several operational factors, such as temperature, depth of discharge, charging, and discharging currents, influence a battery's degradation. Therefore, it is advisable to consider operational conditions while modeling the degradation of the battery [15]. The techniques or algorithms used in an EM can be regarded as a viable option for preventing or reducing component degradation. However, integrating the operational conditions for battery aging into the objective function of an EM system poses challenges, as it adds complexity to the system. Additionally, it is essential to consider the primary objective of the EM system, which is to minimize fuel consumption costs.

1.3 Dissertation Problems and Approaches

Battery degradation poses significant challenges in the context of EVs and HEVs. As these vehicles heavily rely on the performance and longevity of the ESS, any degradation in the battery leads to reduced range, diminished power output, and increased operating costs. The detrimental effects of battery degradation impact the economic viability and long-term reliability of the vehicle. Therefore, there is a critical need to address this issue and develop strategies that minimize battery degradation, ensuring extended operational efficiency and cost-effectiveness.

The aim of minimizing battery degradation in EVs and HEVs brings forth various advantages, encompassing long-term cost reduction and enhanced operational reliability. This dissertation is primarily dedicated to minimizing the degradation of the ESS employed in HEVs, striving for economic viability and prolonged operational reliability. To attain this objective, different algorithms are employed within an EM system. Furthermore, additional devices, such as supercapacitors, are integrated with the battery to mitigate degradation. A distinctive focus of this dissertation involves the incorporation of a Degradation Forecasting (DF) layer into the HEV's control architecture, which is positioned above the EM layer. This layer effectively addresses battery deterioration without requiring additional devices that might escalate vehicle costs. Importantly, the proposed strategy is formulated for real-time implementation.

The following section discusses the problem statement and briefly presents the proposed approaches.

1.3.1 EM's Optimization Problem

The presence of multiple energy-generating sources in HEVs demand for an EM [28, 29]. The primary function of EM is to allocate power among various energy sources within a vehicle, optimizing an objective function in a well-defined manner while also satisfying the specified constraints [30].

Recently, several research has been done to improve the optimization function of the EM. EM techniques can be broadly classified into four main categories, namely, predictive control method, learning method, heuristic method, and globally optimum approach [31]. Utilizing globally optimal methods can lead to minimum fuel consumption when provided with complete information regarding future power demand [32, 33]. Among different algorithms, dynamic programming (DP) and Pontryagin's minimum principle (PMP) are the most commonly used algorithms [30, 34, 35]. The primary limitations of DP implementation are the curse of dimensionality and the considerable computing overhead requirement. Although several DP approximation techniques can alleviate the computational burden, they are still not currently suitable for real-time EM problem-solving [6]. And, for PMP, the iterative nature of the two-point boundary value problem (TPBVP) arising from it leads to longer computation times [36]. The non-convex nature of the optimization problem makes achieving global optimality in distributed energy management a challenging

task in current research.

The approach taken in this dissertation involves the development of an optimization algorithm capable of real-time operation. The objective is to efficiently address the constraints associated with the EM strategy, specifically the reduction of fuel consumption cost. In order to accomplish this, a set of constraints is established to govern the operation of the HEV within a specified range, emulating real-world vehicle conditions.

The optimization problem is formulated as a constrained optimization problem, which means that there are certain conditions and limitations that must be satisfied. The constraints considered for the EM in this dissertation are related to the power limits of the generator or engine and the battery, the total load power, and the state of charge (SoC) of the battery. These constraints ensure that the operation of the HEV remains within a specific range. The goal of the objective function of the EM is to determine the optimal power distribution between the battery and the ICE of the vehicle in order to minimize fuel consumption. The detail explanation of the EM is provided in Chapter 4.

1.3.2 Integrating Degradation Forecasting into Control Architecture of HEV

In recent years, forecasting has gained considerable attention due to its importance and advancements in forecasting and prediction technologies. This has led to the emergence of various forecasting algorithms, such as linear regression, neural networks, and support vector machines. More recently, there has been a growing interest in the degradation forecasting of components used in different sectors. Accurate predictions of component degradation can provide valuable insights for system planning, especially timely maintenance, and prevent potential severe events for the reliable operation of the system. The ability to forecast future events with precision enables systems to make well-prepared plans and mitigate potential risks. This has motivated researchers to explore degradation forecasting techniques alongside other forecasting domains.

To ensure optimal system reliability, it is crucial to develop degradation models in conjunction with suitable decision-making strategies. These strategies enable the integration of component status information with control processes, ultimately contributing to the system's overall reliability. In the automotive sector, real-time control and management activities should encompass planning activities, such as maintenance and unit commitment, in an automated and collaborative manner.

By taking these factors into account, the integration of a forecasting layer into the hierarchical control architecture of a HEV can effectively monitor the degradation of vehicle components, the battery in this dissertation. This integration enables the implementation of degradation models and suitable decision-

making strategies to incorporate component status information into the control system. The developed DF layer considers the degradation of battery used in the vehicle and serves the following purposes:

1. Provides the cost of degradation to the EM so that it can take action to minimize degradation
2. Enhances the reliability of vehicle operation by monitoring the state of health (SoH) of the battery
3. Reduces the overall operating cost of the vehicle.

1.4 Dissertation Organization

This dissertation has seven chapters. Figure 1.7 shows the dissertation chapter flow. The following lists and briefly summarizes the chapters.

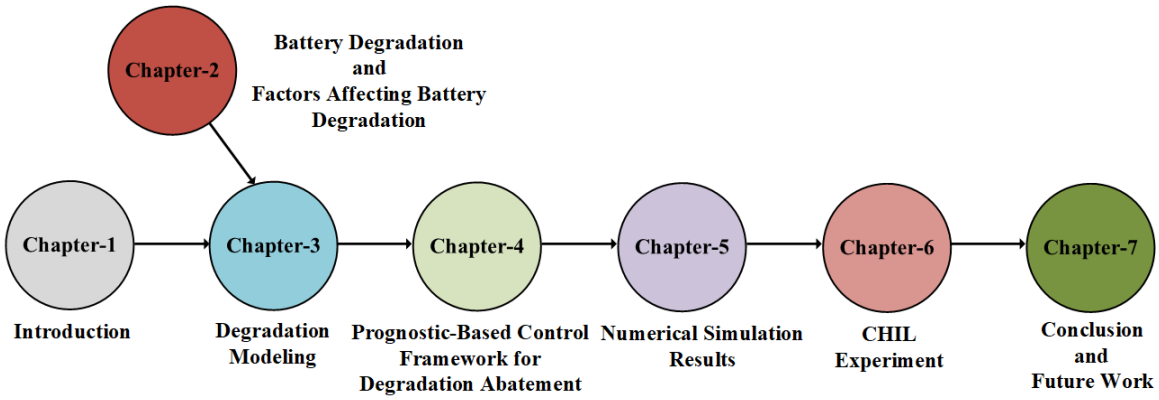

Figure 1.7: Dissertation chapter flow.

Chapter 1: Introduction

In this chapter, the growing importance of electrified vehicles in the current era will be addressed. Detailed discussions are provided to highlight why Li-ion batteries are considered the most suitable choice for automotive applications. Additionally, the chapter gives a summary of existing challenges associated with energy management design from a degradation perspective. These challenges serve as motivation for this dissertation. To summarize, the following problems are identified and outlined as follows:

- The main objective of an EM is to reduce fuel consumption and does not consider the degradation of components used in the vehicle
- This dissertation proposes a strategy named prognostic-based control framework (PBCF) that integrates an additional upper layer to the EM layer in the control architecture to achieve the following aspects:
  - Minimize the degradation of components (i.e., battery in this dissertation)

- Minimize the overall operating cost of the vehicle
- Increase the reliability of operation of the vehicle through monitoring the real-time status of the vehicle's components.

Chapter 2: Battery Degradation and Factors Affecting Battery Degradation

In this chapter, a comprehensive survey of the literature on battery degradation will be presented. The aim is to understand the underlying reasons behind this phenomenon. Also, it will provide a detailed exploration of the various factors that contribute to battery degradation in EVs/HEVs. The emphasis will be on understanding the impact of these factors on the overall lifecycle count of the battery. Through a comprehensive analysis, the aim is to gain insights into the specific factors that influence battery degradation and ultimately affect the longevity of the battery in EVs/HEVs and use these information in modeling the degradation of the battery.

Chapter 3: Analytical and Data-Driven Degradation Models

The battery's health in EVs must be closely monitored and predicted in real time for reliable operation and timely maintenance of the vehicle. In recent years, there has been significant improvement in estimating the life of a battery using different degradation models. In this dissertation, analytical and data-driven methods are used to model the degradation of the battery, and the techniques used to model the degradation will be explained in detail in this chapter.

Chapter 4: Prognostic-based Control Framework for Degradation Abatement

In this chapter, the control strategy proposed in this dissertation will be elucidated. Specifically, the integration of a degradation forecasting (DF) layer into the control architecture of the HEV will be described. This section will provide a comprehensive explanation of the procedure involved in implementing this strategy, outlining the steps and processes in detail. The aim is to offer a thorough understanding of how the proposed control strategy operates within the HEV system.

Chapter 5: Numerical Simulation Results

Within this chapter, numerical simulations will be presented to showcase the efficacy of the strategy proposed in Chapter 4. The simulations serve as practical demonstrations that illustrate the effectiveness and performance of the proposed architecture in MATLAB/Simulink.

Chapter 6: CHIL Experiment

Chapter 5 focuses on the verification of the simulation using MATLAB/Simulink on a personal computer. However, this section goes beyond simulation and presents a real-time implementation of the proposed strategy. Specifically, a controller-hardware-in-loop (CHIL) experiment is conducted in the RT-COOL lab at Clemson University, and the details of this experiment will be thoroughly discussed in this chapter.

Chapter 7: Conclusion and Future Work

This section concludes this dissertation.

The overall sections explained in the chapter above are shown graphically in Figure 1.8.

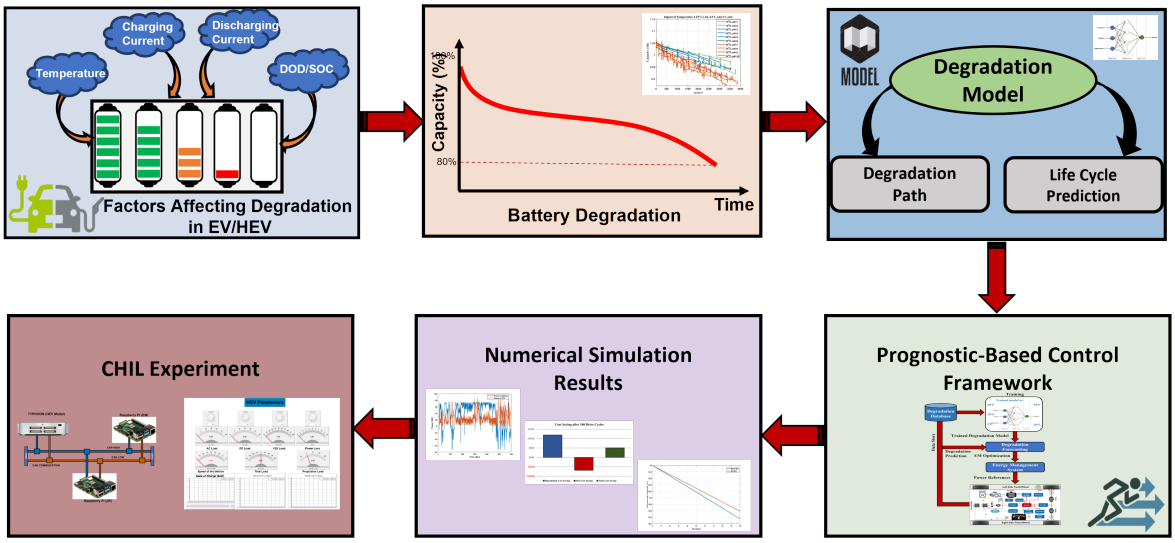

Figure 1.8: Steps followed to complete the dissertation.

Chapter 2

Battery Degradation and Factors Affecting Battery Degradation

Nomenclature

Ah	Ampere-hour
BMS	Battery management system
C-rate	Charging/ Discharging current rate
DoD	Depth of discharge
Li-ion	Lithium ion
LFP	Lithium iron phosphate
LLI	Loss of lithium inventory
LAM	Loss of active materials
NiMH	Nickel-metal hydride
OR	Ohmic resistance
PR	Polarized resistance
SEI	Solid-electrolyte interphase
SNL	Sandia national laboratory
SoC	State of charge
SoH	State of health
Q	Battery capacity
Q_{loss}	Battery capacity loss

2.1 Literature Review in Battery Degradation

The battery is a critical component of an EV, and being one of the most expensive components, it must be thoroughly vetted and operated. The major challenge for the auto industry is to reduce the

cost of the battery and increase the operating life cycle. To achieve the economic viability of an EV, it is required to have a long battery lifetime. The lifetime of a battery depends on how it's been operated and is a complex mechanism [37]. Battery degradation is one of the limiting factors in battery lifetime, therefore, this mechanism must be thoroughly investigated and reduced in order to extend the battery's lifespan.

The battery's lifetime is the length of time it operates to meet the demands of a particular application. In EV applications, the battery's lifecycle is short compared to other components and is considered reliable until it reaches 80% of its initial capacity [38, 39]. A long battery life is necessary for an EV to be economically viable since the battery costs 30% of the price of an EV [40, 11]. The lifetime of a battery depends on its operation and how fast it degrades, which is a complex mechanism [37]. Two prominent metrics are used to assess the level of battery degradation known as capacity fade and power fade. The use of EVs and HEVs for intense cycling results in the degradation of Li-ion batteries, leading to a gradual decline in their capacity to store energy and deliver power. This is commonly known as capacity fade and power fade.

- Capacity fade refers to the reduction in the energy storage capacity of a cell caused by its degradation. A capacity fade emerges as a gradual decline in the amount of battery capacity that can be discharged throughout a battery's lifespan. It is crucial because it depicts the decline in an electric vehicle's usable range.
- Power fade is defined as the decrease in cell power resulting from an increase in cell resistance due to the effects of aging. It is the gradual reduction in a battery's power capacity caused by a steady increase in the battery's cell impedance over time. Power fade is essential for applications in automobiles since it determines how much power the battery can deliver without lowering vehicle speed or activating an engine or power extender.

To analyze the decline in battery capacity, there should be a fundamental understanding of how a Li-ion battery works. A Li-ion cell is shown in Figure 2.1 which consists of a cathode, an anode, a separator, and an electrolyte. The electrolyte facilitates lithium ions to travel between the electrodes, while the separator separates the anode and cathode, preventing shorting between them. During charging, the lithium ions move from the cathode on the positive side of the battery to the anode. Similarly, during discharging, the lithium ions move from the anode to the cathode. From the initial charge, lithium ions react with the solvents of the electrolyte to form a layer known as solid electrolyte interphase (SEI), whose formation plays a vital role in the degradation of the battery [41], which will be discussed in detail further.

The cathode composition used gives the name of the type of lithium battery. Lithium metal oxides such as Lithium Cobalt Oxide (LCO), Nickel Cobalt Aluminum Oxide (NCA), Lithium Cobalt Phosphate (LCP), Nickel Cobalt Manganese Oxide (NCM), Lithium Manganese Oxide (LMO), Lithium Iron Phosphate

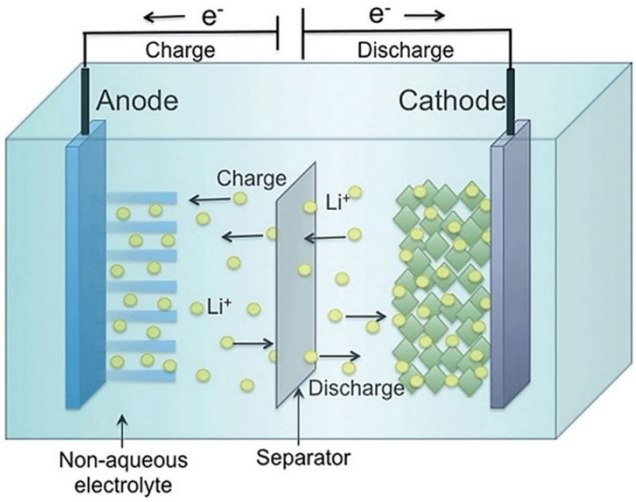

Figure 2.1: Principle of operation of Li-ion battery [13].

(LFP), Lithium Iron Fluorosulphate (LFSF) and Lithium Titanium Sulphide (LTS) have been used as cathode materials owing to their high capacity for lithium intercalation and compatible chemical and physical properties (e.g., for the reversibility of the intercalation reactions) necessary for the movement of lithium ion [42].

The most common material used for anode in lithium batteries is graphite due to its high negative potential. The separator is a porous membrane between the cathode and anode which plays a vital role as it prevents the battery from short circuits but allows lithium ions to pass through it. Li-ion battery's most popular separator materials are made of microporous polyolefin films such as polyethylene (PE), polypropylene (PP), or laminates of polyethylene and polypropylene, offering outstanding chemical stability, mechanical properties, and acceptable cost. The electrolyte infills the space between the separator and electrodes. The electrolyte formulation in lithium batteries is dependent on the electrode materials and operating conditions. The typical electrolyte for lithium batteries is made of a flammable carbonate-based organic solvent such as ethylene carbonate (EC), dimethyl carbonate (DMC), diethyl carbonate (DEC) and ethyl methyl carbonate (EMC), and/or propylene carbonate (PC), with additives including lithium hexafluorophosphate ($LiFP_6$), lithium hexafluoro arsenate monohydrate ($LiAsF_6$), lithium perchlorate ($LiClO_4$), and lithium tetrafluoroborate ($LiBF_4$) to improve cycling [43].

During cycling, side reactions occur in the battery system, and an amount of recyclable active particles irreversibly precipitates in the form of an insoluble SEI file. In addition, the degradation of electrolytes and contact loss between the electrode and the current collector also contribute to the increase of cell resistance. Finally, aged batteries display a reduction in the ability to store energy and deliver power;

performance metrics correlate with a loss in capacity and an increase in internal resistance. During battery cycling, side reactions take place in the system, precipitating a certain amount of recyclable active particles as an insoluble SEI, which cannot be recovered. Moreover, the degradation of the electrolyte and the loss of contact between the electrode and the current collector further contribute to an increase in cell resistance. Ultimately, batteries that have undergone aging exhibit a decline in their capacity to store energy and deliver power, with performance metrics correlated with a decrease in capacity and an increase in internal resistance. To understand the degradation mechanism of a battery, a Li-ion battery is examined since it is a commonly used battery in EVs and has various advantages over the other batteries, as discussed in Chapter 1. Once the battery has been manufactured, it will start to degrade, and different phases of this mechanism are shown in Figure 2.2 [44]. It's worth noting that once the battery reaches 80% of its initial capacity, it can be repurposed as a storage system in power grids. It can be utilized for backup purposes or to assist in frequency regulation, ensuring stability and reliability in the electrical grid.

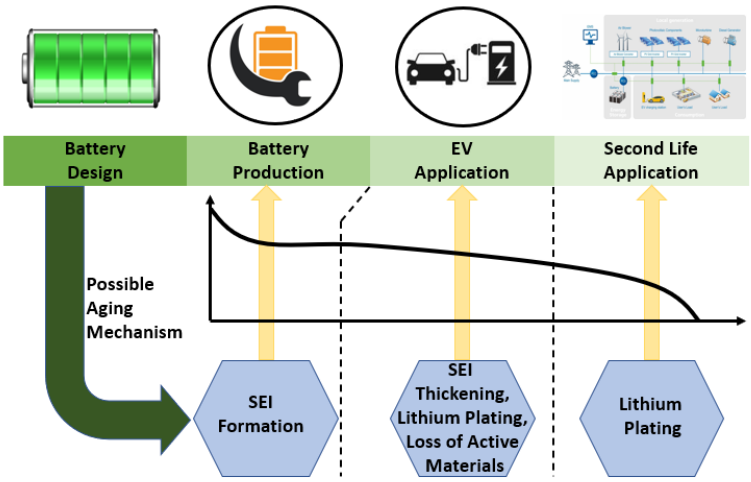

Figure 2.2: Different phases of battery degradation during its lifetime [15].

The Li-ion battery is a complex system to understand, and the aging mechanism is even more complicated. A single factor does not cause capacity and power to fade away but involves several processes and interactions [45, 46]. Battery degradation is determined by different mechanisms and processes depending on the components and chemistry within them. Due to the complex, nonlinear, and path-dependent nature of battery degradation, the aging mechanisms are challenging to analyze and mitigate [47, 48]. According to study [45], the aging trajectories of Li-ion batteries are categorized as linear, sublinear, or superlinear, which are displayed as capacity vs. cycle number or something comparable. Battery aging trajectories are frequently linear or sublinear [49, 50]. Sublinear degradation is commonly considered to be due to side

reactions like SEI growth, which grows nearly with the square root of time or cycle number due to its self-passivating nature. While this degradation is mainly unavoidable, the decelerating degradation rate is a fortunate property for long-lifetime applications. However, the degradation of superlinear batteries is also frequently noticed. They go by several names in different battery literature as knee [51], rollover failure [50], nonlinear aging [52], sudden death [53], saturation [54], second-stage degradation, or two-phase degradation [55], capacity plunge [56], or drop-off [57]. In addition, knees present difficulties for precise onboard state-of-health estimation because batteries with identical states of health could have different remaining useful lives. Avoiding or delaying knees is essential to ensuring long battery lifetimes.

Figure 2.3 shows the different degradation mechanisms in a Li-ion battery cell, where the information provided by [58] and [59] was used to draw this figure. General deterioration is influenced by side reactions, structural changes, and altering chemical compositions. Loss of lithium inventory LLI [46], loss of active materials LAM [46], and loss of electrolyte [57, 60] are the three primary degradation modes identified in the battery aging mechanism [61]. Side reactions at the electrode/electrolyte interfaces, which permanently consume cyclable lithium and produce resistive layers of lithium oxides in the cell, are the primary cause of degradation [59]. The capacity of the cell is reduced (capacity fade) because these Li-ions are no longer cyclable for the intercalation process. Another prominent reason for degradation is the LAM due to electrode delamination, metal dissolution, particle isolation, structural disorder, and film formation [58]. Graphite exfoliation, electrode particle cracking, and dead lithium obstructing the active site pathway reduce the active mass on the negative electrode [62]. Similarly, transition metal dissolution, structural disordering, and electrode particle cracking reduce the active mass of the positive electrode [63, 58, 64, 65]. Electrolyte loss is another key source of deterioration; accumulated lithium on the negative electrode surface interacts with the electrolyte and consumes it [57, 66]. At the end of the battery's life, the reduction of the electrolyte content results in capacity and power fading. The increase in resistance caused by passive film development of the lithium oxides and electrical disconnects between the electrode subcomponents are additional sources of degradation. The most detrimental aging mechanisms impacting graphite anode electrodes are SEI film growth, binder decomposition, and irreversible plating [67]. All these degradation mechanisms can be broadly divided into the following categories:

2.1.1 Loss of free Lithium ions

Lithium ions move from the negative electrode to the positive electrode during discharging and from the positive electrode to the negative electrode during charging in the presence of an electrolyte. While moving from negative electrode to positive electrode and vice-versa, the free Li-ions are consumed by parasitic reactions like SEI formation, decomposition reactions, and lithium plating. Due to these reactions,

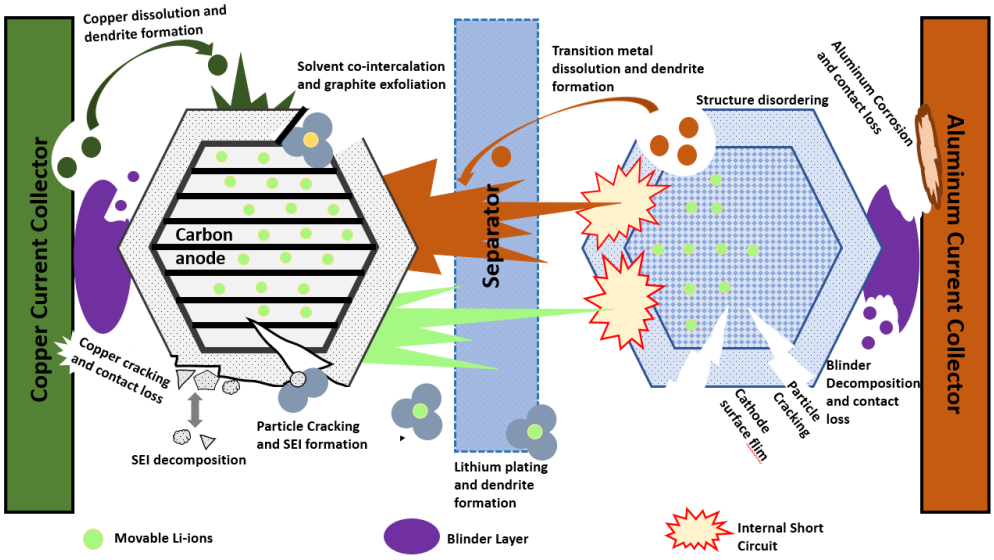

Figure 2.3: Degradation mechanism in Li-ion battery cells [15].

free Li-ions are no longer available for cycling between the positive and negative electrode, resulting in capacity fade and power fade [59]. Two major issues that consume Li-ions during the aging mechanism are described as follows.

2.1.1.1 Solid Electrolyte Interphase

SEI is usually a protective layer formed on the surface of a negative electrode with unique properties that are permeable for lithium ions but impermeable for other electrolyte components and electrons. Typically, the SEI layer protects the electrolyte component from further reduction and the charged electrode from corrosion [60]. Li-ions and other small species can pass through the resultant SEI layer, while bigger species cannot interact with the negative electrode. However, by restricting Li-ion transport and resisting volume changes within the graphitic layers of the negative electrode, the SEI layer can slow down intercalation kinetics at the electrode/electrolyte interface. The SEI layer may break as a result of such a volume change, further exposing the active material in the graphite to reduction processes. The restricted transportation of Li-ions will increase charge-transfer resistance within the battery cell. Also, the consumption of electrolytic compounds decreases charge-transfer capabilities and increases cell impedance.

During the operation of the battery, this SEI layer affects the battery performance in terms of reversible capacity, Coulombic efficiency, and cycling stability [68]. When Li-ions move from the negative electrode to the positive electrode, and vice-versa, they react with the electrolyte to form an additional layer of SEI at the negative electrode, making the SEI layer unstable and increasing its thickness [69]. This

layer grows with time or the number of charging and discharging cycles. When there is chronic charging and discharging of a battery, there is frequent movement of free lithium ions which eventually increases the size of the SEI layer. Due to this, a large number of lithium ions get trapped in this layer and ultimately decrease the battery's capacity [70]. As the thickness of this layer increases, the battery's internal resistance also increases. This SEI layer's growth rate is higher at the early age of the battery and decreases as this layer becomes stable. During the initial 400 cycles, the SEI experiences significant growth. However, after this point and until the battery reaches 80% of its capacity (i.e., EOL), the SEI growth is at a constant rate. When the battery reaches its end of life (EOL), again, the growth of this layer increases rapidly [71], which is not shown in the figure. The SEI formation is believed to be the significant factor affecting the battery cycle life as it consumes the free movable lithium ions and provides resistance to the movement of these ions [72, 57].

High operating temperatures that drive the kinetics of the exothermic parasitic process might increase SEI formation. Furthermore, elevated temperature can change the SEI into lithium salts that are less permeable to lithium ions. On the other hand, a low-temperature operation can reduce the excess lithium ions present at the interface due to slower ion transit, limiting SEI development. Operating the battery at low SoC (i.e., $< 20\%$) or at high SoC (i.e., $>80\%$) can further promote SEI growth because of the increased potential gradient between the active material and the electrolyte. Also, the high charging current can accelerate the growth of the SEI layer due to the high amount of electrons and Li-ions present at the interface.

Study [71] developed a model for the formation of SEI film inside a battery cell and is given by (2.1). Here, L is the battery life, α_{sei} is the portion of charge capacity irreversibly consumed, $f_{d,1}$ is the life lost in one unit of time. The detailed calculation of all these parameters is provided in [71].

$$L = 1 - \alpha_{sei} e^{-N\beta_{sei} f_{d,1}} - (1 - \alpha_{sei}) e^{-N f_{d,1}}. \tag{2.1}$$

2.1.1.2 Lithium plating

Lithium plating is a well-known and innately destructive aging mechanism in Li-ion batteries. It is the deposition of metallic lithium on the graphite negative electrode surface [73]. Lithium plating is considered severe because it not only promotes degradation but also negatively impacts the battery's safety [74]. From a safety perspective, lithium plating in Li-ion batteries can be dangerous as it may result in thermal runaway. This can cause the battery to overheat, catch fire, or even explode. During lithium plating, the electrolyte in the battery is reduced and deposited onto the negative electrode's surface, creating a coating of metallic lithium. Due to this, the battery may experience a short circuit that might result in

a thermal runaway. This can cause the battery to heat up rapidly and produce gases that could cause the battery to rupture or explode [74, 75].

Low operating temperatures, high SoC, high charge currents or fast charging, and high cell voltage are some of the fundamental causes that give rise to lithium plating [59]. While operating the battery at low temperatures, the SEI layer's ability to diffuse lithium is reduced, which enhances the concentration of lithium ions at the electrode/electrolyte interface. Usually, during fast charging, the Li-ions can deposit on the surface of the negative electrode instead of being intercalated between the graphite's atomic layers [76]. These deposited Li-ions can be reversible or irreversible. The irreversible portion of Li-ions reacts with electrolytes to form a secondary layer of SEI that increases the thickness of this layer and increases the internal resistance of the battery cell [75]. Since the free Li-ions are captured to form the SEI layer, it also decreases the energy density of the battery cell. The irreversible portion accelerates the capacity fade, and in the severe case, the accumulated Li-ions might form a dendrite [77]. The formation of lithium dendrites during the lithium plating can cause the tearing of the separator, subsequent short circuits, and instant battery failure. On the other hand, the reversible portion can cause lithium stripping, which is the process where the deposited Li-ions with an electrical contact on the negative electrode interface experience a charge transfer reaction into the electrolyte and then re-intercalate into the negative electrode [45]. This process occurs throughout the discharge or rest period [78, 79]. Lithium plating is also likely to occur when the capacity of the two electrodes is unbalanced or when the positive electrode is physically bigger than the negatively charged electrode [80]. When the electrodes are unbalanced, it promotes lithium plating by polarizing the negative electrode to low potentials. Lithium deposits build up on the negative electrode's edges when the positive electrodes are bigger [45].

The harsh operating conditions, such as high C-rates, charging at a high SoC, and charging at low temperatures, give rise to lithium plating [81]. Due to these harsh conditions, charge transfer kinetics in the electrolyte and solid-state diffusion is delayed, leading the negative electrode potential to fall below the potential of lithium metal, allowing lithium plating to occur. At low temperatures, the power and energy densities of Li-ion batteries are lowered, especially during the charging process, due to three key factors: 1. low ionic conductivity in the electrolyte; 2. poor Li-ion solid diffusivity in the electrode; 3. slow charge transfer rate [82]. Similarly, a high SoC is a condition where the current continues to flow to the battery even though the battery is already full [83]. At such conditions, it is easier for Li-ion to concentrate on the negative electrode surface and exceeds the maximum allowable limit reaching a saturation level. While doing so, dendrite structures are seen in the cells that penetrate the porous separator, resulting in micro-internal short-circuit [84]. The results from [85] show how to avoid lithium plating, which can be achieved by using the battery at increased temperature, low currents, and SoC.

2.1.2 Loss of active materials

When the battery is used for multiple cycles, there will be a point where there is no active mass of negative electrode and positive electrode for the insertion of lithium due to particle cracking, blocking of active sites by resistive surface layers, and structure disordering. These are the phenomenon that causes capacity and power to fade [59]. Depending on the level of lithiation and the afflicted electrode, LAM can be categorized into four groups [46].

- First, the origin of LAM can be the separation of the active material grains from the electrode's ionic or electronic conduction network [86]
- The second is the transition metal's dissolution into the electrolyte solution [87]
- The third is a change in the composition of the electrode [88], and
- The fourth is a modification to the crystal structure of the active material that decreases the degree of lithiation [89].

The LAM is primarily responsible for the degradation of positive electrodes. The structural disordering of the oxide, the dissolving of the metallic ions, and surface modifications such as fracture are examples of the physical degradation of the active materials. High voltages and temperatures increase the electrolyte's disintegration of the oxide particles, raising the impedance. The dissolved species can either move through the electrolyte to interact with the negative electrode SEI, or they can precipitate into new phases on the positive electrode. In either case, the LAM is responsible for lowering the capacity of the positive electrode, which ultimately reduces the cell's capacity. Also, the insertion and extraction of Li-ions put stress and strain on the active material, which leads to micro-cracking. However, due to the bulk amount of active materials, only a minor aging mechanism is expected to occur. The volume change of graphite during Li-ion penetration and removal is not considered significant (typically in the range of 10% or less), and only a minor negative impact on the material's reversibility is expected as a consequence [90]. The structural changes can cause mechanical stress on C-C bonds resulting in cracking or some other structural damage which will have a minor impact on cell aging. But due to solvent co-intercalation, electrolyte reduction inside graphite, and/or gas evolution inside graphite, graphite exfoliation, and graphite particle cracking would most likely result in fast electrode deterioration [90].

Figure 2.4 shows different working conditions of a Li-ion battery and the degradation mechanism associated with that operating condition along with its effect in a graphical form which is a summary of details provided in studies [58] and [59].

The degradation of a Li-ion battery can be characterized by a decrease in capacity over repeated charge and discharge cycles. Capacity is the amount of electrical charge the battery can store when fully

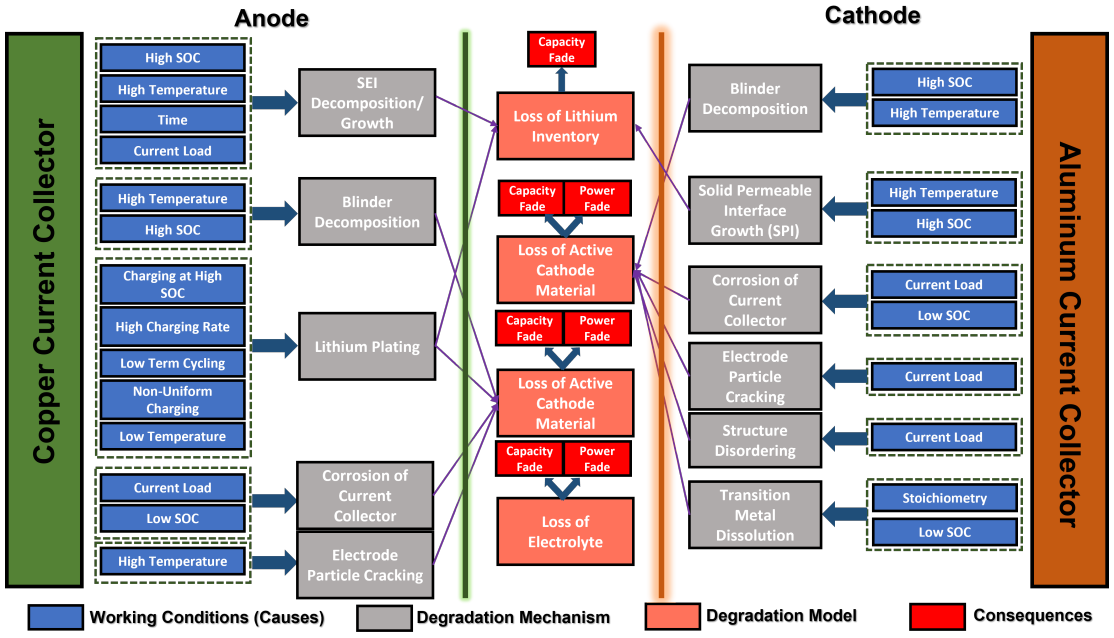

Figure 2.4: Cause and effect of degradation mechanisms and associated degradation modes [15].

charged. For batteries, 80% of the initial capacity is referred to as the point after which it tends to exhibit an exponential decay of capacity and is considered an unreliable power source after this point for EV application [91]. One issue that always comes with battery is self-discharging. Self-discharging means the battery experiences a loss of energy even when it is in an inactive state. It is due to the chemical reactions inside the battery, even though there is no connection between the electrodes. Because of self-discharging, batteries initially have less than a full charge in their first cycle. Generally, the self-discharge for lithium batteries is minimal compared with other types of batteries, about 5% in the first 24 hours and around 1%-2% per month [92].

Besides this self-discharge, a battery's capacity is decreased due to the successive and complex set of dynamic chemical and physical processes that slowly reduce the number of mobile lithium ions and other factors discussed in Section 2.2. High current rates, high discharge conditions, and extreme operating temperatures are the most common factors which put a lot of stress on the battery of EVs [91]. In order to minimize the degradation mechanism and ensure the long-term lifecycle of a battery, the degradation behavior must be thoroughly analyzed.

Once the battery is in use, the degradation process begins, and there are two types of aging mechanisms: calendar aging and cycling aging. Calendar aging occurs when the battery is in rest condition; there are no continuous charging and discharging cycles. Cycling aging occurs when the battery is used

and depends on the frequency of charging and discharging cycles. Calendar aging begins shortly after the batteries are made and progresses over time, whereas cycling aging occurs when the battery is employed and depends on its operating conditions.

In modern Li-ion batteries, the main issue in calendar aging is the formation of the SEI layer on the negative electrode [93]. SEI formation is accelerated at high levels of temperature and SoC that gives rise to the impedance of the battery resulting in lower activation energy [94]. The capacity loss of the battery when stored at a different level of SoC can be calculated using a semi-empirical equation (2.2) proposed by [95, 96] with the value of the parameter provided by the study [97].

$$Q_{loss} = \alpha_1.exp(\beta_1.T^{-1}).\alpha_2.exp(\beta_2.SoC).t^{0.5} \tag{2.2}$$

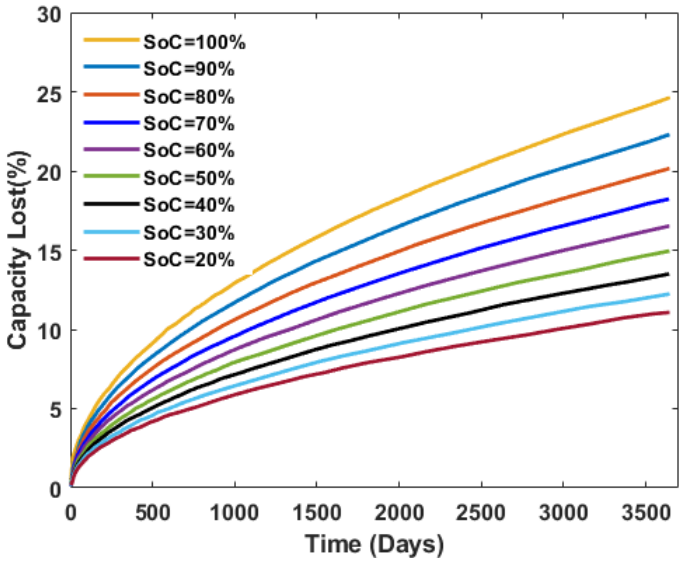

Figure 2.5: Effect of SoC on calendar aging [15].

In this model, t is the storage time in days, T is the storage temperature, and $\alpha_1, \beta_1, \alpha_2$, and β_2 are the fitting parameters. Using this model, the capacity fade of the battery when stored for a long period of time at different storage SoC can be calculated and is shown in Figure 2.5 [96]. The capacity fade is calculated by varying the SoC from 20% to 100% at a constant temperature of $25°C$. For an equal temperature of $25°C$, the capacity loss is not the same at different SoC. The amount of ions on the electrode is given by SoC. A high SoC implies large potential disequilibrium at the electrode/electrolyte interface, which stimulates chemical reactions. Clearly, it can be concluded from the figure that the capacity loss of the battery goes on increasing as the storage SoC of the battery is increased, which is also verified in [98]

and [99].

Similarly, the effect of temperature on the calendar aging of a battery is investigated in [71], and its result is shown in Figure 2.6. The battery is stored at five different temperatures from $15^{\circ}C$ to $55^{\circ}C$, keeping the SoC at 50%. Looking at the figure, it can be inferred that as the temperature increases, the capacity loss of the battery also increases. Study [100] has derived a mathematical model represented by (2.3) to find the capacity loss of a battery cell due to temperature, SoC, and time individually during calendar aging. $k_{temp,Q_{loss}}$ denotes the influence of temperature, σ denotes the influence of SoC, and t denotes the influence of time.

$$Q_{loss}(T, \sigma, t)[\%] = k_{temp,Q_{loss}}.(\sigma).\sqrt{t} \tag{2.3}$$

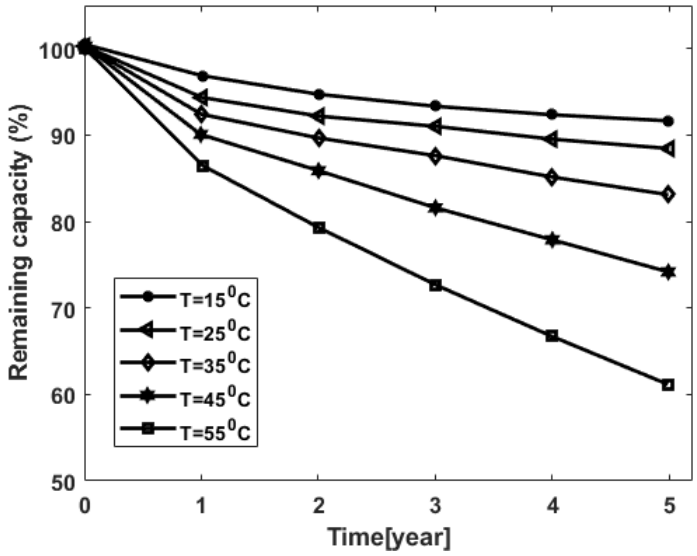

Figure 2.6: Effect of temperature on calendar aging [71].

The temperature influence factor $k_{temp,Q_{loss}}$ can be modeled using Arrhenius equation as given by (2.4). Arrhenius equation is generally used to model the dependency of temperature on the aging of battery as done in studies [101], and [102]. The value of $k_{ref,Q_{loss}}$ can be calculated by dividing the measured value of Q_{loss} at the end of the aging study from the test point with $T = 25^{\circ}C$ and soc= 100%.

$$k_{temp,Q_{loss}} = k_{ref,Q_{loss}}.exp\left(-\frac{E_{a,Q_{loss}}}{R}\left(\frac{1}{T} - \frac{1}{T_{ref}}\right)\right) \tag{2.4}$$

The impact of temperature on the capacity loss based on the experimental data and developed mathematical model is shown in Figure 2.7. This figure is plotted based on the experimental data and

(2.3) and (2.4) provided in [100]. The analysis from this study and Figure 2.7 concludes that the storage of batteries at high temperatures results in higher capacity loss. Also, the result of one year study of a 2.3 Ah graphite/lithium-iron-phosphate (LFP) cell under storage conditions at $25°C$ and $45°C$ was presented in [103]. The result found that the aging was sensitive to temperature, and the battery cell operated at $45°C$ had capacity loss up to four times more than the battery cell operated at $25°C$. This capacity fade was dominated by the loss of cyclable Li-ions along with a minor loss of graphite active material.

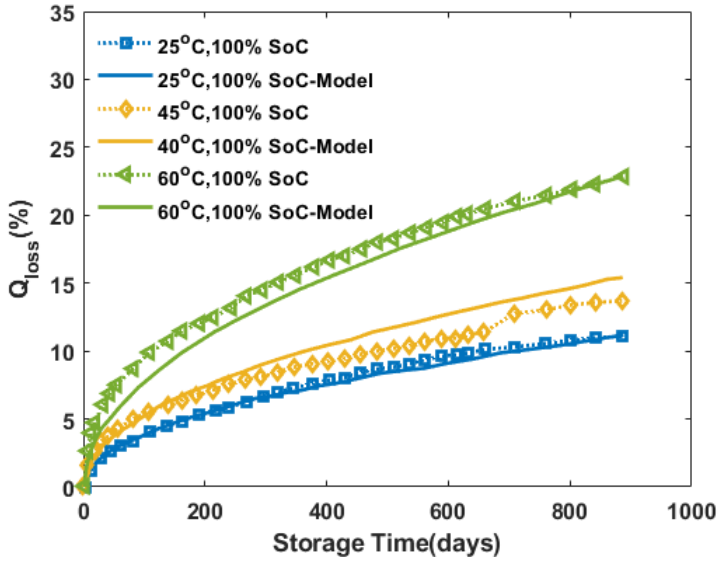

Figure 2.7: Impact of temperature on calendar aging based on experimental data and developed model [100].

Several studies have been conducted on Li-ion batteries at various operating temperatures, charging and discharging current rates, and DoD to determine their impact on battery aging. All these factors have a different impact on the battery that accelerates the aging mechanism. Knowing these factors and how they affect battery capacity is vital for minimizing battery capacity loss. One common parameter associated with all these factors that have a severe impact on battery degradation is internal resistance [104]. The change in internal resistance with the change of aforementioned parameters is examined in detail in [105]. The resistance in a Li-ion battery can be divided into two categories: ohmic resistance (OR) and polarization resistance (PR) [105, 106]. The first one includes electrolyte materials resistance, electrolyte resistance, separator resistance, and contact resistance, whereas the second is the resistance caused by polarization in the electrochemical reaction [107]. The change in these resistances with the increase in cycle number, along with the capacity fade, is shown in Figure 2.8 [105]. It can be analyzed from this figure that with the increase in cycle number, both the resistances (OR and PR) of the battery increase, whereas the battery's

capacity starts to decline. There are several factors that stimulate battery degradation, which is already summarized in Figure 2.4, where different causes of degradation are shown along with their effects on the battery. Predicting the degradation rate and remaining lifetime of a battery is a demanding task due to the complex nature of the degradation process. However, to ensure reliable operation and timely maintenance, it is essential to determine the remaining lifetime of a battery.

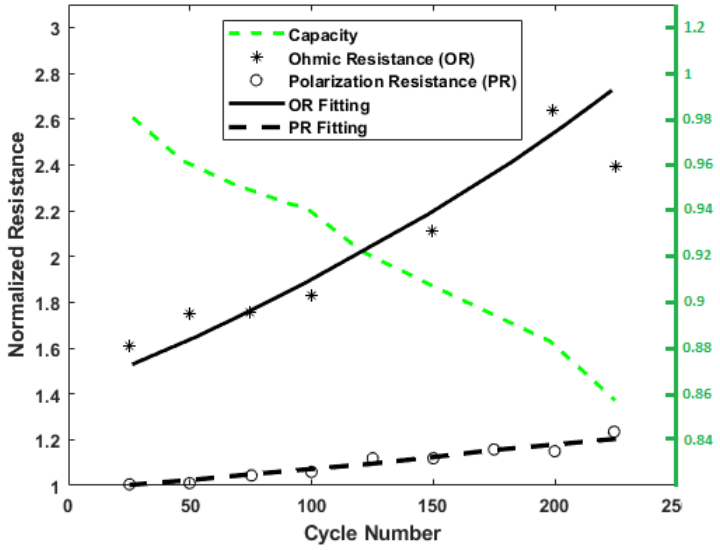

Figure 2.8: Change in parameters of battery with cycle count [105].

The most common factors that affect the battery capacity and give rise to degradation are [108]:

1 Temperature

2 Discharging current

3 Charging current

4 Depth of Discharge (DoD)

These parameters have impacts depending on the mode of operation of the battery. If the battery is stored for some time, then the temperature and SoC of the battery have a great impact on its degradation. When the battery is in operation, all these factors have different effects on the battery and result in degradation. The battery in EVs is subjected to various stresses due to high current rates, deep discharge conditions, and operating temperatures. Table 2.1 provides a summary of the impact of these factors on the degradation of the battery, along with the corresponding references that were used to investigate their effects. The subsequent subsections delve into a detailed discussion of these factors.

Table 2.1: Factors affecting battery degradation

Factors	Affects	Causes
High Temperature	Anode	Mechanical instability due to decomposition of blinder Growth in SEI layer and decrease in accessible surface area due to SEI growth Electrolyte decomposition resulting in loss of cyclable lithium and further SEI growth Parasitic side reactions exposing fresh graphite to electrolyte and increased SEI growth Phase change in active material due to metal dissolution
	Cathode	Increase in phase changes in active material Blinder decomposition Increase in phase changes in active material Loss of cyclable lithium and gas evolution due to oxidation of electrolyte
Low Temperature	Anode	Lithium plating during charging at high SoC
High Current Rates	Anode	Metallic lithium plating and subsequent electrolyte decomposition by metallic lithium SEI growth at locations where Li metal is exposed to electrolyte Contact loss of active material particles and particle cracking due to volume changes Expose of fresh graphite to the electrolyte and further SEI growth
	Cathode	Trasnsition metal dissolution Active material crumbling Volume changes and tensile compressive stresses causing particle cracking
High DoD	Both Anode and Cathode	Particle cracking due to mechanical stress caused by volume changes Contact loss of active material particles due to volume change during cycling
High SoC	Both Anode and Cathode	Blinder formation Electrolyte decomposition
	Anode	Lithium plating at high charging rates
	Cathode	Current collector corrosion
Low SoC	Both Anode and Cathode	Blinder formation Electrolyte decomposition
	Anode	Current collector corrosion
	Cathode	Transition metal dissolution

2.2 Factors Affecting Battery Degradation

2.2.1 Temperature

Temperature is a crucial factor that significantly impacts the health, performance, cycle lifetime, and safe operation of Li-ion batteries [109]. As the temperature in the battery changes, the chemical reaction inside the battery changes. One of the positive impacts of higher temperature on the battery is that it increases the performance and storage capacity of the battery [109]. This is because the electrolyte conductivity increases and the electrode wetting characteristics are improved at higher temperatures [110]. When the temperature was raised from $25°C$ to $45°C$ in [109], the maximum storage capacity rose by 20%. However, this increase in capacity comes at a cost, reducing the battery's longevity. Similarly, the operation of the battery under low temperatures is not favorable as it leads to faster aging of the battery [111].

The effect of temperature on different components of the battery is the reason behind the degradation. The study of the impact of high temperatures on lithium batteries from [112] concludes that a blinder layer is formed on the positive electrode's surface, resulting in poor Li-ion intercalation. Also, the change in the composition of the SEI layer depends on the operating temperature, which is different at different operating temperatures [113]. The X-RAY analysis in this study showed that the capacity loss is mainly related to the sei film growth on the negative electrode. The elevated temperature escalates the formation of the sei layer on the negative electrode [114]. The formation of the sei layer was the main contributor to the increase in the cell's internal resistance [115]. This decreases the performance of the battery by reducing its efficiency. Similarly, Lithium plating and subsequent interaction with the electrolyte, resulting in the loss of cyclable lithium, is the most common aging mechanism at low temperatures [116].

To investigate the apparent effect of temperature on the lifecycle of the battery, the study [91] is considered as a reference. The tests is carried out at four distinct temperatures: $40°C$, $25°C$, $0°C$, and $-18°C$, with the results displayed in figure 2.9. When the temperature is at room temperature ($25°C$), the cycle count of the battery is maximum at 2600. The cycle count of the battery diminishes when the temperature rises over this point. It was found to be 1850 at $45°C$, and the cycle count continues to plummet as the temperature rises. The instability of the SEI causes the battery's lifespan to decline beyond $25°C$ because the SEI layer consumes free Li-ions during each charge cycle, reducing the number of free Li-ions available to represent the battery's capacity. Also, with the instability of SEI, the internal resistance of the cathode surface will increase, and there will be a mismatch in the electrochemical process of the battery, due to which the lifecycle of the battery decreases, and the capacity fade increases [110]. The cycle count of the battery will decrease when the temperature drops below the ambient temperature. The cycle count was lowered to 2070 when the temperature reached 0°C. The battery's life cycle is substantially reduced when

the temperature drops beyond this point; at $-18^{\circ}C$, the cycle count was found to be only 200.

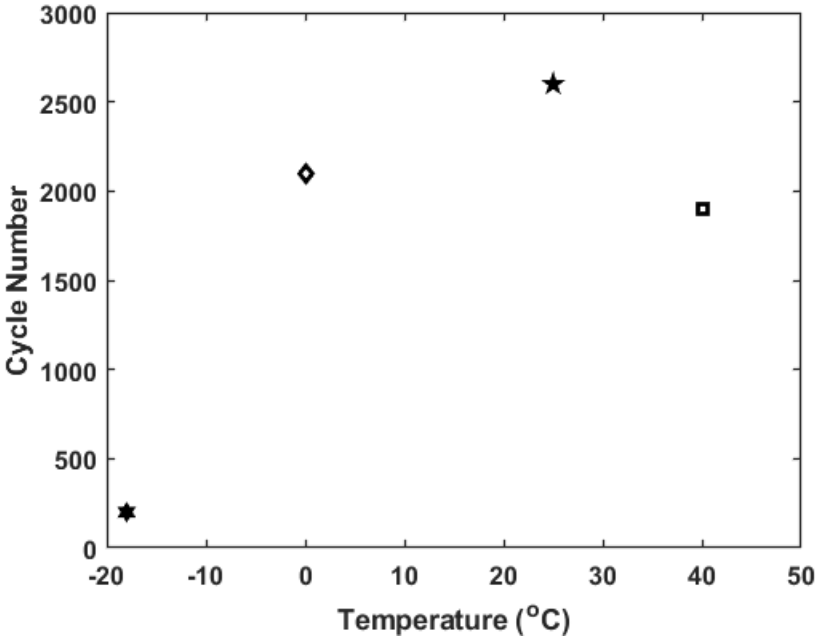

Figure 2.9: Effect of temperature on lifecycle [91].

The impact of temperature on the dataset considered in this dissertation is investigated. The dataset used in this study comprises data collected from laboratory experiments conducted at the University of Wisconsin-Madison, focusing on different 2.9 Ah Panasonic 18650 PF battery cells. Figure 2.10 illustrates the effect of temperature on five of these battery cells, specifically at temperatures of $-20^{\circ}C$, $-10^{\circ}C$, $0^{\circ}C$, $10^{\circ}C$, and $25^{\circ}C$. Upon analysis, it is observed that the battery cell operated at $-20^{\circ}C$ exhibits the most rapid degradation path, followed by the battery cell operated at $-10^{\circ}C$. Conversely, the battery operated at ambient temperature $25^{\circ}C$ demonstrates the slowest degradation path. These findings align with the analysis conducted in a previous study [91] and are consistent with the results reported in the paper [15].

The second dataset considered in this dissertation is obtained from Sandia National Laboratory (SNL), featuring different 1.1 Ah LFP 18650 battery cells. Figure 2.11 illustrates the impact of temperature on the degradation path of these battery cells, considering a total of 10 cells. Specifically, the figure showcases two cells operated at $15^{\circ}C$, four cells operated at $25^{\circ}C$, and four cells operated at $35^{\circ}C$. Notably, the figure demonstrates that the degradation paths of battery cells at the same temperature vary, highlighting the complex nature of degradation mechanisms within batteries. This complexity is influenced by multiple factors, as explained in Chapter 1. It is observed that as the battery temperature increases, the degradation rate accelerates. At $15^{\circ}C$, the battery exhibits a slower degradation rate, while at $35^{\circ}C$s, the battery

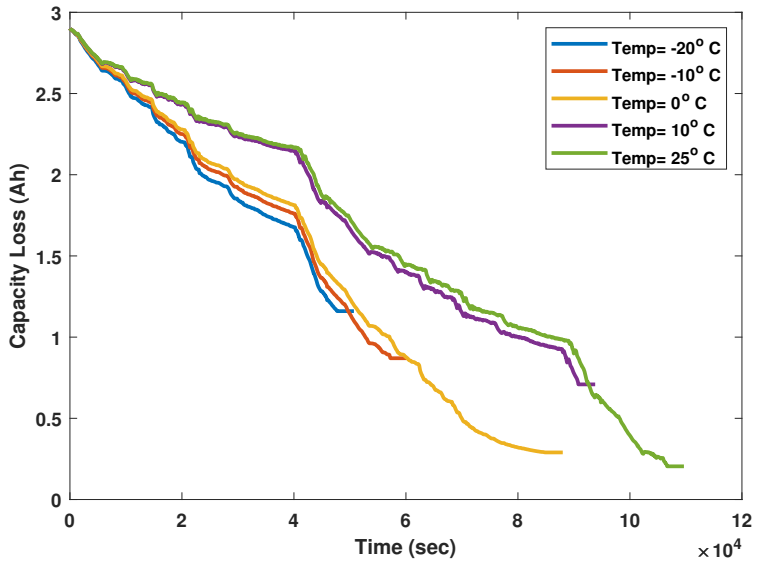

Figure 2.10: Impact of temperature on capacity of battery for University of Wisconsin-Madison dataset.

experiences the fastest degradation path. These observations are consistent with the findings of studies [91] and [15]. The underlying reasons for battery degradation are elaborated in detail in the paper [15], which was published during the period of this dissertation. This paper provides comprehensive insights into the degradation mechanisms and factors contributing to battery performance decline.

2.2.2 Discharging Currents

The discharge current is the amount of current at which the battery is being discharged. The discharge current rate is expressed as Q/h rate, where Q is rated battery capacity, and h is discharge time in hours. Sometimes discharge and charge rate is defined as C-rate, where 1C rate means that the discharge/charge current will discharge/charge the entire battery in 1 hour. The cycle count of a battery depends on the rate at which the battery is discharged. Numerous literature [117, 118, 119, 120] state that the discharge rate greatly impacts the performance and different amounts of discharge current have a different impact on the degradation of the battery.

The primary reason behind this higher capacity fade is the increase in loss of secondary material (i.e., carbon) at higher C-rates which is verified in study [121]. In the third case of this study, when C-rate was 3C, out of the total capacity loss of 16.9% of the whole cell, 10.6% of the capacity loss was due to the carbon electrode material alone. This increase in capacity fade at a higher discharge current for the carbon

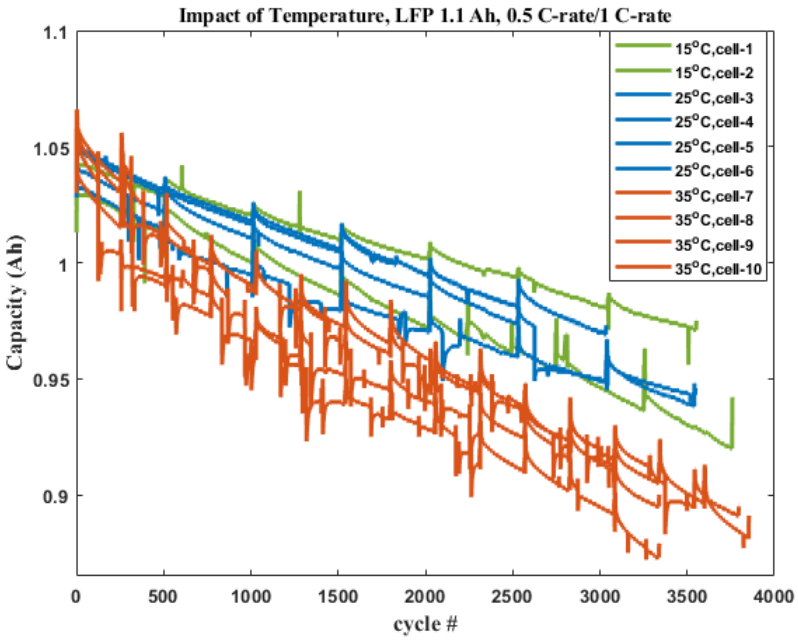

Figure 2.11: Impact of temperature on capacity of battery for SNL battery dataset.

material was correlated to the increase of the internal resistance [122]. Hence, one way to reduce the capacity fade in a battery is by reducing the amount of discharge current that is fed by the battery to the load [123].

The capacity fade of the battery under high discharge current is again correlated to the increase in internal resistance [124]. Studies [91] and [122] analyzed the deviation in the internal resistance of a battery. They found that with the increase in discharge current, there is an increase in internal resistance, which increases the temperature of the battery and further decreases the capacity of the battery. This effect of change in internal resistance with the change in discharge current is further verified in [105], [125], and [126]. All the degradation mechanism is explained in the study [15], which is one of the reference paper for writing this dissertation.

An in-depth analysis of the impact of discharge current on battery cell performance is conducted using the dataset used in this dissertation. The aim is to understand how different discharge rates affect the degradation behavior of the battery cells. The dataset obtained from SNL for different discharge currents is shown in Figure 2.12. This figure shows the degradation paths of nine distinct battery cells, subjected to three different discharge rates. The figure presents the degradation paths of four cells under a 1C-rate discharge, two cells under a 2C-rate discharge, and three cells under a 3C-rate discharge. By observing the degradation paths, a clear trend emerges: higher discharge currents lead to accelerated battery degradation. The impact of discharge current on battery performance is significant. As the discharge current increases,

the degradation of the battery becomes more pronounced. This correlation suggests that higher discharge currents impose greater stress on the battery cells, resulting in faster degradation and reduced overall lifespan as explained in the studies [15].

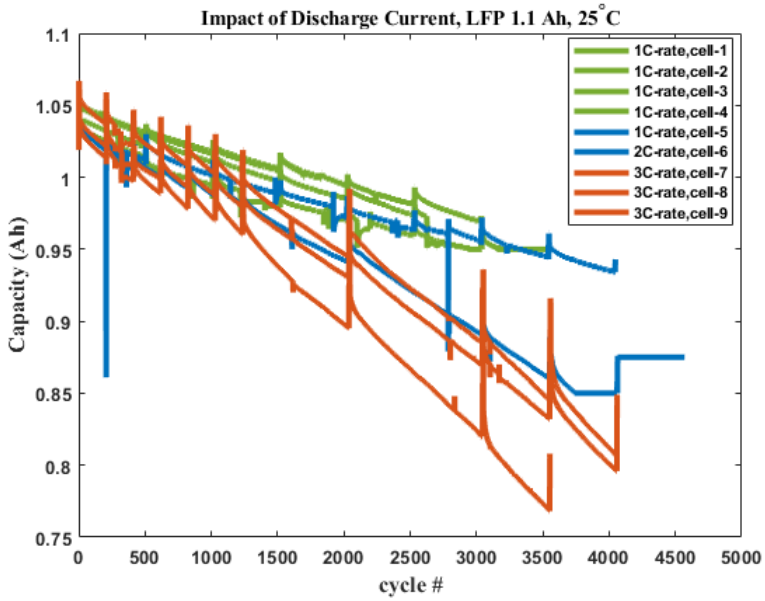

Figure 2.12: Impact of discharge current on the capacity of battery cells.

2.2.3 Charging Current

Most EVs and commercial batteries have been using the concept of fast charging [127]. Vehicle charging time is a crucial factor in the adoption of EVs. Long charging time, usually more than 30 minutes, strongly reduces the sales of EVs [128]. This is because it increases waiting time in the queues, which acts as a barrier to EV adoption [129]. This is why all EV manufacturing companies are shifting towards fast or ultra fast-charging systems for their vehicles [130]. The U.S . Department of Energy has classified charging of electric vehicles into three levels:

- Level 1 is regular charging, which happens when the charge power is less than 5 kW,
- Level 2 is fast charging, which occurs when the charge power is between 5 kW and 50 kW, and
- Level 3 is super-fast charging, which occurs when the charge power is higher than 50 kW [131, 132].

An off-board charger is used for Level 3 charging, which means the charger is located outside the car. Because of the high-power charging levels of Level 3 charging, carrying the requisite power electronics onboard is unfeasible owing to space limits. To overcome this limitation and reduce the mass, a Level 3 charge usually

conveys the DC power to the vehicle, whereas Level 1 and Level 2 charging usually have onboard electronic converters that allow AC energy transmission [133].

Most EVs use Level 2 chargers, and Level 3 chargers are in the adoption phase. With the use of an AC level 2 charger, the LLI, and LAM in the negative electrode were found to be the primary aging modes in the cells in the study [134]. These fast-charging technologies can help to increase EV adoption but can have a serious impact on the battery. High charging currents result in increased heat generation, which can lead to elevated operating temperatures. Excessive heat can degrade the battery's active materials, reduce electrolyte stability, and accelerate chemical reactions contributing to degradation processes. Elevated temperatures can also lead to thermal runaway and safety concerns in extreme cases. Hence, there should be a better understanding of the effects of fast charging on Li-ion batteries [125, 23]. Studies [135, 136, 137, 138] investigated the effect of fast charging on Li-ion batteries and observed a more robust capacity fade at higher charging rates. Also, fast charging at a low temperature has a negative impact on the battery [9, 139]. Several failure modes were noted at a high charging current rate after the postmortem analysis of the cells, like lithium plating, graphite exfoliation, jelly-roll deformation, active materials crumbling, aluminum corrosion, and an abnormal SEI formation [140, 141]. The capacity loss is mainly due to the lithium plating that causes irreversible loss of cyclable lithium [142]. Under high charge current or fast charging, heat generation within the cell accelerates the side reactions [143]. Lithium plating, ohmic heat, and increase in impedance are significant issues during fast charging that deteriorates the battery faster [23]. The studies of X-ray diffraction analysis (XRD), transmission electron microscopy (TEM), and scanning electron microscope (SEM) on the individual electrodes done in [144], indicate that the capacity fade during rapid charging and discharging of the battery can be correlated to two leading causes. First, the formation of the defects such as cation disorder and cracks in the positive electrode's active material $LiCoO_2$. Second, the continuous increase in the passive film thickness on the negative electrode is due to the reduction of the electrolyte.

Also, overcharging a battery is another issue during the operation of EVs. Paper [145] investigates the overcharge-induced capacity fading behavior of 20Ah commercial pouch Li-ion batteries with NCM + LMO as a positive electrode and graphite as a negative electrode. A prognostic/mechanistic model and incremental capacity analysis were used to investigate the capacity deterioration process (ICA). This model was used to calculate the LAM in the positive and negative electrodes and the LLI at various overcharge phases. The analysis shows no noticeable capacity degradation until overcharged to 120% SoC. Above this SoC, LLI occurs as a result of lithium deposition, with LAM in the $Li_yMn_2O_4$ of the composite positive electrode [146]. The thickening of the SEI film is confirmed by the increase in internal resistance. When the battery is overcharged above 140% SoC, LAM occurs in both the positive and negative electrode. Also,

due to the electrolyte oxidation, the battery starts to swell. When the battery was overcharged to 150% or more SoC, the battery cell started to rupture, with all the stored energy released instantly due to an internal short circuit, and pinholes on the separator surface was observed after dissembling the batteries.

Similar to the impact of discharge current, the charging current also plays a significant role in the lifecycle count of the battery. Like the discharging current, a higher charging current leads to faster degradation of the battery. To further investigate the influence of charging current, the dataset from the University of Wisconsin-Madison is utilized. The dataset includes different drive cycle data (that will be explained in detail in Chapter 3), which involve varying discharging and charging rates applied to the battery. This allows for a comprehensive analysis of the impact of both charging and discharging currents on battery degradation. Figure 2.13 illustrates the degradation paths of nine distinct battery cells subjected to different drive cycles, which can be correlated with the corresponding charging and discharging currents. Each cell exhibits a unique degradation path, influenced by the specific charging and discharging currents associated with the drive cycle. Notably, cells subjected to lower charging/discharging currents exhibit a slower degradation path, while cells exposed to higher charging/discharging currents display a faster degradation path. This correlation further supports the understanding that a higher charging current accelerates battery degradation.

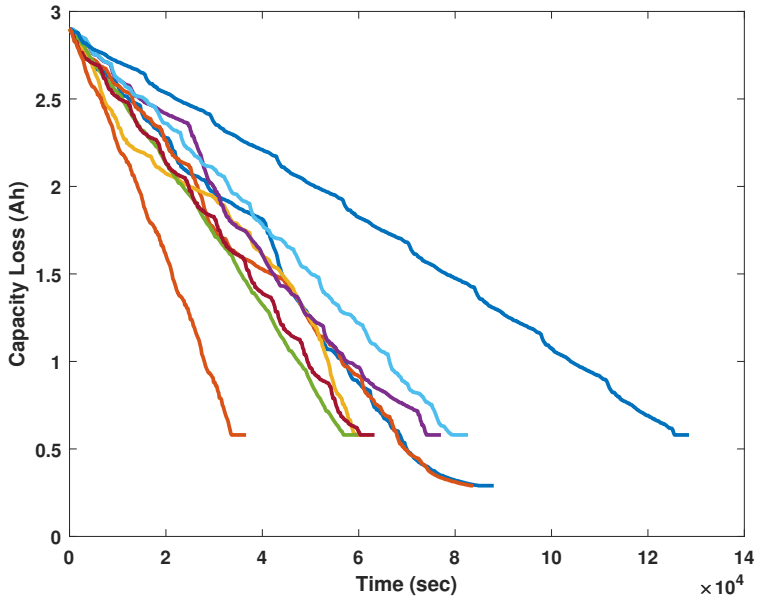

Figure 2.13: Impact of charging and discharge current on the capacity of battery cells.

2.2.4 Depth of Discharge

The DoD is the portion of electrical charge discharged or charged during a cycle with respect to the maximum possible charge that a battery can hold. Or, in simple words, it is the percentage of battery capacity (rated capacity) to which a battery is discharged. Generally, the withdrawal of at least 80% of battery capacity is referred to as a deep discharge [91, 147]. A higher DoD indicates higher discharge of the battery, accelerating the battery aging and increasing the battery life cycle cost [148]. The study [149] finds that the deep discharging of batteries used in PHEV for bulk energy services during vehicle-to-grid (V2G) operation led to the annual replacement of battery packs across all EV charging regimes. Nevertheless, when compared to PHEV, charged opportunistically at home or worked, the battery pack was replaced once in 3 years. This concludes that the regular deep discharge of the battery can reduce the life span by more than one-third. These phenomena are mainly due to the degradation of a positive electrode and growth of the SEI layer [150].

The change in DoD in a Li-ion battery cell can be electrically linked with the change in internal resistance. The internal resistance of the battery increases with the degree of DoD [91]. The percentage increase in internal resistance is lowest for the battery cell that was discharged at 20% DoD, which was found to be 112%. In contrast, the battery cell that was fully discharged (100%) had the highest percentage increase in the internal resistance of 132%. The higher the DoD, the higher the increase in internal resistance, which further assists in the battery's aging mechanism, which is further verified in [151, 152, 153].

Figure 2.14 illustrates the impact of Depth of Discharge (DoD) on battery degradation using the SNL dataset. The plot displays the degradation paths of three battery cells operated at a constant temperature of $25^{\circ}C$, with consistent charging and discharging rates of 0.5C and 3C, respectively. The cells were subjected to three different DoD levels: 100%, 60%, and 20%. It can be observed that the battery cell discharged to its full capacity (DoD = 100%) experiences the most rapid degradation, while the cell with a DoD of 20% exhibits the least degradation. These results align with the findings reported in various research papers, which underscores their relevance in the context of this dissertation.

In this Chapter, a comprehensive review of the factors that impact the degradation and lifecycle count of batteries is done. These factors are crucial in understanding the behavior of batteries and predicting their degradation paths. To ensure the accuracy and reliability of the dataset employed in this dissertation, the degradation pattern under different factors from several studies is also compared and verified in this Chapter. Among the various factors considered, temperature plays a significant role in battery degradation. Fluctuations in temperature can accelerate the degradation process and reduce the overall lifecycle count. Charging current and discharging current are additional factors that influence battery performance and degradation. Higher currents can cause increased stress on the battery, leading to faster degradation and a

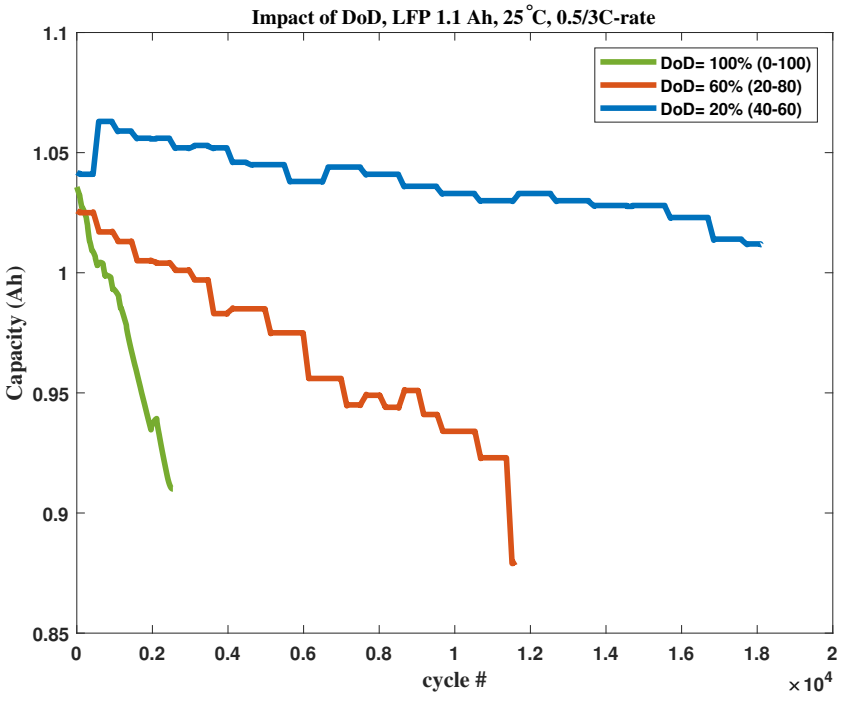

Figure 2.14: Impact of DoD on the capacity loss of battery cells.

shorter lifecycle. DoD is another critical factor considered in this analysis. Deep discharge can lead to more severe degradation, impacting the overall performance and lifespan of the battery. By incorporating these factors into the degradation model (explained in detail in Chapter 3), this dissertation predicts the degradation path of batteries more accurately and assesses the impact of different factors on their performance.

Chapter 3

Analytical and Data-Driven Degradation Models

Nomenclature

Ah	Ampere-hour
K	Number of time instants
Q_{loss}	Percentage of battery capacity loss,
s	Power source index
T	Transition matrix
d_s^e	Estimated degradation signal of power source s
d_s^a	Actual degradation signal of power source s
σ_s	Error of degradation estimation
λ	Degradation rate
$\mathbb{P}_s$	Maximum expected capacity of component s
Δ_s	Loss of capacity
ρ_s	Cost per unit of component s
δ_{train}	Training dataset
δ_{test}	Testing dataset
$\delta_{validation}$	Validating dataset

3.1 Literature Review in Degradation Modeling

Battery safety and reliability are crucial for the operation of EVs. The fundamental restriction of Li-ion-based EV batteries is aging since the battery goes through a complicated degradation process throughout the operation of the vehicle. The degradation occurs over time, resulting in a lower driving

range due to reduced capacity. The operating conditions or factors giving rise to degradation are explained in detail in Chapter 2. Battery states, battery aging, driving behavior, and environmental conditions are all possible, relevant elements influencing EV usage and energy consumption. The expensive ESS, which accounts for a large portion of the entire cost of an EV, and the restrictive driving environment, which limits the performance and acceptance of EVs, are two concerns in the battery application. As a result, minimizing the degradation through precise modeling, extending battery life, and optimizing battery capacity are the primary objectives for maximizing EV lifetime value. One of the most challenging tasks in modeling the degradation trend of an EV battery is identifying the factors that contribute to it. The major factors leading to degradation are already explained, and these factors have a different impact on the battery, making it challenging to establish a degradation model through existing methods. The diversity and number of research literature on battery degradation give useful information that analyzes EV battery aging mechanisms, impacts, and features. Several researchers studied the approaches used to simulate the degradation mechanisms in EV batteries based on the explored factors.

In every system, components degrade over time, some degrading faster than others based on their robustness and application. In HEV, there are several components whose life cycle count decreases once the vehicle is in operation. However, this study is focused on the degradation of the power-generating sources present in the HEVs. While ICE can also degrade, batteries are particularly prone to it. This study focuses on battery degradation since HEVs with high hybridization factors (HF) are used nowadays. This means batteries with higher capacity are used and can cost up to 30% of the price of the entire vehicle as mentioned previously.

In automotive applications, the battery's lifecycle is shorter compared to other components, and it is considered unreliable to operate after it reaches 80% of its initial capacity. The initial cost of a battery is high, so it is necessary to have a longer life for the operation of the vehicle to be economically viable. A battery's lifetime depends on its operation and degradation rate, which is a complex mechanism. Battery degradation is a significant limiting factor in battery lifetime; thus, it is essential to investigate this mechanism thoroughly and reduce it to extend the battery's lifetime.

Several factors stimulate battery degradation, and predicting the degradation path of a battery is a demanding task due to the complex nature of the process. However, it is crucial to determine the degradation path to ensure reliable operation and timely maintenance. Identifying the factors that accelerate the aging process can help to minimize the degradation process. The most common factors that affect battery capacity and give rise to degradation are temperature, discharging current, charging current, and DoD [15]. These parameters have impacts depending on the mode of operation of the battery or vehicle. When the battery or vehicle is in operation, all these factors have different effects on the battery and result in degradation.

The battery in EVs is subjected to various stresses due to these extreme factors.

The battery's health in EVs must be closely monitored and predicted in real time for reliable operation and timely maintenance of the vehicle [154]. In recent years, there has been significant improvement in estimating the life of a battery using different degradation models. They can be classified into different categories where the literature [155, 156, 157] groups the methods into three main categories

1. Model-based approach,
2. Data-driven approach, and
3. Hybrid approach.

The model-based approaches are based on physics-based modeling of degradation behavior, in which an empirical model is built to represent the system's diminishing path based on the real diffusion phenomenon. This model demonstrates the degrading behavior of a battery using a combination of algebraic and differential equations or an empirical equation. Since the deterioration of the battery is nonlinear, predicting long-term performance can be rugged [158]. The main drawback of this model is its lack of flexibility and parametrization difficulty. It can easily lead to poor model design due to a lack of prior understanding of the system. To construct a robust model, the designer must have a proper understanding of the numerous aspects of the system, including mechanical, electrical, electronic, chemical, and other physical characteristics.

Data-driven approaches (commonly known as black-box models) are based on empirical observations with little or no understanding of the underlying processes. This method depends heavily on evaluating data from the process; therefore, designers do not need to gain a thorough, domain-specific grasp of the background process to use it. The data-driven method uses statistical theories or machine learning techniques to derive a model from measured data [159]. This method creates a mathematical model from data gathered in the lab through large-scale testing under various aging circumstances, rather than utilizing a specific physical-based model, and forecasts the battery's deterioration trajectory. It has lately become the most popular method since it is more adaptable and practical and removes the need for sophisticated physics-based models. These models are self-adaptive, model-free, and have the ability to learn from previous data on their own. Data-driven approaches include techniques such as artificial intelligence, statistical analysis, Wiener process, and signal processing [59].

The data-driven approaches rely heavily on data; therefore, the model's accuracy and effectiveness are mainly determined by the data quality. Unbalanced data, for example, might lead to decision-making bias (also known as overfitting and underfitting) in a model. In essence, if a large amount of relevant data is readily accessible, a data-driven strategy would be beneficial. However, in the absence of this data, the application of a data-driven strategy would be limited. Recently the concept of featured-based data-driven

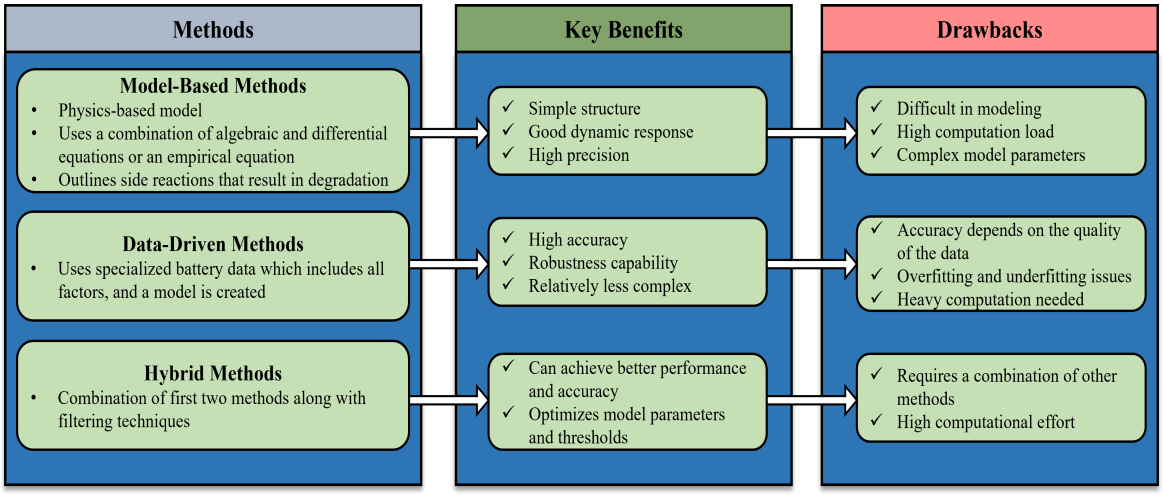

Figure 3.1: Methods for modeling battery degradation.

models has been widespread. In this technique, certain features are retrieved from the voltage and current during the preprocessing stage using knowledge about the behavior of the cell's physical properties. Then, these attributes are used as a input to the algorithm used in the process. This method has the advantage of producing less complex inputs by preprocessing the raw data that is supplied for the input. Studies [160, 161, 162] have used this concept of feature-based data-driven models to predict the RUL of the battery. Also, the study [163] explains the concept of generating synthetic data that are equivalent to the actual battery data for the data-driven approach. The generated datasets were compared to the battery's actual behavior, which yielded identical results. These large synthetic datasets can be used to train algorithms for data-driven approaches and diagnoses. As a result, these datasets can help evaluate various algorithms and enhance these techniques.

Similarly, the hybrid method incorporates the strengths of both model-based and data-driven models. This method is useful when there is limited or biased data, as the data-driven method can lead to imprecise forecasts or wholly misleading outcomes. In battery life estimation, hybrid techniques that combine model-based and data-driven methods to produce accurate forecasts have become a hotspot of study. The main advantage of this method is that it can extrapolate beyond the training data more precisely than the data-driven method. The use of this approach in studies [164, 165, 166] demonstrated promising results. The only issue to adopt this approach is lack of openly available field data, which should be validated with the results obtained from lab data [167]. All these three methods are summarized in Figure 3.1.

As discussed in Section 2.2, various factors give rise to the degradation of the battery. Each factor has a different impact on the aging mechanism. The cycle life experiment conducted under one operating

condition for a battery may not be valid for other operating conditions, making it difficult to predict the RUL of the battery. To conduct experiments at continuously varying operating conditions would cost years of testing, causing such experiments to become infeasible. The development of precise battery performance and life prediction models would be hampered by the absence of comprehensive experimental data. However, despite the lack of degradation data, several types of studies have been conducted on accurately forecasting the cycle life of a battery. A dynamic battery degradation capacity model based on a semi-empirical equation has been used in several studies like [71, 168, 169, 170]. In this model, the effect of four parameters are considered, which are time, temperature, DOD, and discharge current rate. This semi-empirical model is based on the original formula of the Arrhenius degradation model shown in (3.1). Here, Q_{loss} is the percentage of battery capacity loss, A is the pre-exponential factor, Ea is the activation energy, 78.06 (J), R is the gas constant, 8.314 J/mol/K, T_{bat} is the absolute temperature of battery(K), Ah is the Ah-throughput, z is the time factor, C_{Rate} is the battery discharge rate, B is the compensation factor of C_{Rate}

$$Q_{loss} = Ae^{-\left(\frac{E_a+B.C_{RATE}}{RT_{bat}}\right)}(A_h)^z \tag{3.1}$$

According to the cumulative damage theory, the capacity fade model of the battery illustrated by the aforementioned equation can be utilized to predict battery degradation [171]. The dynamic degradation model's discrete formula is given by (3.2) as done in [172].

$$Q_{loss,p+1} - Q_{loss,p} = \Delta A_h z A^{\left(\frac{1}{z}\right)} e^{\left(-\frac{E_a+B*C_{RATE}}{RT_{bat}}\right)} (Q_{loss,p})^{\frac{z-1}{z}} \tag{3.2}$$

Here, $Q_{loss,p}$ and $Q_{loss,p+1}$ are the accumulated battery capacity loss at instantaneous time t_p and t_{p+1}, and ΔA_h is the Ah-throughput from t_p and t_{p+1}, which can be found by using (3.3)

$$\Delta A_h = \frac{1}{3600}\int_{t_p}^{t_p+1} |I_{bat}|\, dt \tag{3.3}$$

The modeling technique described above focuses solely on temperature and discharging current as factors influencing battery capacity loss. However, it is important to acknowledge that these factors are not the sole contributors to capacity loss in batteries used in EVs, as discussed in Chapter 2 and study [15]. Other significant factors, namely charging current and DoD, as highlighted in [15], should also be incorporated into the modeling technique to enhance prediction accuracy.

Therefore, this dissertation employs analytical and data-driven approaches. The analytical method employs a Markov-chain-based model, while the data-driven method utilizes three prediction techniques with NNs to model the degradation path and predict battery capacity loss. This is achieved by implementing the following models:

- Markov Chain Model
- Neural Network Models
  - Feedforward Neural Network (FNN)
  - Recurrent Neural Network (RNN)
  - Deep Neural Network (DNN)

In data-driven approaches, such as the ones mentioned above, training data is essential for developing a predictive model that can accurately estimate future battery degradation. However, predicting battery degradation in EVs poses a significant challenge due to the scarcity of available battery data. While institutions like NASA Ames, the University of Maryland, Stanford University, and the Hawaii Natural Energy Institute provide lab conducted battery data, access to real-world battery data used in EVs is limited. This restricted access to actual EV battery data has been a persistent issue for researchers.

To address this limitation, the data utilized in this dissertation were obtained from two distinct laboratories. By employing datasets from different laboratory settings, the aim was to validate the effectiveness of the proposed methodology irrespective of whether the data originated from a controlled lab environment or actual EVs. This approach ensures that the proposed method remains robust and applicable in various scenarios, providing insights into battery degradation prediction that can be beneficial across different contexts.

3.2 Battery Datasets

This dissertation utilizes two distinct battery datasets obtained from different laboratories, namely

- Sandia National Laboratory (SNL)
- University of Wisconsin-Madison

The Sandia National Laboratory conducted extensive testing on three chemistries of 18650 form cells: LFP from A123 Systems (APR18650M1A, 1.1 Ah), NCA from Panasonic (NCR18650B, 3.2 Ah), and NMC from LG Chem (18650HG2, 3 Ah) [173]. This dataset contains a total of 86 cells, comprising 30 LFP cells, 24 NCA cells, and 32 NMC cells. The resulting dataset from this research is publicly accessible on the battery archive website [174]. For the purpose of this dissertation, 30 LFP cells of 1.1 Ah from this laboratory are utilized for training the Markov chain model, which is elaborated on in detail in Section 3.3.

During the testing phase, the cells underwent cycling at various temperatures ($15^{\circ}C$, $25^{\circ}C$, and $35^{\circ}C$) with different depths of discharge (DoDs) ranging from 0% to 100%, 20% to 80%, and 40% to 60%, respectively. Various discharge currents (0.5C, 1C, 2C, and 3C) were also applied. For each combination of

temperature, DoD, and discharge current (12 groups), at least two cells from each chemistry were cycled. All cells were charged at a fixed rate of 0.5C. The cycling process continued until the cells reached their end-of-life (80% state of health). The dataset encompasses in-cycle measurements of current, voltage, temperature, capacity (Ah), and energy (Wh). Additionally, it provides per-cycle measurements of the charged and discharged capacity within the designated DoD range, along with other relevant summary statistics.

Similarly, the University of Wisconsin-Madison's battery research group released a battery testing dataset encompassing four commonly used driving cycles: US06, HWFET, UDDS, and LA92. This dataset is available on the Mendeley data website [175]. It consists of data collected from different 2.9 Ah NCA Panasonic 18650PF cells. The cell underwent cycling based on the aforementioned driving cycles, along with additional cycles labeled as Cycle 1, Cycle 2, Cycle 3, Cycle 4, and NN. These nine cycles systematically covered a range of temperatures ($25^{\circ}C$, $10^{\circ}C$, $0^{\circ}C$, $-10^{\circ}C$, and $-20^{\circ}C$, in that order). The accompanying "ReadMe" file provided with the dataset provides a comprehensive description of the experimental procedures. The dataset includes characterization data obtained from Hybrid Power Pulse Characterization (HPPC) and electrochemical impedance spectroscopy (EIS) tests. Additionally, it contains in-cycle measurements captured during the driving cycles, including voltage, current, capacity, energy, and temperature. The data is available in both '.mat' and '.csv' file formats, and it follows a well-structured organization based on temperature, test type, and drive cycle.

This dataset is utilized to train the NNs mentioned earlier in this dissertation. The voltage, current, capacity, and temperature data are used as inputs to the NNs, while the capacity serves as the output from the NNs.

3.3 Markov Chain based Degradation Model

The binary model is widely used to represent a system as either a working or failing state because of its simplicity and computational efficiency. However, the multistate model is often used instead of a binary model to provide a more accurate representation of the system. This increases the granularity of the binary model. A model with four states is chosen as a compromise between precision and complexity because increasing the number of states can lead to a more complex and computationally demanding model.

In various studies, components have been represented using a multi-state model with four states to represent the system accurately. For instance, a component has been represented using four states as perfect, useful, pseudo-fault, and fault in [176]. Similarly, transformers have been described using four states, namely good, fair, poor, and very poor, in study [177]. In [178], drivetrain components of wind turbines have been represented by normal working, degraded, critical, and functional failure states. Moreover, in [48], different power-generating sources in microgrids have been defined as four states denoted by the number 1,2,3,4. In

line with these studies, this dissertation also follows a multistate model where four states are defined based on a component's degradation signal $d_s^e(t_k)$. Where, $d_s^e(t_k)$ represents the degradation signal of source s at time t_k which is the sum of actual degradation $d_s^a(t_k)$ and the error of the estimation $\sigma_s(t_k)$ represented as follow:

$$d_s^e(t_k) = d_s^a(t_k) + \sigma_s(t_k) \tag{3.4}$$

The assumptions for the degradation are formally stated as follows:

Assumption

1. There is no improvement in the degradation of a component between two consecutive maintenance or repair times.
2. The maximum of the actual degradation $d_s^a(t_k)$ is 1.
3. Between two consecutive maintenance or repair times, the actual degradation $d_s^a(t_k)$ exhibits a monotonically decreasing behavior.

The degradation signals in study [48] were converted into 4 states by dividing the range of signals into intervals and assigning each interval a specific state. Similar approach is followed in this dissertation and adopts 4 states, namely perfect, good, degraded, and unreliable, each represented by a maximum capacity. The conversion of degradation signals into states is defined in the following points. Additionally, for batteries used in automotive applications, they are typically used from 100% to 80%. Therefore, this dissertation specifically defines four states based on the remaining capacity of the battery ($\rho_x = Q_{rem}$), as follows:

- State 1 (Perfect): In this state, the hard constraint for this state is $d_s^a(t_k) \geq \rho_1$. For the battery, $\rho_1 = 90\%$.
- State 2 (Good): In this state, the hard constraint for this state is $\rho_1 \geq d_s^a(t_k) \geq \rho_2$. For the battery, $\rho_1 = 90\%$ and $\rho_2 = 85\%$.
- State 3 (Degraded): In this state, the hard constraint for this state is $\rho_2 \geq d_s^a(t_k) \geq \rho_3$. For the battery, $\rho_2 = 85\%$ and $\rho_3 = 80\%$.
- State 4 (Unreliable): In this state, the hard constraint for this state is $\rho_3 \geq d_s^a(t_k)$. For the battery, $\rho_3 = 80\%$. When the battery reaches this state, the operation of battery in EV application is considered unreliable and needs to be replaced.

Based on the above observations, a degradation model that is dependent on load is utilized. The model is designed using a Markov chain and comprises four states to predict the degradation process of a

component. Markov chain is a valuable algorithm for anticipating future outcomes. One merit of leveraging these tools lies in their simplistic design, making them easily understandable to multiple user levels, even those with no background in statistical methods. Apart from their approachability feature, these models boast flexibility regarding modeling various nuances. They can integrate diverse inputs such as historical data, which enhance precision towards future predictions significantly. Markov chain models also possess commendable computational efficiency, acting as a considerable strength concerning substantial data systems management requirements- particularly in real-time applications calling for rapid and precise prognoses. Consequently, this technique's wide-ranging adaptability, teamed with speed and ease of use, secure its applicability across multiple applications [179].

Modeling the degradation process of a component can be a challenging task due to the influence of future operating conditions in addition to the current state of the component. To address this issue, this study utilizes a degradation model based on Markov chain theory. The Markov chain model takes into account the future operating conditions, allowing for a more accurate representation of the degradation process of the component.

Let $x_{s,i}$ denote the probability that the component s is at state $i, i \in \{1, 2, 3, 4\}$, where x_s is the vector of all $x_{s,i}, i.e., x_s = [x_{s,1}, x_{s,2}, x_{s,3}, x_{s,4}]$. Therefore, for the Markov model depicted in Figure 3.2, the transition from state x_s at time t_k to x_s at time t_{k+1} is mathematically represented by the following formula:

$$\mathbf{x_s}(t_{k+1}) = \mathbf{x_s}(t_k)\mathbf{T} \tag{3.5}$$

where $\mathbf{T}$ is the transition matrix

$$\mathbf{T} = \begin{bmatrix} \pi_{11} & \pi_{12} & \pi_{13} & \pi_{14} \\ \pi_{21} & \pi_{22} & \pi_{23} & \pi_{24} \\ \pi_{31} & \pi_{32} & \pi_{33} & \pi_{34} \\ \pi_{41} & \pi_{42} & \pi_{43} & \pi_{44} \end{bmatrix} \tag{3.6}$$

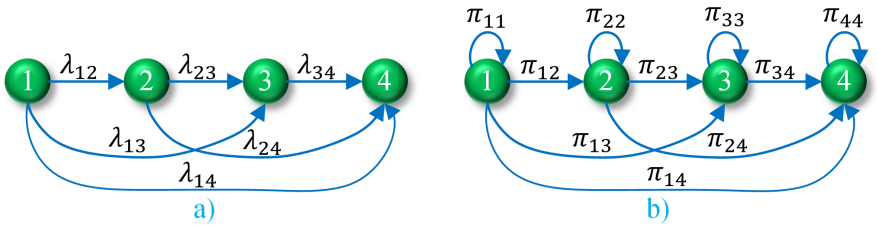

Figure 3.2: Markov's chain degradation prediction model.

The transition matrix in the above model is now derived. It is typically assumed that the sojourn

time in a state is the exponential distribution [180]. Denote λ_{ij} as the degradation rate from state i to state j, with $i \neq j$. The following equation can be obtained by looking at the inflow and outflow of state i in Figure 3.2 (a):

$$\frac{dx_i(t)}{dt} = -x_i(t) \sum_{j=i+1}^{4} \lambda_{ij} + \sum_{j=1}^{i-1} x_j(t)\lambda_{ji} \tag{3.7}$$

In (3.7), the term $x_i(t) \sum_{j=i+1}^{4} \lambda_{ij}$ denotes the intensity of transitioning from state i to the other states. Similarly, the term $\sum_{j=1}^{i-1} x_j(t)\lambda_{ji}$ denotes the intensity of transitioning to state i from the other states. Solving (3.7) and discretizing the solutions with sampling time Δt, following equations can be obtained [181]

$$\pi_{11} = e^{-(\lambda_{14}+\lambda_{13}+\lambda_{12})\Delta t} \tag{3.8a}$$

$$\pi_{12} = \frac{\lambda_{12}}{\lambda_{14}+\lambda_{13}+\lambda_{12}}(1 - e^{-(\lambda_{14}+\lambda_{13}+\lambda_{12})\Delta t}) \tag{3.8b}$$

$$\pi_{13} = \frac{\lambda_{13}}{\lambda_{14}+\lambda_{13}+\lambda_{12}}(1 - e^{-(\lambda_{14}+\lambda_{13}+\lambda_{1,2})\Delta t}) \tag{3.8c}$$

$$\pi_{14} = \frac{\lambda_{1,4}}{\lambda_{1,4}+\lambda_{13}+\lambda_{12}}(1 - e^{-(\lambda_{14}+\lambda_{13}+\lambda_{12})\Delta t}) \tag{3.8d}$$

$$\pi_{21} = 0 \tag{3.8e}$$

$$\pi_{22} = e^{-(\lambda_{23}+\lambda_{24})\Delta t} \tag{3.8f}$$

$$\pi_{23} = \frac{\lambda_{23}}{\lambda_{23}+\lambda_{24}}(1 - e^{-(\lambda_{23}+\lambda_{24})\Delta t}) \tag{3.8g}$$

$$\pi_{24} = \frac{\lambda_{24}}{\lambda_{23}+\lambda_{24}}(1 - e^{-(\lambda_{23}+\lambda_{24})\Delta t}) \tag{3.8h}$$

$$\pi_{31} = 0 \tag{3.8i}$$

$$\pi_{32} = 0 \tag{3.8j}$$

$$\pi_{33} = e^{-\lambda_{34}\Delta t} \tag{3.8k}$$

$$\pi_{34} = 1 - e^{-\lambda_{34}\Delta t} \tag{3.8l}$$

$$\pi_{41} = 0 \tag{3.8m}$$

$$\pi_{42} = 0 \tag{3.8n}$$

$$\pi_{43} = 0 \tag{3.8o}$$

$$\pi_{44} = 1 \tag{3.8p}$$

This study assumes that a component's degradation rate remains constant when the load is at or below P^{norm}. However, the degradation rate increases exponentially once the load surpasses P^{norm}. This

assumption is based on the fact that the operating temperature of the component starts to rise exponentially as the load increases from this point, resulting in an exponential increase in the degradation rate [48, 182, 183]. It should be noted that the control system includes an EM and thus limits P to be less than its maximum capacity $\overline{P}$, which is one of the optimization constraints. $\underline{\lambda_{ij}}$ represents the degradation rate when the component operates in the range of $P < P_{norm}$, while $\overline{\lambda_{ij}}$ represents the degradation rate when the component operates at the maximum capacity $\overline{P}$. The degradation rate when the component operates between P_{norm} and $\overline{P}$ is calculated as follows.

$$\lambda_{ij} = \eta e^{\zeta P} \tag{3.9}$$

where,

$$\zeta = \frac{\ln(\underline{\lambda_{ij}}/\overline{\lambda_{ij}})}{P^{norm} - \overline{P}} \tag{3.10a}$$

$$\eta = \frac{\underline{\lambda_{ij}}}{e^{\zeta P^{norm}}}. \tag{3.10b}$$

3.4 Neural Network based Degradation Model

Artificial neural networks (ANNs) have become a popular tool for modeling complex systems and making predictions based on data. This algorithm is designed to mathematically mimic the neural activity of the brain through a network of interconnected neurons. The NN's internal structure consists of a large number of these neurons, as shown by circles in Figure 3.3, which shows a simplified NN.

NNs are created to learn from data and then make predictions based on that learning. Neurons are the center of a NN, the fundamental computing units that process input data and generate output. Weighted connections link neurons to one another, creating a network of interconnected nodes. Each neuron in the network gets information from one or more other neurons, processes that information, and then transmits the outcome to one or more other neurons [184, 185].

To predict the degradation paths of the component, a degradation model based on NN is constructed. The degradation of the component is impacted by its working conditions. For example, the degradation path of the battery is impacted by the working temperature, charging and discharging cycles, and depth of discharge [15]. In the previous Section 3.3, Markov chain-based model is used to predict the degradation path. However, there are several drawbacks of Markov Chain models, which are highlighted by the following points:

- **Assumption of independence**: Markov chain models assume that the future state is only deter-

mined by the present state and ignores other factors. This can be a limitation in cases where there are other factors that influence the future state, such as external events or changes in the environment.

- **Static data-generating system**: Markov chain models assume that the data-generating system is static, meaning that the relationships between the variables do not change over time. This can be a limitation in cases where the relationships between the variables are dynamic and change over time which can make the predictions less reliable.
- **Overfitting**: Markov chain models have a tendency to overfit data, meaning that they learn the patterns in the training data too well and are not able to generalize to new data. This can lead to incorrect predictions when the model is used to make predictions on new data.
- **Difficulty modeling complex relationships**: Markov chain models have difficulty modeling complex non-linear relationships. This can be a limitation in cases where the relationships between the variables are complex and non-linear.
- **Computational complexity**: The need to compute the transition matrix can slow down the computational process. This can be a limitation in cases where the model is being used to make real-time predictions.

In addition to these limitations, Markov chain models can also be sensitive to the choice of parameters and the quality of the data. As a result, it is important to consider Markov chain models' limitations before using them for future prediction.

There has been a significant enhancement in model-free/data-driven algorithms, like NNs in recent years. These algorithms offer a range of benefits, including their ability to model complex non-linear relationships between inputs and outputs, resulting in their suitability for a variety of applications. Furthermore, they have the capability to generalize from training data to new, unseen data, making them practical for real-world scenarios. Additionally, NNs can automatically extract relevant features from input data, reducing the requirement for manual feature engineering. They are also well-suited for big data applications, as they can handle large amounts of data. Finally, they are able to learn from unstructured data, such as images, audio, and text, broadening the range of problems they can be used to solve [186]. Hence, in this section, instead of Markov's chain model, a more advanced learning algorithm, i.e., a NN (data-driven method), is used to predict the degradation path of the battery.

3.4.1 Feedforward Neural Network (FNN)

This section uses a three-layer feedforward NN architecture consisting of an input layer, a hidden layer, and an output layer to predict battery capacity loss, as shown in Figure 3.3. Before feeding the data to

the model, they are pre-processed, and the necessary features, voltage, current, temperature, and capacity, are extracted. The NN's input layer accepts three inputs, namely current, voltage, and temperature, while the output layer predicts the capacity of the battery. The number of hidden layers is one, and the number of neurons is 32. The reason for choosing 32 hidden neurons is to compare the results with LSTM and DNN networks where they also use 32 number of neurons in hidden layers. The following sets of data denote the separation of data into training, testing, and validating data

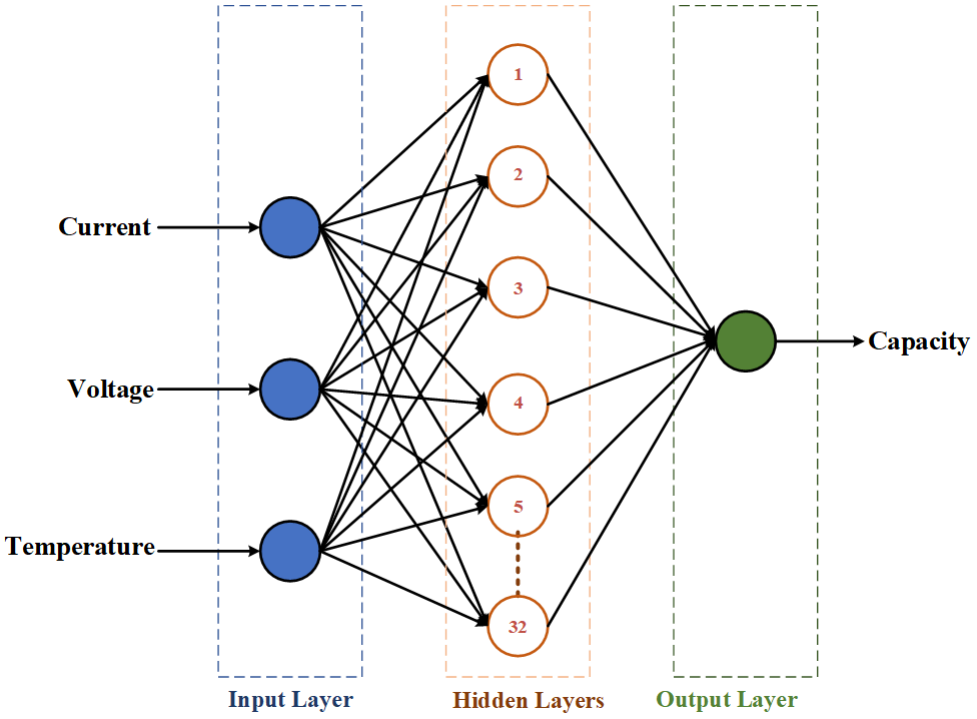

Figure 3.3: A simple neural network with three inputs and one output .

$$\delta_{train} = [(x_1, Y_1), (x_2, Y_2), (x_3, Y_3).....(x_n, Y_n)] \tag{3.11}$$

$$\delta_{test} = [(x_{n+1}, Y_{n+1}), (x_{n+2}, Y_{n+2}), (x_{n+3}, Y_{n+3}).....(x_s, Y_s)] \tag{3.12}$$

$$\delta_{validation} = [(x_{s+1}, Y_{s+1}), (x_{s+2}, Y_{s+2}), (x_{s+3}, Y_{s+3}).....(x_t, Y_t)] \tag{3.13}$$

where, x and Y represent the data extracted from the raw data. x is the input to the NN and has three variables voltage, current, and temperature as $x_i = (V_i, i_i, T_i)$. Similarly, Y is the output from the network, which represents the capacity of the battery. The δ_{train} is used to train the NN, whereas δ_{test} and $\delta_{validation}$ are used to test and validate the model developed using train data sets.

3.4.2 Recurrent Neural Network (RNN)

A recurrent layer consists of specific neurons that have recurrent connections, allowing them to retain information from previous time steps, usually just one. This type of computational cell is highly advantageous when there is a need to capture the temporal dynamics of a sequence of inputs [187]. In many cases, the output value is influenced by the historical context of the corresponding inputs. However, models like MLPs, as discussed earlier, are stateless, meaning their output is solely determined by the current input. To address this limitation, recurrent Neural Networks (RNNs) offer an internal memory mechanism that can capture both short-term and long-term dependencies, enabling them to retain and utilize information from previous time steps [188].

LSTM, which stands for Long Short-Term Memory, is a specific type of RNN that addresses the challenges posed by the vanishing gradient problem and the need to capture long-term dependencies in sequential data. LSTM has demonstrated its effectiveness in various applications, such as time series prediction, speech recognition, and natural language processing [189]The key aspect that sets LSTM apart is its utilization of memory cells, which enable the network to retain information across long sequences. These memory cells are updated at each time step, allowing them to store and preserve information from previous time steps. By incorporating this memory mechanism, LSTM can learn and capture long-term dependencies that would otherwise be challenging for traditional RNNs.

The LSTM architecture includes various components that regulate the flow of information. The input gate controls the intake of new information into the memory cell, while the forget gate decides which parts of the previous memory cell state should be discarded. The memory cell stores information from previous time steps and is updated based on the input and forget gates. The output gate determines the final output of the LSTM cell by combining the current input, previous hidden state, and updated memory cell state. These components work together to manage the flow and storage of information within the LSTM model.

The detailed explanation and derivation of the equation for each gate and cell are obtained from [190]. The LSTM NN model is constructed and trained using the PyTorch library with a specific configuration in Python and deployed in Raspberry Pi 4 Model B, which is shown in Figure 3.4. The first layer added to the model is an LSTM layer. LSTM is a type of RNN layer that is designed to handle sequential data and capture long-term dependencies. In this case, the LSTM layer has 32 units (or nodes), and the input shape is specified as (1, 3), indicating that the input data has a sequence length of 1 and three features, which are current, voltage, and temperature, respectively. The next layer added is a dense layer with a single unit. This layer is a fully connected layer, which means that each neuron in this layer is connected to every neuron in the previous layer. The dense layer is commonly used for the final output layer in regression tasks.

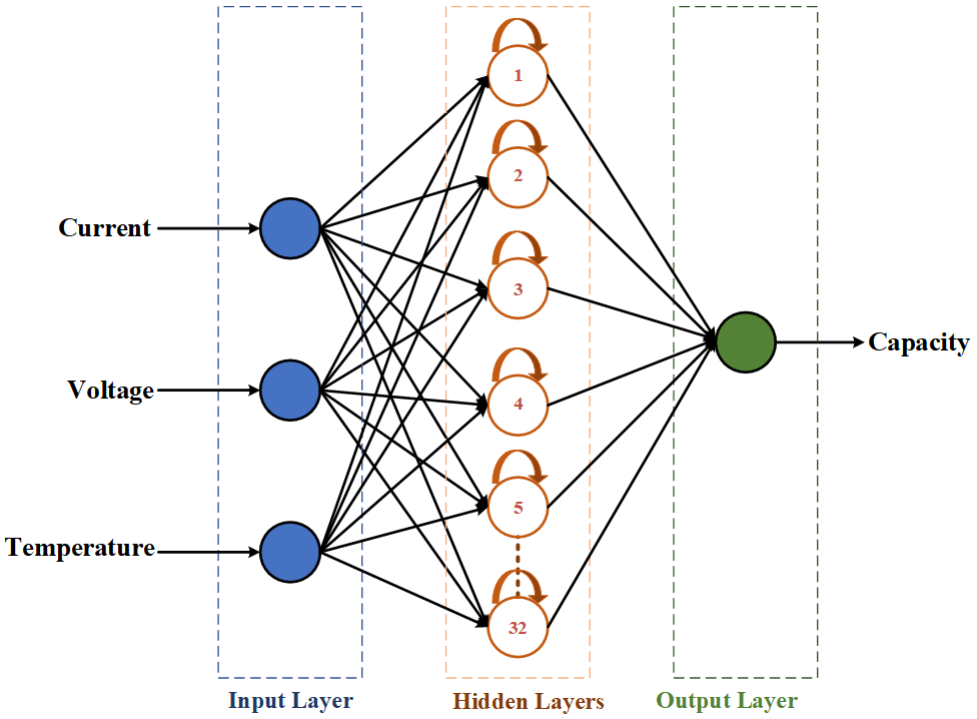

Figure 3.4: Neural network considered for LSTM.

Here, the goal is to predict the capacity loss of the battery. The model is compiled using the mean squared error (MSE) as the loss function and the Adam optimizer. The MSE loss function measures the average squared difference between predicted and true output values. During training, the model uses the Adam optimizer, which is a popular optimization algorithm known for its effectiveness in updating the model's parameters based on the calculated gradients. The Adam optimizer adjusts the parameters of the LSTM model to minimize the defined loss function. The forward function, which is responsible for executing the forward pass of the model, is used in the code. It takes the input data, passes it through the LSTM layer to obtain the hidden state, and then applies the fully connected layer to generate the model output.

The model is trained and developed using the PyTorch library, which takes the training data and corresponding target values as defined in (3.11). The training is performed for 100 epochs, where the entire training dataset is passed through the network 100 times. During training, the model adjusts its internal parameters to minimize the defined loss function and improve its predictive performance.

3.4.3 Deep Neural Network (DNN)

Deep Neural Networks (DNNs) are a type of ANN that have multiple hidden layers between the input and output layers. The number of hidden layers is what makes a DNN "deep." The more hidden layers

a DNN has, the more complex patterns and representations it can learn from data. DNNs have gained significant popularity in recent years and have been deployed successfully in various domains, including computer vision, natural language processing, speech recognition, and many other machine-learning tasks. The reasons why DNNs have been so successful are that they can learn complex patterns and representations from data, they can be trained on large amounts of data, and also they are able to generalize to new data [191].

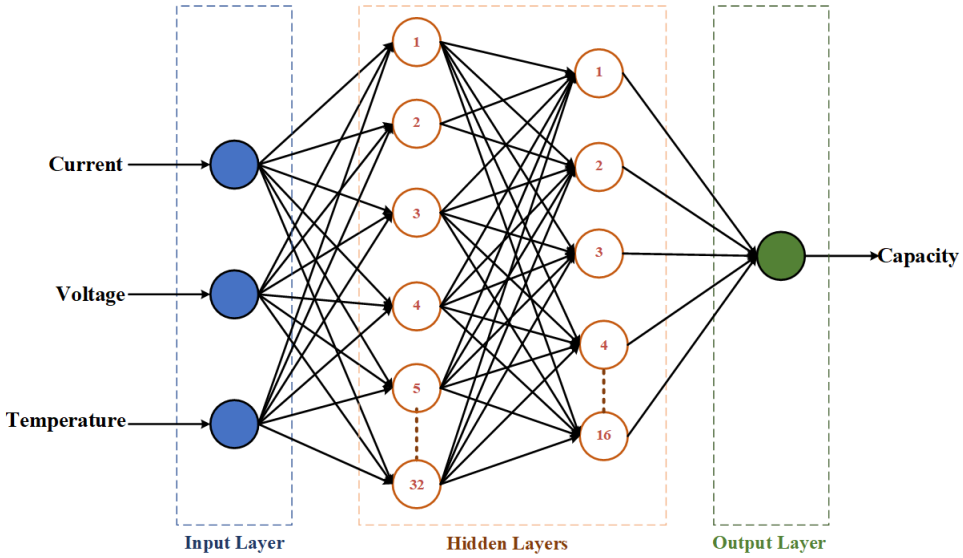

Figure 3.5: Neural Network model considered for DNN.

In this dissertation, a DNN for the degradation prediction is created using Python and run in a Raspberry Pi 4 Model B. The network diagram is shown in Figure 3.5. The Sequential function is utilized to create a sequential model, ensuring that layers are sequentially stacked. The model's first dense layer consists of 32 neurons. The input data contains three features, namely voltage, current, and temperature, as mentioned earlier for the two cases. The activation function applied in this layer is the sigmoid function, introducing non-linearity and enhancing the model's capacity to learn complex relationships within the data. A second dense layer with 16 neurons is used model. The Rectified Linear Unit (ReLU) activation function is employed in this layer. ReLU is commonly used in hidden layers as it enables the model to learn intricate non-linear relationships, contributing to enhanced predictive performance. Finally, the output comprises a single neuron, as the regression task aims to predict the capacity loss of the battery. No activation function is specified for the output layer, ensuring that it produces raw output values, directly representing the predicted continuous output.

The MSE is chosen as the loss function, which measures the average squared difference between the predicted output from the model and the actual output values obtained from the lab. The Adam optimizer

is employed, which adapts the learning rate during training to update the model's weights more efficiently, as explained earlier so that it would be easy to compare the prediction results among these three techniques.

The model for DNN is trained and created using the training dataset and corresponding target values as given by (3.11). The training process iterates over the entire dataset 100 times. During training, the model's parameters, including weights and biases, are adjusted using backpropagation and gradient descent. The goal is to minimize the defined loss function (i.e., MSE), thereby improving the model's ability to predict continuous outputs accurately.

There are different numerical algorithms that can be employed to optimize θ , including Levenberg-Marquardt (LM), Adaptive Moment Estimation (Adam), Adagrad, Broyden-Fletcher-Goldfarb-Shanno (BFGS) and Stochastic Gradient Descent (SGD) [186]. Here, Adam optimizer algorithm is used in all of these three networks mentioned above. Adam is an optimization algorithm that builds upon stochastic gradient descent (SGD) to efficiently handle non-convex problems. It offers faster convergence and requires fewer computational resources than other optimization methods. Particularly, Adam excels in scenarios with large datasets, as it maintains more accurate gradients over multiple iterations of learning. By integrating the benefits of two other stochastic gradient techniques, namely Adaptive Gradients and Root Mean Square Propagation, Adam presents a novel learning approach that effectively optimizes various types of NNs.

Now, the main objective is to minimize the estimation error $J(\theta)$ and the difference between the actual capacity and the estimated capacity from the NN denoted by $f(x_i, \theta)$

$$J(\theta) = \frac{1}{2}\sum_{i=1}^{n}(f(x_i, \theta) - Y_i)^2 \tag{3.14}$$

Now, Adam algorithm is used for efficient stochastic optimization, which uses following equations to update the parameter θ.

$$m_t = \beta_1 * m_{t-1} + (1 - \beta_1) * g_t \tag{3.15a}$$

$$\theta_t := \theta_{t-1} - \alpha.m_t \tag{3.15b}$$

$$v_t = \beta_2 * v_{t-1} + (1 - beta_2) * g_t^2 \tag{3.15c}$$

$$\hat{m_t} = \frac{m_t}{(1 - \beta_1^t)} \tag{3.15d}$$

$$\hat{v_t} = \frac{v_t}{(1 - \beta_2^t)} \tag{3.15e}$$

$$\theta_t = \theta_{t-1} - \alpha * \frac{\hat{m_t}}{\sqrt{(\hat{v_t} + \epsilon)}} \tag{3.15f}$$

where, g_t is the gradient obtained by the derivation of the objective function. m_t is the moving

average of the gradients which is used to update the parameter θ. v_t is the moving average of the squared gradients $\hat{m}_t$ is the bias-corrected moving average of the gradients, $\hat{v}_t$ is the bias-corrected moving average of the squared gradients, w_t is the weight at iteration t, α is the learning rate, and ϵ is a small constant to prevent division by zero. The term β (β_1 and β_2) are the decay rate of the average of the gradients, which controls the moving average and its value is between [0,1) [192]. The main objective here is not to develop new learning algorithms for the NN, but rather to utilize existing algorithms to determine the capacity loss. To achieve this, accurate data is collected to serve as the input and output of the network. The details about the NNs and optimizer are taken from [192, 193], which can be referred to for further details.

Chapter 4

Prognostic-based Control Framework for Degradation Abatement in HEV

Nomenclature

CHIL	Controller-Hardware-In-the-Loop
DF	Degradation forecasting
EM	Energy management
PBCF	Prognostic-based control framework
c^F	Cost of fuel
$f_s(P_s)$	Objective function based on fuel cost for EM
$f_s^d(P_s)$	Degradation cost sent by DF layer

This chapter introduces a framework for degradation forecasting and abatement. The primary focus of this section is to provide a detailed discussion of the proposed strategy and highlight its key objectives, which revolve around minimizing the total degradation cost. The HEV model considered in this dissertation is explained first to establish a foundation for the framework. Then, a critical analysis of the drawbacks and limitations of the traditional control strategy is done. By highlighting these shortcomings, an improved strategy is proposed to address the challenges effectively. A detailed explanation is provided for the proposed strategy, which uses two distinct methods for predicting degradation.

4.1 Electrical Model of Hybrid Electric Vehicle

Hybrid electric vehicles (HEVs) are becoming increasingly popular as they offer a more sustainable solution to transportation. HEVs use multiple energy sources to provide propulsion power, with at least one of them delivering electrical energy to drive an electric motor. HEVs can be classified into different types depending on the sources of energy and the architecture used to deliver the power. The most common type of HEV uses an internal combustion engine (ICE) and a battery as a source of power to meet the vehicle's power demands. Depending on how ICE and electric motor contribute to a vehicle's transmission, HEVs can be classified into different architectures, such as series hybrid, parallel hybrid, series-parallel hybrid, and complex hybrid [194].

This dissertation considers a series hybrid architecture due to its simplicity and flexibility in control. In a series HEV, the ICE is not connected directly to the drivetrain. Instead, its output is converted into electricity via a generator. The electricity generated is then used to either charge a battery or power an electric motor that drives the vehicle's wheels. This configuration allows for greater control over the power delivered to each wheel, which simplifies traction control [195, 196]. Figure 4.1 shows a configuration of a series HEV, which includes an engine and a battery as power-generating sources. The use of power electronics technology has greatly improved the efficiency and reliability of HEVs. The series hybrid architecture offers several benefits, including improved fuel efficiency, reduced emissions, and greater control over the power delivered to each wheel. Additionally, the lack of direct connection between the ICE and the drivetrain allows for greater flexibility in control and simplifies the traction control [185].

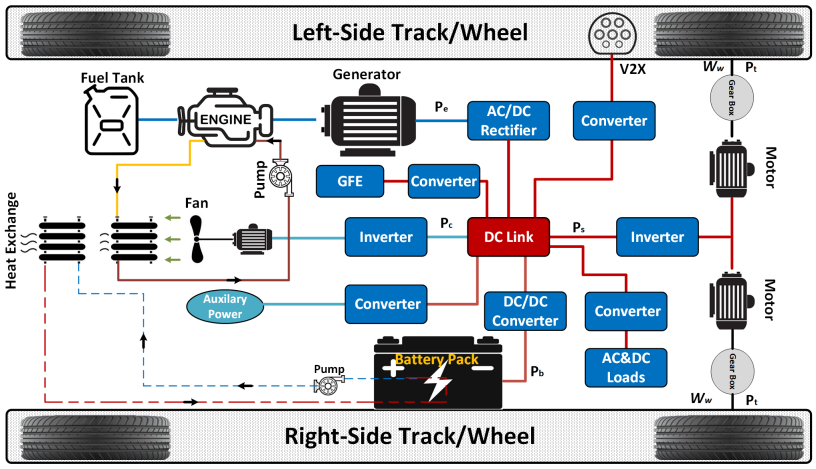

Figure 4.1: Series HEV powertrain configuration considered in this dissertation.

A brief discussion of the electrical model is presented here. The model houses a 600 V_{DC} bus powered by an ICE and an ESS. As can be seen in the figure, energy sources and loads are decoupled from

the bus by the power electronics converter interface. The development of power electronics devices has played an important role in the development of electrified vehicles [197, 198]. This design is economically feasible because of recent advancements in power electronics and the reduction in power electronic device costs [199, 200, 201]. Because of the decoupling, the implementation of EM is eased as the issues of power split in HEVs are relaxed. In particular, this design allows various constraints in EM due to the dynamics of propulsion loads and the ICE to be relaxed. This design also contains a V2X outlet, which allows the vehicle-to-grid (V2G) and the vehicle-to-vehicle (V2V) mode [202].

The series HEV model considered in this project is developed based on the power flow equation of the vehicle and deployed in MATLAB/Simulink in Chapters 5 and the digital real-time simulator (DRTS) Typhoon HIL 606 for real-time simulation in Chapters 6, respectively. No vehicle dynamics are considered to ease the complexity of the vehicle. The vehicle is driven by predefined drive cycles. All the parameters of the HEV needed to find the propulsion power using Ansys Motor-CAD for the drive cycles are used from study [203]. The battery's state of charge (SoC) is obtained mathematically based on the amount of power it is supplying to the vehicle as allocated by the EM.

$$i_{bat} = \frac{P_{bat}}{V_{dc}} \tag{4.1a}$$

$$\dot{SoC}_{bat} = \begin{cases} -\frac{1}{\eta_{coul}} \frac{i_{bat}(t)}{Q_{norm}} & \text{if } i_{bat}(t_k) < 0 \\ -\eta_{coul} \frac{i_{bat}(t)}{Q_{norm}} & \text{if } i_{bat}(t_k) > 0 \end{cases} \tag{4.1b}$$

where P_{bat} is the power allocated by the EM to be supplied by the battery, V_{dc} is the DC link voltage, which is assumed to be constant to $600V$, η_{coul} is the Coulombic efficiency or charge efficiency, which accounts for charge losses and depends on current operating conditions [204], and Q_{norm} is the nominal capacity of the battery.

The initial SoC of the battery is considered to be 80% and the SoC is varied between predefined boundaries of lower and upper limits of 40% and 80% for the efficient operation of the battery as shown by 4.2.

$$\underline{SoC_{bat}} \leq SoC_{bat} \leq \overline{SoC_{bat}} \tag{4.2}$$

4.2 Energy Management

The series HEV explained above consists of an ICE and an ESS i.e., a battery supplying the power demanded by the vehicle for its operation. Here, due to the presence of multiple power-generating sources

in the vehicle, it demands EM system. The objective of the EM is to distribute the power demanded by the vehicles among ICE and other ESSs by reducing the overall fuel consumption [30]. Recently, several research has been done to improve the optimization function of the EM [205, 206]. EM techniques can be broadly classified into four main categories, namely, predictive control method, learning method, heuristic method, and globally optimum approach [31]. Utilizing globally optimal methods can lead to minimum fuel consumption when provided with complete information regarding future power demand [32, 33]. Among different algorithms, dynamic programming (DP) and Pontryagin's minimum principle (PMP) are the most commonly used algorithms [30, 34, 35]. The primary limitations of DP implementation are the curse of dimensionality and the considerable computing overhead required. Although several DP approximation techniques can alleviate the computational burden, they are still not currently suitable for real-time EM problem-solving [6]. And, for PMP, the iterative nature of the two-point boundary value problem (TPBVP) arising from it leads to longer computation times [36]. The non-convex nature of the optimization problem makes achieving global optimality in distributed energy management a challenging task in current research. A dual-objective approach for distributed energy management is proposed in [207]. The approach involves two distinct steps. In the initial phase, several requirements of the EM optimization problem are relaxed to employ a method that converges to global optimality. The findings of the first stage are then utilized to modify the constraints of the overall optimization problem. The utilization of EMs in HEVs is common due to their ability to save fuel [33]. However, it is important to note that various powertrain configurations may require different optimization formulations for EM, resulting in different strategies. In the case of a series HEV shown in Figure 4.1 (explained in detail in Section 4.1), the optimization of EM can be generally presented as follows where an optimization function is used whose objective is to reduce the fuel cost.

$$\min \sum_{s \in \mathcal{S}} f_s\big(P_s(t_k)\big) \tag{4.3a}$$

$$P_s(t_k) \in \mathcal{P} \tag{4.3b}$$

$$\mathbf{x}_s(t_k) \in \mathcal{X} \tag{4.3c}$$

where t_k is the time instant in the discrete domain, $\mathcal{S}$ is the set of indices of energy sources, and $P_s(t_k)$ is power generated by source s at t_k, $\mathbf{x}_k(t_k)$ is the set of states of system s, and $\mathcal{P}$ and $\mathcal{X}$ are correspondingly the constraints set of $P_s(t_k)$ and $\mathbf{x}_s(t_k)$. For the sake of presentation, t_k is omitted. Besides these there are several constraints which should be considered and is explained in detail in this section.

The optimization problem used as the EM is a constrained optimization, where different constraints are considered for the EM. The constraints include the power limits of the vehicle's sources, the total load

demanded, and the state of charge (SoC) of the battery. To solve the optimization problem, SQP (Sequential Quadratic Programming) algorithm is used. SQP is an iterative method designed for solving nonlinear programming problems with constraints. It aims to find the minimum or maximum of an objective function while adhering to the specified constraints. The SQP algorithm follows a sequential approach, where it approximates the original constrained optimization problem using a sequence of quadratic subproblems. During each iteration, it solves a quadratic subproblem that serves as an approximation to the original problem. The solution obtained from the subproblem is then used to update the current solution. The main steps of the SQP algorithm can be summarized as follows:

- Initialization: Begin with an initial feasible solution and set the iteration counter to zero.
- Quadratic Programming: Solve a quadratic programming subproblem, which is derived by linearizing the objective function and constraints around the current solution and constructing a quadratic model.
- Update: Update the current solution using the solution obtained from the quadratic subproblem. This update step determines both the direction and magnitude of the adjustment made to the current solution.
- Convergence Check: Examine convergence criteria to determine whether the algorithm should terminate. These criteria often involve assessing the changes in the objective function, constraints, and other stopping conditions.
- Iteration: If the convergence criteria are not met, increase the iteration counter and repeat steps 2 to 4 with the updated solution.

The SQP algorithm combines concepts from gradient-based methods, utilizing gradients of the objective and constraint functions, as well as quadratic programming techniques involving the solution of a sequence of quadratic subproblems. This approach proves effective for solving nonlinear optimization problems encompassing both equality and inequality constraints.

4.2.0.1 Cost Function

The power supplied by the ICE (P_{ICE}) and the battery (P_{Bat}) sources can be adjusted to gain economic objectives formed in the following function:

$$f_s(P_s) = c^F \Big(\alpha_s (P_s)^2 + \beta_s P_s + \gamma_s \Big), \alpha_s > 0 \tag{4.4}$$

where c^F (\$/gallon) is the cost of fuel. P_s represents the power supplies by the sources present in the vehicle (i.e., P_{Bat} and P_{ICE}). α_s represents the quadratic term in the cost function. It is a positive parameter

($\alpha_s > 0$) that influences the curvature of the cost function. A higher value of α_s increases the weight of the quadratic term in the cost function, making the optimization process more sensitive to deviations from the desired reference powers. β_s represents the linear term in the cost function. It captures the impact of the reference powers (P_s) on the overall cost. The value of β_s determines the weight of the linear term in the cost function. It can be positive or negative, indicating the preference for a specific power split or penalizing deviations from the desired split. And finally, γ_s represents the constant term in the cost function. It represents any additional costs or benefits associated with the power split that is not captured by the quadratic or linear terms.

It is worth noting that every energy source has its generation capacity limits. Therefore, one of the constraints of (4.3b) is lower and upper generation limits as

$$\underline{P_{bat}} \leq P_{bat} \leq \overline{P_{bat}} \tag{4.5a}$$

$$\underline{P_{ICE}} \leq P_{ICE} \leq \overline{P_{ICE}} \tag{4.5b}$$

The main goal of powertrains is to supply loads properly. The total generation should be met the total load and any losses as shown in figure 4.2. With the considered configuration, the following constraint can be formed.

$$P_{bat} + P_{ICE} = P_{AC\ load} + P_{DC\ load} + P_{propulsion} + P_{V2X} + P_{loss} \tag{4.6}$$

where P_{bat} is power generated by the battery, P_{ICE} is power generated by the ICE, $P_{AC\ load}$ is AC load, $P_{DC\ load}$ is DC load, $P_{propulsion}$ is propulsion load, P_{V2X} is power used for V2X mode, and P_{loss} is the total loss.

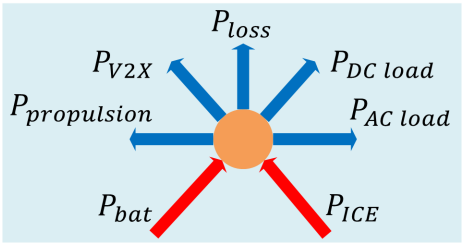

Figure 4.2: Power flow model.

Each system has its own internal constraints, i.e., (4.3b) and (4.3c). The components considered in this study are ICE and battery; hence, the following constraints are assumed for these power-generating sources.

$$|P_{ICE}(t_{k+1}) - P_{ICE}(t_k))| < rr_{ICE} \tag{4.7a}$$

$$|P_{bat}(t_{k+1}) - P_{bat}(t_k)| < rr_{bat} \tag{4.7b}$$

$$\underline{SoC_{bat}} \leq SoC_{bat} \leq \overline{SoC_{bat}} \tag{4.7c}$$

$$SOC_{bat}(t_{k+1}) = SOC_{bat}(t_k) - \frac{\delta T i_{bat}}{Q_{nom}} \tag{4.7d}$$

where $\delta T = t_{k+1} - t_k$. Constraints (4.7a) and (4.7b) are understood both the battery and the ICE have ramp rate limits when adjusting their generation. Constraints (4.7c) and (4.7d) are the battery's State of Charge (SoC) constraints.

The main goal of this EM is to efficiently distribute power between the power-generating sources in order to achieve economic objectives while also taking into account the limitations of the system [27]. EM considers fuel consumption as an economic objective and tries to reduce it by allocating more power to the battery.

However, fuel cost is not only the operating cost of the vehicle; the degradation of the components should also be included in the operating cost of the vehicle. For example, when the EM allocates additional power to the battery to minimize fuel consumption, the battery experiences accelerated degradation. Consequently, this results in the economically unviable operation of the vehicle, as the accelerated deterioration necessitates the faster replacement of the battery. It's noteworthy that the battery stands out as one of the costly components of the vehicle.

Therefore, the following two observations can be summarized from the EM's optimization problem:

- Observation 1: EM looks into the operating condition of the vehicle and calculates the power references to be supplied by the multiple sources into the vehicle.
- Observation 2: The amount of power supplied by the sources or operating condition of the components impacts its degradation process. The higher the power supplied or power flow from the source or components, the higher is the degradation rate. For example, in batteries, higher the amount of charging/discharging current higher is the degradation [15].

Over time, the capacity of components decreases due to degradation, and different components may degrade at different rates. As a result, it is essential to factor in degradation costs when optimizing operating costs based on the degradation path of the components. Energy management can help regulate component degradation in a way that satisfies vehicle load demands.

4.3 Prognostic-based Control Framework

The decreasing cost and increasing capability of computational devices have enabled the widespread use of power electronic devices in vehicles, making it easier to implement computationally intensive algorithms and strategies for efficient vehicle operation. This includes optimization and forecasting functionalities, which are essential for effective vehicle control. In this section, a hierarchical control strategy (shown in Figure 4.3) with an upper layer to an EM layer of degradation forecasting (DF) is introduced, and the operation of each layer is explained in detail. This multilevel control strategy takes advantage of the developments in computational technology, allowing for cost-effective and efficient vehicle operation.

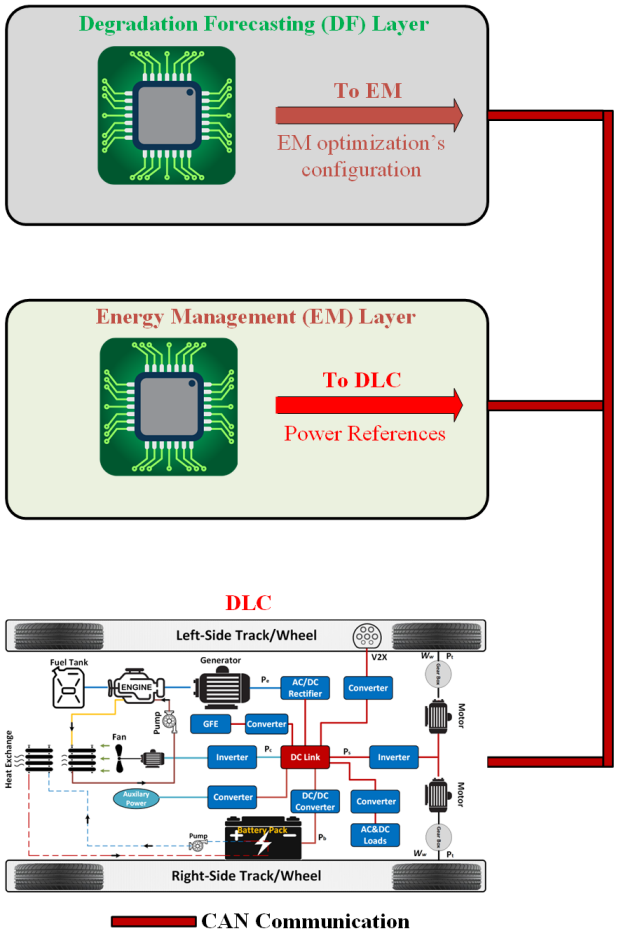

Figure 4.3: Hierarchical control architecture.

The conventional HEV architecture, depicted in Figure 1.6 in Chapter 1, primarily focuses on vehicle control without considering the degradation of its components. The main objective of this control system is to minimize fuel costs, as discussed earlier. A multilevel control architecture is proposed to address

this limitation and incorporate degradation-aware control. This architecture consists of two layers and the HEV model, where each layer serves a distinct purpose.

The first layer is the degradation forecasting layer (DF), which utilizes degradation prediction models to estimate the degradation levels of various components within the vehicle. By leveraging these models, the DF layer provides valuable insights into the expected degradation behavior and performance of the components over time. The second layer is the energy management (EM) layer, which is responsible for power allocation among the different sources within the HEV. This layer takes into account the predicted degradation cost obtained from the DF layer and optimizes power distribution to minimize the impact of degradation on system performance. The process of including the degradation cost of the components into the objective function of EM is explained in Section 4.3.2. The final is the HEV model, which integrates the control strategies developed in the previous layers and enables the effective operation of the HEV system based on the insights gained from degradation forecasting and energy management.

The integration of the degradation forecasting layer into the control architecture of the HEV that can communicate with both the vehicle and EM is called the prognostic-based control framework (PBCF) in this dissertation. This framework redefines the objective function of energy management and aims to enhance the overall performance and longevity of the HEV system by considering the degradation of its components (especially the battery) and minimizing them.

4.3.1 Degradation Forecasting Layer

The primary contribution of this dissertation lies in the innovative integration of the degradation forecasting (DF) layer within the control architecture of the hybrid electric vehicle. Also, this dissertation explores the prediction of battery degradation using two different algorithms, as discussed in detail in Chapter 3. The objective is to design a degradation forecasting layer that incorporates these algorithms effectively into the control architecture of an HEV. The first algorithm employed is the Markov chain model, whereas the second one is the NNs.

4.3.1.1 Markov Chain based Degradation Model

In the degradation forecasting layer the data from SNL is used to construct a model capable of predicting the battery's degradation path and the overall steps for this technique is shown in Figure 4.4. To begin, the battery dataset undergoes a preprocessing step to extract and filter out four crucial parameters: voltage, current, temperature, and capacity. These parameters play a vital role in understanding the battery's behavior and degradation patterns. Once the relevant data is extracted, it is utilized to train and develop a Markov chain model.

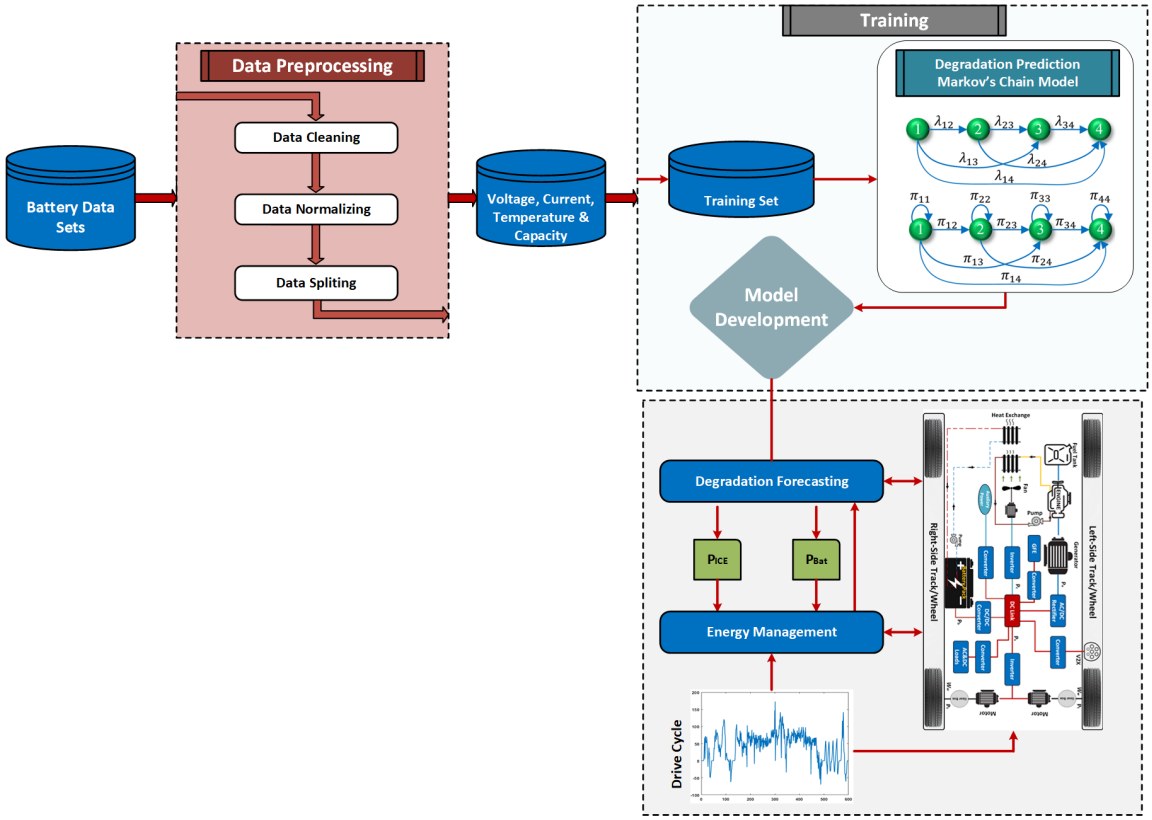

Figure 4.4: Overall schematic diagram of the proposed system using Markov chain model.

The Markov chain model captures the transitions and dependencies between different degradation states of the battery as explained in 3.3. By analyzing the historical data from SNL, the model learns the probabilities of transitioning between various degradation levels. This information forms the basis for predicting the future degradation trajectory of the battery. After constructing the Markov chain model, it is integrated into the DF layer. This layer acts as the interface between the HEV model and the EM of the overall control system. It utilizes the developed Markov chain model to forecast the battery's degradation, taking into account the current operating conditions and the historical data captured during training.

The predictions generated by the DF layer are then sent into the EM. By incorporating the degradation cost, which is obtained from the predicted degradation of the battery, into the objective function of the EM system, the EM optimizes the power allocation between the ICE and the battery. This optimization aims to minimize the degradation and maximize the overall system performance.

4.3.1.2 Maximum capacity expectation degradation (Markov chain model)

The degradation prediction layer outputs the degradation rate cost, which is then incorporated into the objective function of the EM layer. While the previous section and Chapter 2 focused on explaining the prediction of the degradation path, this section will now elaborate on the approach for determining the degradation cost, which serves as the output from the DF layer. The approach is to incorporate a cost factor based on the degradation results into the objective cost of the EM. To quantify the degradation of component capacity, a new parameter is introduced as follows: Let $\mathbb{P}_s(t_k)$ denote the maximum expected capacity of component s at time t_k resulting from the degradation prediction. This parameter is mathematically defined as:

$$\mathbb{P}_s(t_k) = \sum_{i=1}^{4} x_i(t_k)\overline{P_i} \tag{4.8}$$

The aim is to quantify the degradation of $\mathbb{P}_s(t_k)$ over a period of time. Assuming the forecast of component degradation is made from t_0 to t_k, a metric $\Delta_s(t_K)$ is presented to gauge the decline in the capacity of component s from t_0 to t_k.

$$\Delta_s(t_K) = \mathbb{P}_s(t_0) - \mathbb{P}_s(t_K) \tag{4.9}$$

Let ρ_s denote the cost per unit of capacity of component s at the initial time. The degradation cost is penalized by adding the following term to the objective cost of the EM.

$$f_s^d(P_s) = \rho_s \Delta_s P_s \tag{4.10}$$

Now, how this degradation cost $f_s^d(P_s)$ is added into the objective function of the EM as shown in Section 4.3.2.

4.3.1.3 Neural Network based Degradation Model

In the DF layer of the proposed system, the dataset obtained from the University of Wisconsin-Madison is utilized to construct the neural network (NN) models. The primary objective of this layer is to accurately predict the degradation rate of the battery using a data-driven technique, i.e., Neural Networks. The overall steps involved in PBCF using NNs are illustrated in Figure 4.5.

To begin, the dataset undergoes a preprocessing stage where it is carefully prepared for training and testing the NN models. The data is divided into three subsets: training, testing, and validation sets. Approximately 70% of the total data is allocated as the training dataset, which is used to train the NN models. This allows the models to learn and capture the underlying patterns and relationships between

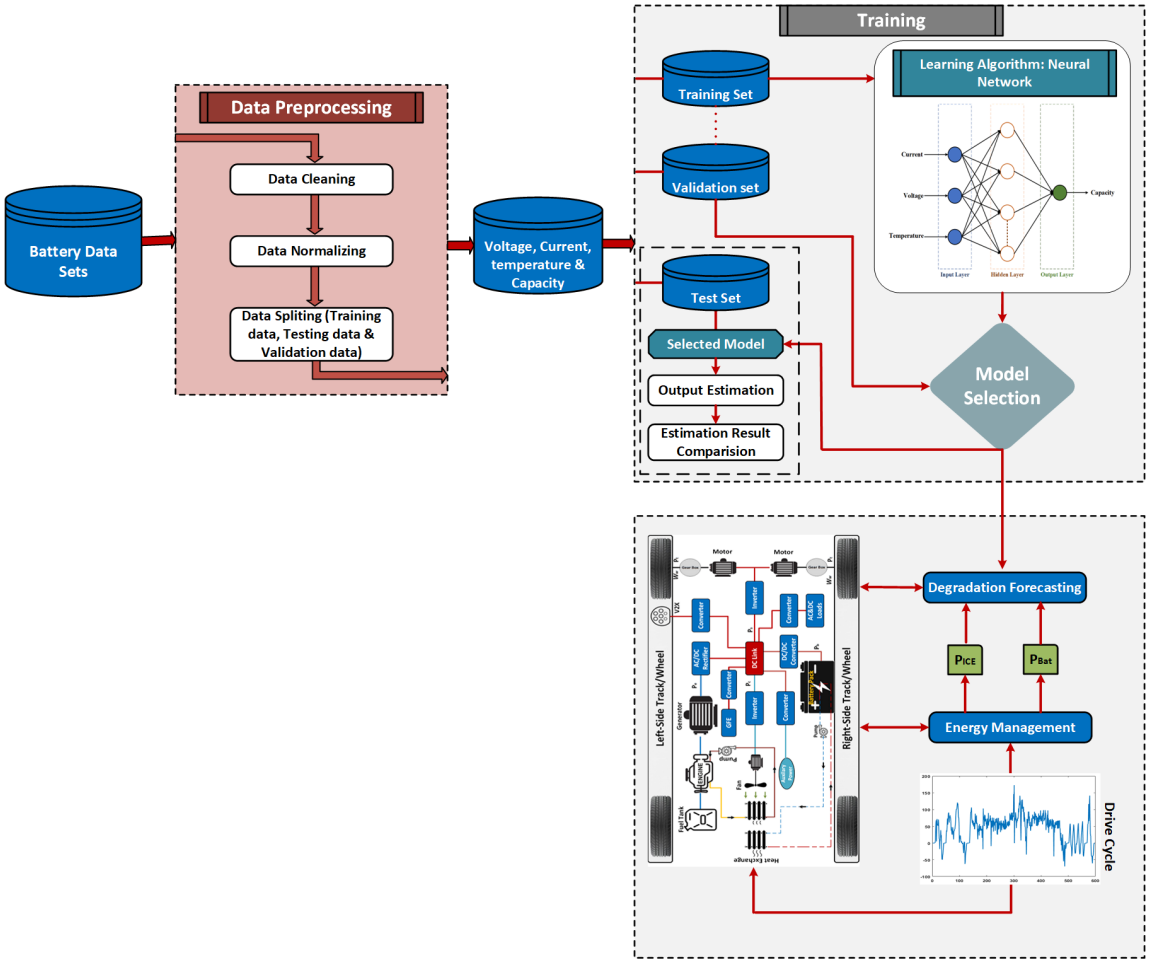

Figure 4.5: Overall schematic diagram of the proposed system using NNs.

the battery's performance parameters, such as voltage, current, temperature, and capacity. The remaining 30% of the dataset is split equally between the testing and validation sets. The testing dataset is used to evaluate the performance of the trained models by comparing their predictions with the actual outputs. The validation dataset, on the other hand, is used to fine-tune the models and make adjustments if necessary.

During the training process, the NN models are iteratively adjusted and optimized using various techniques, as explained in Chapter 3. The goal is to minimize the prediction errors and enhance the accuracy of the degradation forecasts. If the model's performance on the validation dataset is satisfactory, indicating good generalization and predictive capability, the model is considered suitable for integration into the DF layer. However, if the model's performance falls short of the desired level, adjustments are made to the architecture of the NN models, particularly the number of neurons in the hidden layer. The models are then retrained using the updated architecture, and the performance evaluation process is repeated. This iterative procedure continues until a satisfactory level of accuracy is achieved, ensuring that the NN models

effectively capture the complex degradation patterns of the battery.

Once a suitable NN model is obtained, it is incorporated into the DF layer. This layer utilizes the trained NN model to predict the degradation path of the battery. By analyzing the input parameters, such as voltage, current, and temperature, the DF layer generates accurate capacity loss predictions. As explained earlier, this capacity loss is used to find the degradation rate cost which is then fed into the EM layer. The action of EM after obtaining this degradation rate cost is explained in the Section 4.3.2.

4.3.1.4 Maximum capacity expectation degradation (NN model)

The degradation prediction layer outputs the degradation rate cost, which is then incorporated into the objective function of the EM layer similar to as discussed in Section 4.3.1.2. The difference from the Markov Chain in predicting the degradation capacity using NNs is that, after running the simulation from time t_0 to t_k, the output from the network is the capacity loss by the battery during this period which is given by $\Delta_s(t_K)$ as follow:

$$\Delta_s(t_K) = \Delta\mathbb{P}_s(t_k) \tag{4.11}$$

Let $\mathbb{P}_s(t_0)$ represent the maximum capacity of component s at the beginning when time is t_0, $\mathbb{P}_s(t_k)$ be the remaining capacity of the component s at time t_k. Then, the remaining capacity of the battery can be obtained as follows.

$$\mathbb{P}_s(t_K) = \mathbb{P}_s(t_0) - \Delta_s(t_K) \tag{4.12}$$

Now, if ρ_s denotes the cost per unit of capacity of component s at the initial time similar to (4.9). Then, the degradation cost is penalized by adding the following term to the objective cost of the EM.

$$f_s^d(P_s) = \rho_s \Delta_s P_s \tag{4.13}$$

The utilization of this degradation cost $f_s^d(P_s)$ in this dissertation is explained in detail in the following Section 4.3.2.

4.3.2 Reconfiguration of EM's optimization problem

The calculation of degradation cost $f_s^d(P_s)$ using the Markov Chain model and NN models are discussed in detail in previous sections and is given by (4.10) and (4.13), respectively. Now, in this section how this cost is included into the objective function of EM is discussed. The proposed system is graphically represented in Figure 4.6, where a Markov chain model or NNs are trained and utilized to predict the

component's degradation, and subsequently, the degradation cost is calculated in the degradation forecasting layer. The degradation cost is then incorporated into the EM's objective function, as shown in (4.14a) and (4.14b), through the proposed mechanism called the Prognostic-based control framework.

$$\min \sum_{s \in \mathcal{S}} \left(f_s\left(P_s(t_k)\right) + f_s^d(P_s) \right) \tag{4.14a}$$

$$\min \sum_{s \in \mathcal{S}} \left(f_s\left(P_s(t_k)\right) + \rho_s \Delta_s P_s \right) \tag{4.14b}$$

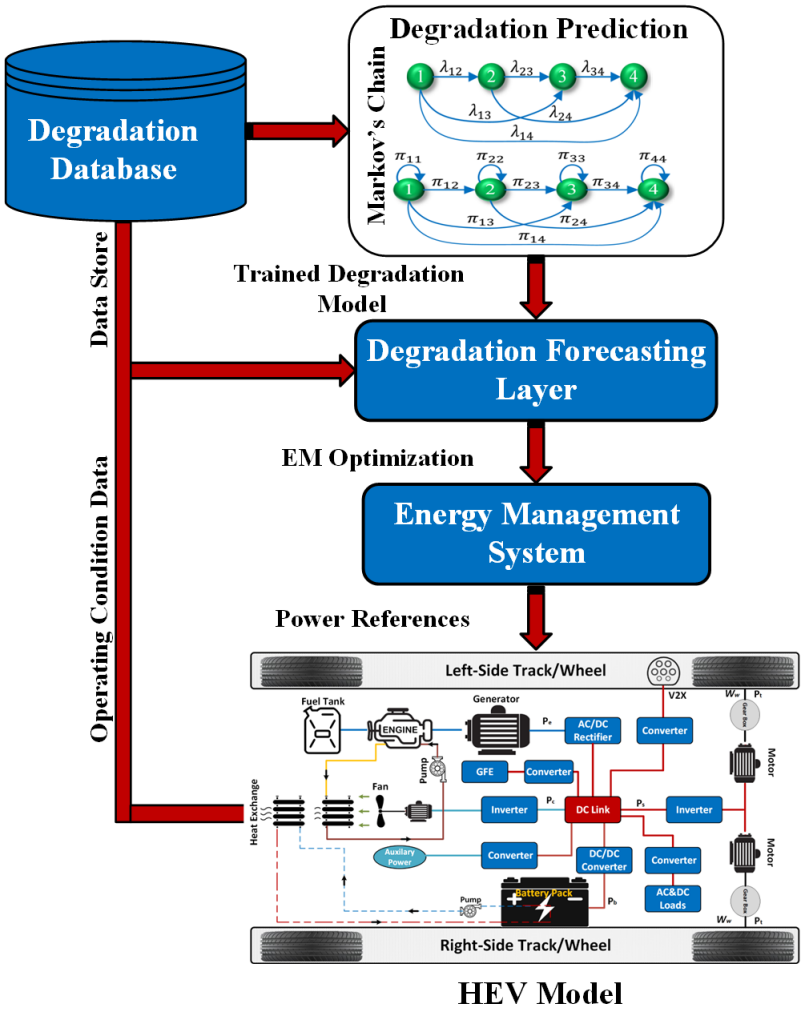

Figure 4.6: Prognostic-based control framework.

Figure 4.7 shows the process involved in PBCF to update the objective function of the EM. Initially, the EM distributes power between the battery and the engine with the goal of minimizing fuel consumption.

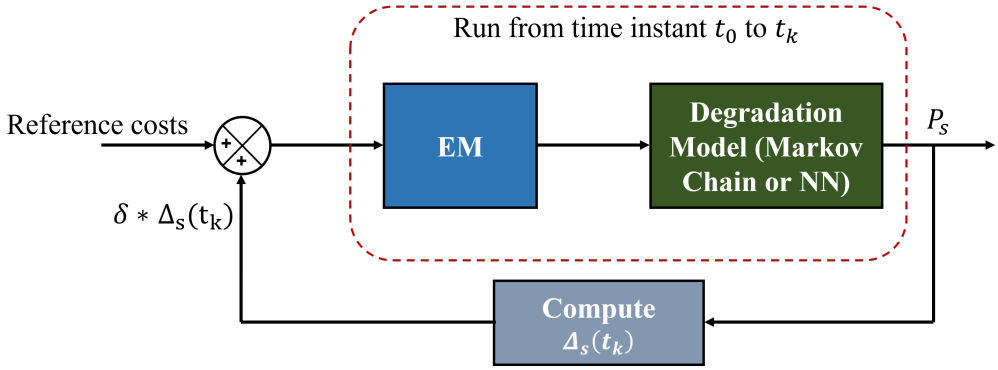

Figure 4.7: Diagram for updating the objective function of EM in PBCF.

Utilizing the power allocated to the battery, the degradation prediction model within the DF layer forecasts the degradation rate and computes the associated degradation cost using equations (4.10) or (4.13). Subsequently, based on the degradation cost, the objective function of the EM is adjusted as given by (4.14a) or (4.14b), leading to a reallocation of power between the sources.

Chapter 5

Numerical Simulation Results

This chapter presents and thoroughly discusses the results of the simulation conducted on MATLAB/Simulink for the proposed system. The numerical simulation is divided into two sections depending upon the technique used to predict the battery degradation: the utilization of the Markov chain and Neural Network models for predicting battery degradation.

5.1 System Description

Numerical simulations are used to validate the proposed framework on a personal computer. The HEV powertrain, illustrated in Figure 4.1 with two power sources, ICE and battery, is used for this purpose. Since this dissertation focuses on reconfiguring the objective function of EM through the proposed framework, an HEV model based on the power flow equation is developed in MATLAB/Simulink. It does not consider the system's dynamics for simplicity and reduced complexity while deploying it on MATLAB/Simulink or to a real-time simulator. All vehicle parameters are considered from the study [203], which is then used to calculate the propulsion power for the US06 and WLTP drive cycles using Ansys Motor-CAD. Figure 5.1 illustrates a sample of the propulsion load for the US06 drive cycle used in this study. The vehicle operates for 598 seconds and 8.01 miles in one drive cycle. The HEV's ICE capacity can generate up to 180 kW to provide the DC bus, and the battery has a capacity of 73 kWh. The propulsion load is typically the highest among the other loads when operating vehicles. In this dissertation, a few samples of propulsion loads are used. Also, the SoC of the battery is operated within certain limits, where the minimum SoC is 40%, and the maximum SoC is 90%.

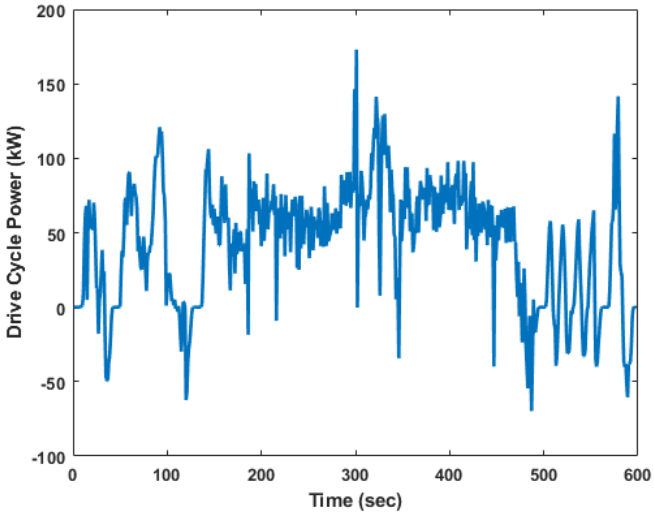

Figure 5.1: Sample of propulsion load.

5.2 Markov Chain based Model

5.2.1 Degradation data

Accessing battery degradation data used in HEVs/EVs by the automotive industry is challenging since it is kept confidential. Therefore, in this section for the Markov Chain model, SNL datasets are utilized, as discussed previously. The battery cell data on degradation is used to develop the degradation model, which was already explained in Chapter 3, Section 3.3, and then scaled up to the battery capacity used in this study. From the generated data, different degradation paths for different cells are used to obtain minimum degradation intensity matrix $\underline{\lambda} = [\underline{\lambda_{ij}}]_{4x4}$ using Algorithm 1. Algorithm 1 utilizes the array d_y to store a degradation path while the array S_y holds the state of all elements in d_y . Y denotes the total number of generated degradation paths. The algorithm is designed to calculate the transition probability from state i to state j. Additionally, the maximum degradation intensity matrix $\overline{\lambda} = [\underline{\lambda_{ij}}]_{4x4}$ can also be computed using this algorithm. Similarly, the Wiener process is used to model ICE degradation, as explained in detail in the study [48]. The same model is used in this dissertation, with the efficiency curve given by (5.1). The model and the code are developed and deployed in MATLAB/Simulink in this section.

$$f(x) = 0.00052x^2 + 0.0152x + 0.65 \tag{5.1}$$

To evaluate the economic feasibility of the proposed framework, it is essential to consider the initial costs of both the ICE and battery. According to recent reports from [208], the average cost per kWh of the Li-ion battery used in EVs is around $151 in 2023. Furthermore, the cost of the ICE is considered

approximately $7000 [11].

Algorithm 1 Training minimum degradation intensity matrix

1. Input: Degradation paths $d_y, y \in \{1, ..., Y\}$
2. Initialize: $\underline{\lambda} = [0]_{4x4}$
3. **for** $y := 1$ *to* Y **do**
   Assign state for $d_y(l) : \ S_y(l) \ = \ i, \ i = 1$ *or* $i = 2$ *or* $i = 3$ *or* $i = 4$
   for $l := 2$ *to* $length(d_y) - 1$ **do**
   Assign state for $d_y(l) : \ S_y(l) \ = \ i, \ i = 1$ *or* $i = 2$ *or* $i = 3$ *or* $i = 4$
   $\underline{\lambda}(S_y(l-1), S_y(l)) = \underline{\lambda}(S_y)(l-1), S_y(l) + 1$
   end
   end
4. Normalize $\underline{\lambda}$
5. **return** $\underline{\lambda}$

5.2.2 Numerical simulation results and discussion

The simulation is conducted to evaluate the effectiveness of the PBCF in minimizing degradation and optimizing the operation of the HEV. The result compares two simulations: one without implementing the PBCF and another with the PBCF strategy integrated into the system.

If the PBCF is not applied, the DF layer, responsible for predicting vehicle component degradation, remains inactive. Conversely, with PBCF implementation, the DF layer integrates a Markov chain model to anticipate degradation. The predicted degradation cost obtained from the DF layer is then integrated into the objective function of the EM system as explained in Chapter 4, Section 4.3.2, which allocates the power among the sources in the HEV. Figure 5.2 illustrates the power allocation by the EM with and without PBCF.

During the simulation, the degradation forecasting is performed for both the battery and the ICE at a temperature of $25^{\circ}C$ after running 75 drive cycles. Figure 5.3 analyzes and presents the simulation results. Figure 5.3a clearly demonstrates the positive impact of the PBCF strategy on the battery degradation path. The implementation of degradation prediction allows the system to make proactive decisions on power allocation, thereby reducing the stress on the battery and slowing down its degradation rate. On the other hand, as shown in Figure 5.3b, no significant change is observed in the ICE degradation path. This can be explained by the relatively gradual degradation of the ICE compared to the battery, as ICE tends to have a longer lifespan. Furthermore, due to the limitation of the simulation to only 75 cycles, no notable enhancement is observed in the minimization of degradation of the ICE. For this reason, the results in the subsequent cases do not display the degradation of the ICE but instead concentrate solely on the degradation of the battery.

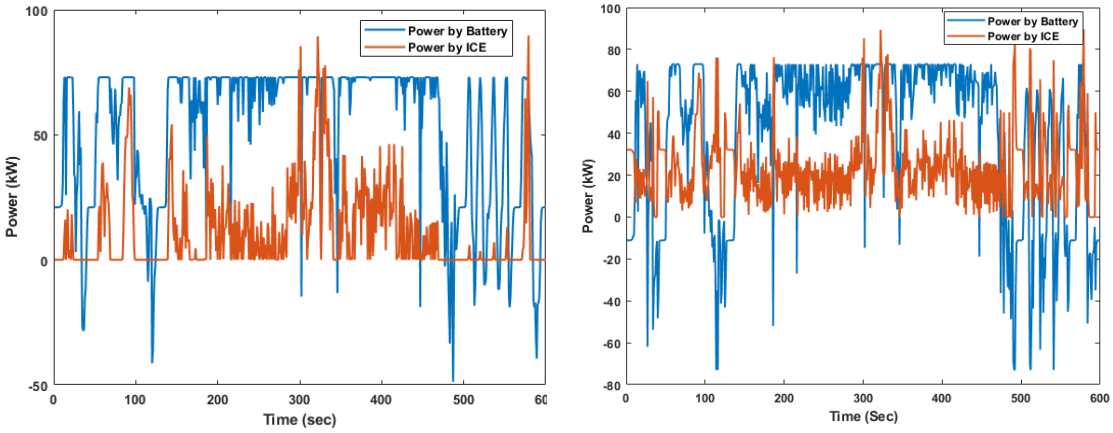

(a) (b)

Figure 5.2: Power allocation by EM: (a) without PBCF (b) With PBCF.

Figure 5.3c provides valuable insights into the economic implications of implementing the PBCF strategy. The results show a reduction in the degradation costs of both the battery and the ICE, amounting to \$10.8045. However, it is important to note that there is an increase in fuel cost of \$5.9808 due to the higher power supplied by the ICE, which can be seen in Figure 5.2b. Nevertheless, when considering the overall operating costs, the PBCF strategy resulted in a net reduction of \$4.8237 after 75 drive cycles.

These findings highlight the potential benefits of the PBCF strategy in terms of prolonging the lifespan of the battery, reducing degradation costs, and optimizing the operation of the HEV. By effectively mitigating battery degradation, the PBCF strategy offers promising prospects for improving the performance and longevity of HEV systems, ultimately leading to cost savings and enhanced sustainability.

5.3 Neural Network based Model

In Chapter 3, three different neural network architectures are employed to forecast the degradation trajectory of the battery. A distinct battery dataset, not utilized during the model's training, testing, and validation phases, is employed to compare the predictions of these three networks. Figure 5.4 depicts the forecasted degradation paths generated by these networks alongside the actual degradation path of the battery.

Upon analyzing Figure 5.4, it becomes apparent that all three techniques exhibit good prediction performance. However, the FNN exhibits the least accurate predictions while comparing the three networks. On the other hand, both the LSTM and DNN models demonstrate similar fitting capabilities. To assess the models more comprehensively, metrics such as mean absolute error (MAE), mean square error (MSE),

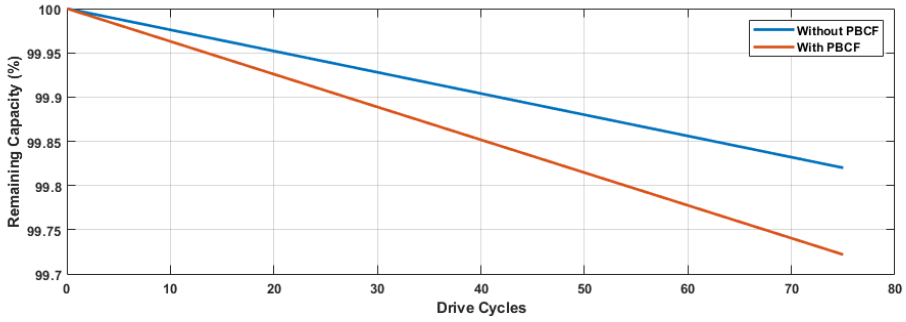

(a)

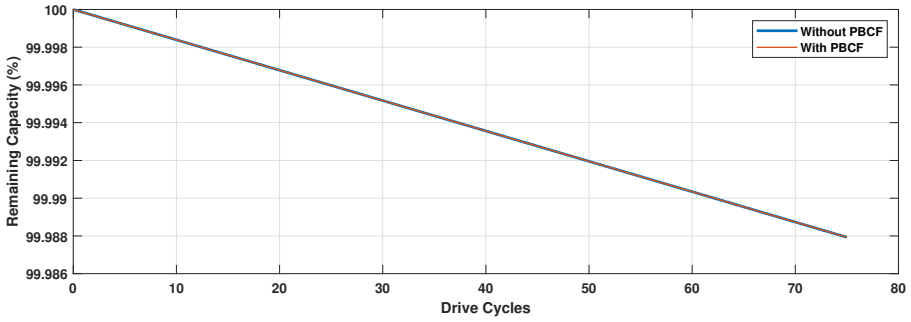

(b)

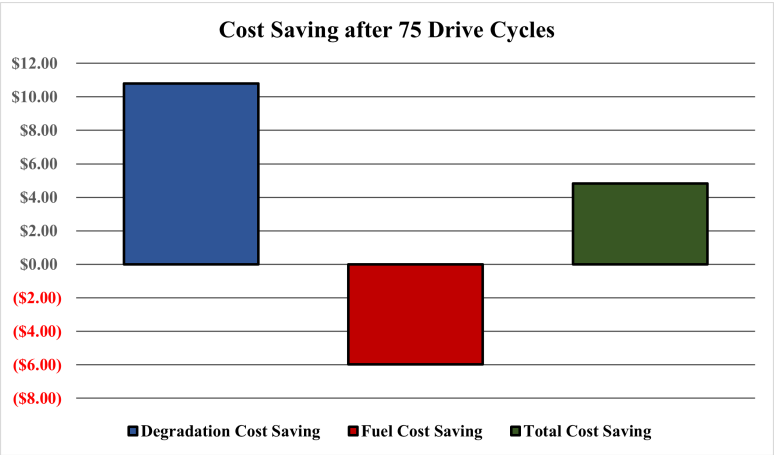

(c)

Figure 5.3: Simulation results: (a) Battery degradation abatement (b) ICE degradation abatement (c) Cost savings by the proposed PBCF.

and R-squared (R2) are used, which are calculated using (5.2). The MAE provides an absolute measure of prediction accuracy, while the R2 value indicates how well the model captures the variability in the data.

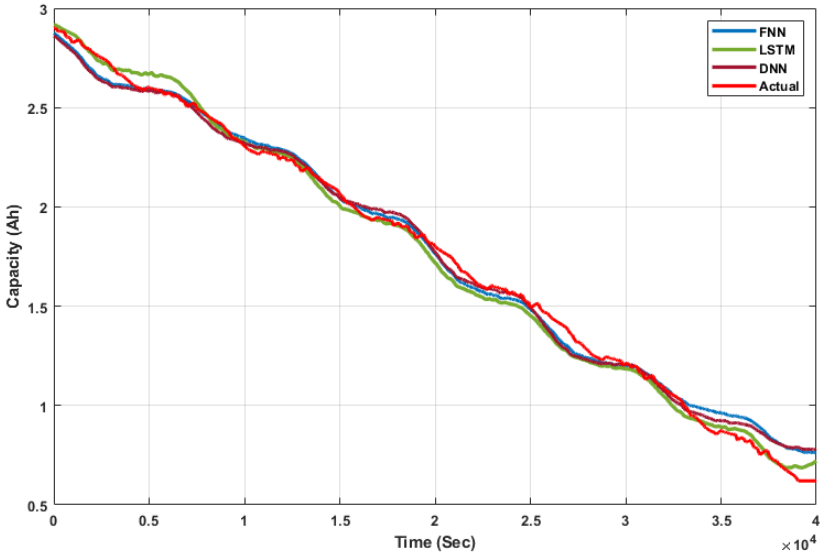

Figure 5.4: Degradation prediction using different NNs.

$$
\begin{aligned}
MSE &= \frac{1}{N}\sum_{i=1}^{N}(y_i - \hat{y}_i)^2 \\
MAE &= \frac{1}{N}\sum_{i=1}^{N}|y_i - \hat{y}_i)| \\
R^2 &= \frac{\left(N\sum_{i=1}^{N} y_i\hat{y}_i - \sum_{i=1}^{N} y_i \sum_{i=1}^{N} \hat{y}_i\right)^2}{\left(N\sum_{i=1}^{N} {y_i}^2 - \left(N\sum_{i=1}^{N} y_i\right)^2\right)\left(N\sum_{i=1}^{N} {\hat{y}_i}^2 - \left(\sum_{i=1}^{N} \hat{y}_i\right)^2\right)}
\end{aligned}
\tag{5.2}
$$

Table 5.1 compares the fitting of the three different networks. The first three rows display the MAE, MSE, and R2 values for the testing dataset used during model training, while the last three rows exhibit the MAE, MSE, and R2 values for the unseen data that was not part of the training, testing, and validation process. It is evident from the table that the LSTM network outperforms the other two networks, exhibiting lower MAE values and higher R2 values for both the training/testing dataset and the unseen dataset. Additionally, the DNN model demonstrates the second-best fitting performance, while the FNN lags behind in terms of accuracy.

Looking at the development of the networks, DNN might be considered an advanced network compared to LSTM networks. However, it's important to experiment with different network architectures and evaluate their performance on the specific task and dataset. There is no one-size-fits-all answer, and the performance of DNNs and LSTM networks can vary depending on the context. DNNs do not always give

Table 5.1: Comparison of different NNs

Parameters	**FNN**	**RNN (LSTM)**	**DNN**
MAE	0.0789	**0.0687**	0.0697
MSE	0.0129	**0.0091**	0.0096
R-square	0.9743	**0.984**	0.9808
MAE (new data)	0.8167	**0.0728**	0.0882
MSE (new data)	0.0212	**0.0088**	0.0119
R-square (new data)	0.9556	**0.9860**	0.9749

better results than LSTM networks. The choice of the network architecture depends on the specific task, the characteristics of the data, and the available resources.

If the data has a sequential nature, such as a time series, LSTM networks are specifically designed to handle such sequences. LSTM networks excel at capturing long-term dependencies and modeling temporal patterns. Their memory mechanism allows them to retain information over time, making them particularly effective for tasks involving sequential data. LSTM networks have a distinct advantage in capturing context and understanding dependencies between elements in a sequence. They can learn to remember important information from the past and selectively forget irrelevant details. Hence, in this analysis from Figure 5.4 and Table 5.1, the LSTM model exhibits superior prediction performance compared to the DNN due to the sequential nature of the battery degradation dataset.

To ensure the robustness and generalizability of the proposed framework, the Markov Chain-based model is simulated using the US06 drive cycle, while the neural network-based models undergo simulation using two different drive cycles. The first drive cycle utilized is the US06, while the second drive cycle combines the US06 and WLTP drive cycles, providing a comprehensive evaluation of the framework's performance across different driving scenarios. Additional information about the combined drive cycle is elaborated upon in Section 5.3.2.

5.3.1 Case-I

The US06 drive cycle, previously depicted in Figure 5.10, is employed in this study, consisting of a total duration of 598 seconds and covering a distance of 8.01 miles per cycle. The simulation is run for 75 consecutive drive cycles, equivalent to a total distance of 600 miles. The LSTM NN degradation model developed in Chapter 3, Section 3.4 is utilized to predict the degradation path in this section, and the power allocation by the EM after implementing the PBCF is illustrated in Figure 5.5. It is worth noting that the power allocation without PBCF remains consistent with the depiction in Figure 5.2a, as discussed in Section 4.3.2 of Chapter 4.

The implementation of PBCF results in a notable change in the power supplied by the battery and

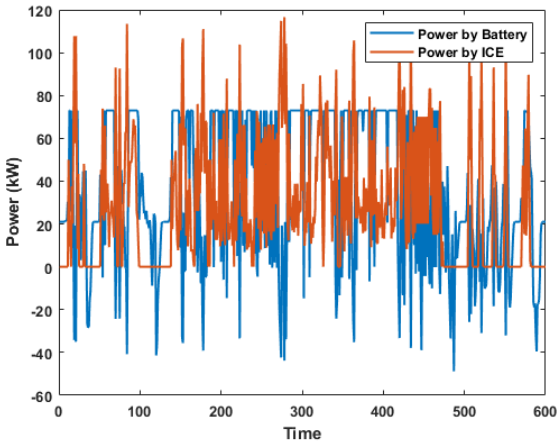

Figure 5.5: Power allocation by EM after the implementation of PBCF.

the engine. This is evident from the graph presented in Figure 5.5, where the ICE also supplies additional power compared to the previous case (i.e, without PBCF) to meet the vehicle's load demand and charge the battery. To further validate this observation, the SoC of the battery can be observed in Figure 5.6. In the case of the PBCF applied vehicle, after conducting simulations for 75 drive cycles, the battery's SoC reaches 76%. On the other hand, in the non-PBCF scenario, the SoC decreases to 65%. Hence, implementing the PBCF leads to more frequent battery charging at shorter intervals. The increased charging frequency allows the battery to maintain a higher SoC.

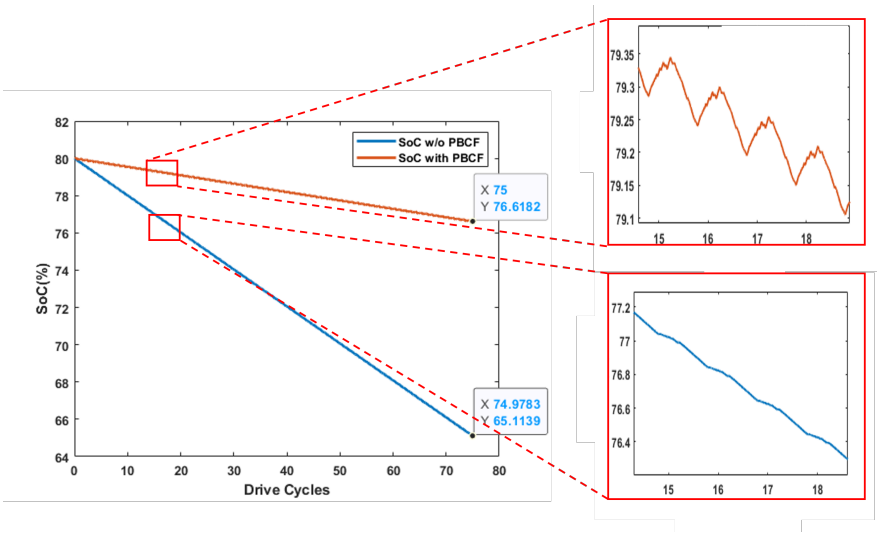

Figure 5.6: SoC of battery with and without PBCF.

Lastly, Figure 5.7 showcases a reduction in the degradation path after implementing PBCF. The

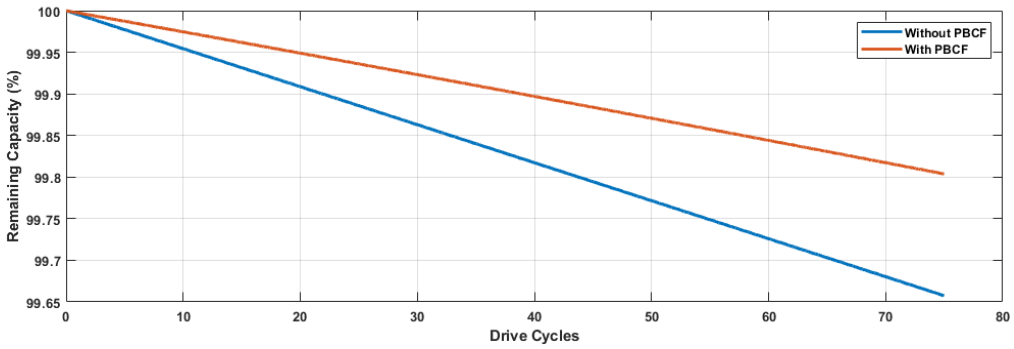

(a)

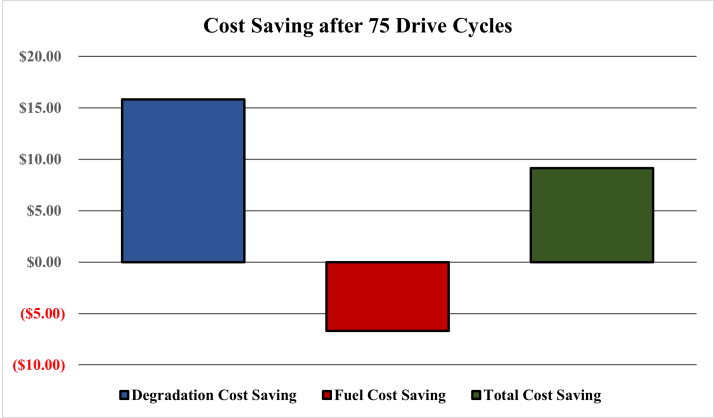

(b)

Figure 5.7: (a) Degradation abatement of battery using PBCF. (b) Cost savings after implementing PBCF.

capacity loss of the battery without PBCF is found to be 0.3425%, whereas the capacity loss with PBCF is observed to be 0.1961% after driving for 75 drive cycles, which results in a saving of 0.1464% capacity loss. Figure 5.7b provides valuable insights into the economic implications of implementing the PBCF strategy. The results show a reduction in the degradation costs of the battery, amounting to $16.13. However, it is important to note that there is an increase in fuel cost of $6.7019 due to the higher power supplied by the ICE. Nevertheless, when considering the overall operating costs, the PBCF strategy resulted in a net reduction of $9.4357 after 75 drive cycles.

5.3.2 Case-II

To evaluate the feasibility and effectiveness of the proposed strategy across various driving scenarios, a drive cycle is created by combining the characteristics of two distinct drive cycles: the US06 and WLTP drive cycles. The inclusion of the WLTP drive cycle is driven by its ability to replicate real-world driving

conditions, incorporating a range of driving maneuvers such as starts, accelerations, and stops within a controlled environment, which is shown in Figure 5.8.

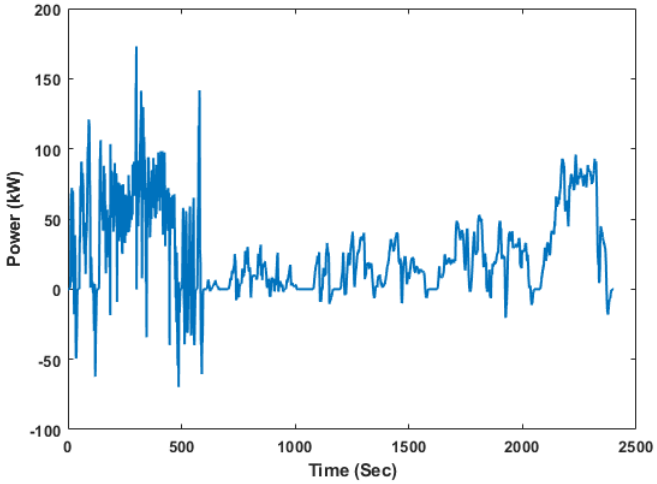

Figure 5.8: Sample of propulsion load for combined drive cycle.

In the combined drive cycle, the vehicle initially runs to the US06 drive cycle for a duration of 598 seconds, simulating specific driving conditions and patterns. Following this period, the WLTP drive cycle is seamlessly integrated, extending for a duration of 1800 seconds. Throughout this combined drive cycle, the vehicle covers a total distance of 22.46 miles. The vehicle operates under the US06 drive cycle for 8.01 miles, replicating the corresponding driving conditions and load profiles associated with this specific drive cycle. Subsequently, the vehicle transitions to the WLTP drive cycle, covering an additional distance of 14.45 miles.

To capture the propulsion load profile demanded by this combined drive cycle, an in-depth analysis is conducted using Ansys Motor-CAD, considering the dynamics of an HEV from study [203]. The load profile, as illustrated in Figure 5.8, provides valuable insights into the power demands and fluctuations experienced by the vehicle throughout the combined drive cycle.

The power allocation strategy of the EM is depicted in Figure 5.9. Initially, during the US06 drive cycle, the power distribution involves the battery supplying a significant portion of the demanded power while the ICE supplements the remaining power required by the vehicle. This allocation scheme remains consistent with the previous section's discussion.

However, as the drive cycle transitions to the WLTP phase beyond 598 seconds, a different power allocation pattern emerges. During this phase, the power demand from the vehicle decreases, and the battery becomes capable of meeting the vehicle's power requirements independently until 2100 seconds. The ICE remains inactive until the power demand exceeds the battery's capacity, at which point it engages to fulfill

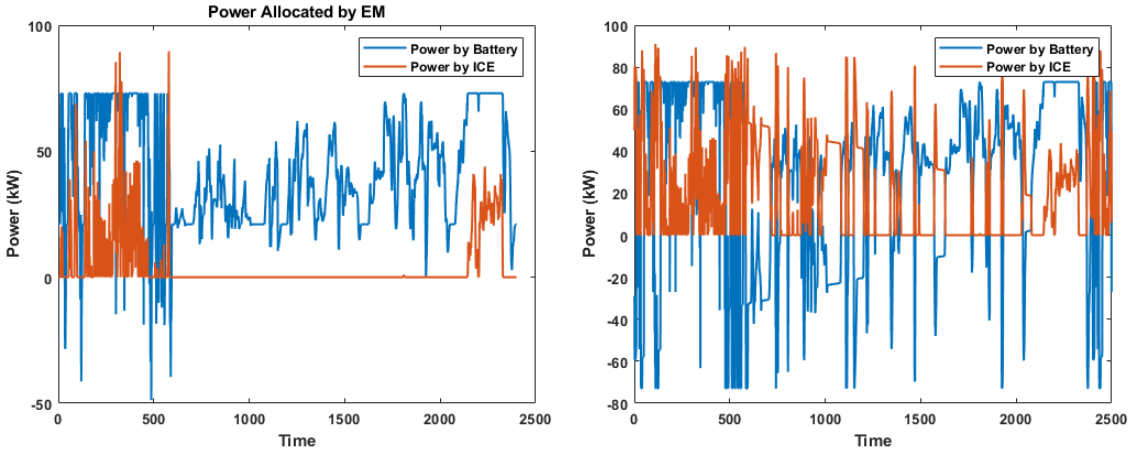

(a) (b)

Figure 5.9: Power allocation by EM: (a) without PBCF (b) With PBCF.

the additional power needs.

Consequently, the battery predominantly supplies power throughout the drive cycle, with minimal instances of charging. Upon implementing the PBCF, the power allocation undergoes adjustment, resulting in the ICE contributing power and charging the battery more frequently, as depicted in Figure 5.9b. This reallocation of power improves the state of charge (SoC) of the battery. Without PBCF, after 27 drive cycles, the battery's SoC is recorded at 62%, whereas with the application of PBCF, the battery's SoC reaches 68%.

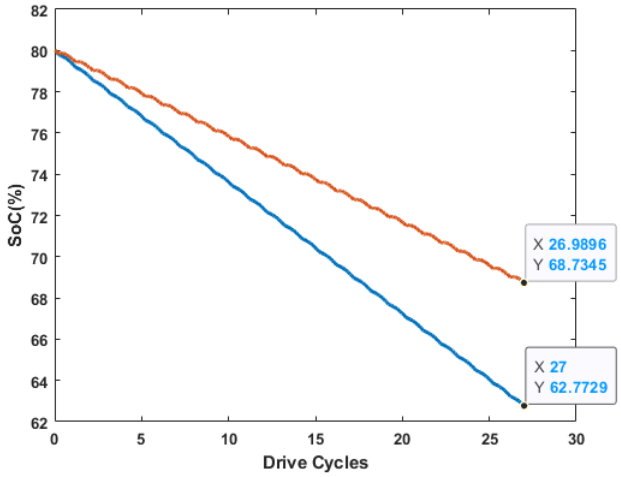

Figure 5.10: SoC of battery with and without PBCF.

Furthermore, Figure 5.11a showcases a reduction in the degradation path after implementing PBCF. The capacity loss of the battery without PBCF is found to be 0.4588%, whereas the capacity loss with PBCF

is observed to be 0.2856% after driving for 27 drive cycles. Hence, the capacity loss saving of 0.1732% is achieved after the implementation of PBCF. Figure 5.11b provides valuable insights into the economic implications of implementing the PBCF strategy. The results show a reduction in the degradation costs of the battery, amounting to $19.47. However, it is important to note that there is an increase in fuel cost of $8.49 due to the higher power supplied by the ICE. Nevertheless, when considering the overall operating costs, the PBCF strategy resulted in a net reduction of $10.98 after 27 drive cycles.

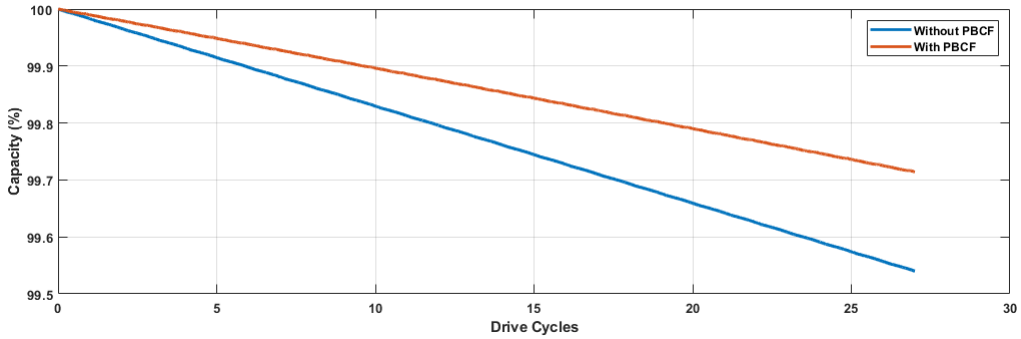

(a)

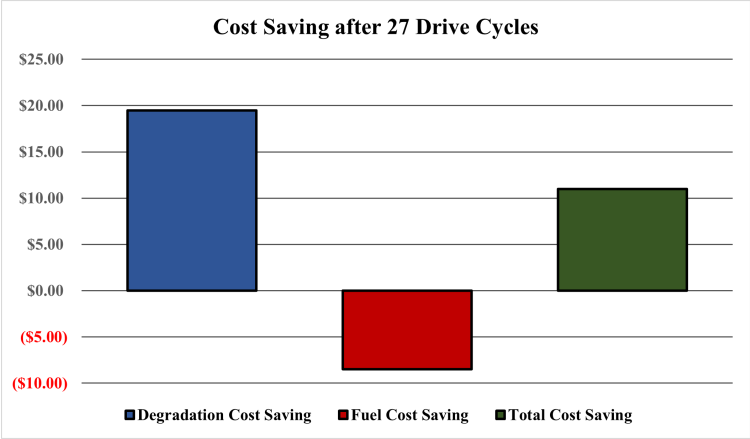

(b)

Figure 5.11: (a) Degradation abatement of battery using PBCF (b) Cost saving using PBCF.

Chapter 6

Controller Hardware in Loop

The controller hardware-in-the-loop (CHIL) experiments are conducted to test and validate algorithms or frameworks in real-time systems using real-time simulators and controllers [209, 210, 211]. This chapter presents and thoroughly discusses the real-time implementation of the proposed strategy. The implementation of the proposed strategy is demonstrated through a CHIL experiment conducted on a series HEV system, as explained in Section 4.1. The equipment from Clemson University's Real-time Control and Optimization Laboratory (RT-COOL) is used to integrate the DF layer with the EM for implementing PBCF. The objective of a CHIL experiment utilizing laboratory equipment is to demonstrate the viability of implementing the proposed framework in real-time application and efficient integration of DF layer with the existing EM layer. The subsequent section presents further information on the CHIL implementation and the experimental outcomes.

6.1 System Modeling

The series HEV is simulated in the schematic editor in Typhoon HIL control center software. HEV model based on the power flow equation is developed in the schematic editor. This model is then compiled and loaded into HIL SCADA, which is then deployed into the DRTS Typhoon HIL 606. In Section 4.1, a model is developed using the power flow equation instead of developing a comprehensive vehicle dynamic model. In this dissertation, the identical model is utilized in Typhoon, as the primary focus of this dissertation is on formulating a control strategy for distributing power among multiple sources to meet the vehicle's load demand rather than delving into an examination of the vehicle's dynamics. This approach simplifies the model's complexity in contrast to utilizing the complete dynamic model of the vehicle.

In order to manage multiple power sources in a vehicle, an EM is necessary, as discussed in Chapter

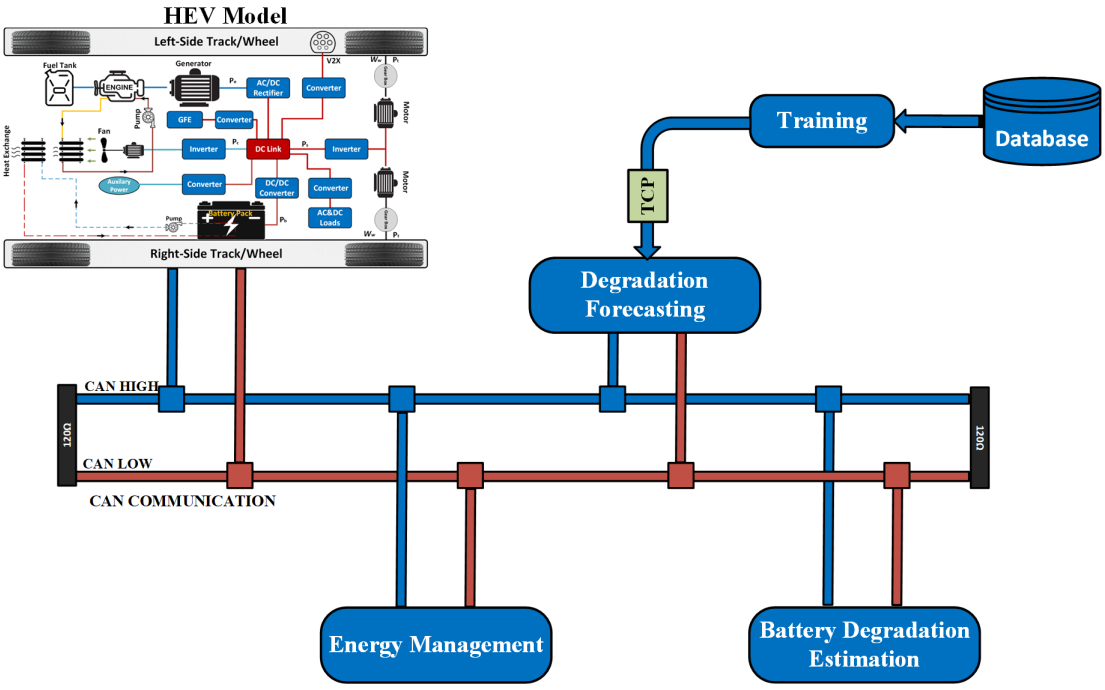

Figure 6.1: CHIL implementation for real-time PBCF.

4, Section 4.2. In the automotive industry, EM algorithms are typically deployed in a controller called Electronic Control Units (ECUs). Here, a Raspberry Pi 4 Model B is used as the ECU to run the EM algorithm, whose objective is to reduce fuel cost. The real operating parameters from the HEV model (i.e., Typhoon) are sent to the Raspberry Pi, which runs the EM algorithm to determine the optimal reference power to be supplied by the battery and ICE. This reference power is then sent back to the Typhoon.

The EM employs three threads running in parallel (utilizing three out of the four cores of the Raspberry Pi). The first thread waits for the signal (whether the system has started or not) to begin the EM algorithm, while the second thread handles communication protocol, receiving the battery's SoC and all the loads demanded by the vehicle. Finally, the third thread runs the EM algorithm and returns the reference power back to Typhoon using the communication protocol deployed in the second thread. The standard communication protocol used in the vehicles is Controller Area Network (CAN) communication. Therefore, this dissertation uses CAN communication to transfer data between the simulator and the ECUs. Figure 6.1 illustrates the implementation of the proposed strategy in real-time through a CHIL setup.

6.2 Integrating Degradation Forecasting into the EM

The previous section explains the EM's approach, which aims to minimize fuel costs and allocate power across each source used in the vehicle. The EM, however, won't evaluate the degradation of the components, which may increase the vehicle's overall running costs. The DF layer is integrated above the EM for this reason. Now, the reference powers generated by the EM are fed into the HEV model and also to the DF layer to predict the degradation of the components using CAN communication.

The proposed DF algorithm is developed using the Python environment and is deployed in a real-time ECU, the Raspberry Pi 4 Model B. This ECU receives signals from another ECU that hosts the EM and DRTS, where the HEV model is deployed. Depending on the signals received, the ECU predicts the degradation rate using the developed Markov chain model and Neural Network models, as explained in Chapter 3. The trained models (either the Markov Chain model or Neural Network models) are obtained from a computer acting as a server, with its functionalities implemented using a Python script. The server's functionalities involve storing and training data using Algorithm 1 to obtain the maximum and minimum degradation intensity matrices for each information source for the Markov Chain model and storing and training data for Neural Network models. Additionally, it sends trained models whenever the real-time controller that implements the DF requests them and stores the necessary scripts for the EM and DF in their respective controllers. Finally, the DF controller collaborates with the server to run the degradation model and predict the components' degradation rate.

The degradation cost is estimated using (4.10) and (4.13), based on the degradation path and the capacity lost over time. This cost is then transmitted to the EM, which incorporates it as a penalized degradation cost in its objective function as given by (4.14a) and (4.14b) and adjusts the power allocation between the sources accordingly. The communication between the ECUs and the DRTS is facilitated through CAN communication, which is explained in the following Section 6.3.

6.3 Communication

Controller Area Network (CAN) is a widely used communication protocol for transferring data in automotive and industrial applications. In a CAN network, data is transferred between different ECUs, also known as nodes, through two wires: CAN HIGH (CAN-H) and CAN LOW (CAN-L).

All the nodes are connected to the CAN bus, and when a node wants to transmit data, it checks the bus to ensure it is idle. If the bus is free, the node begins transmitting its message by placing it on the bus. Each node on the network receives the message and checks the identifier. Here each message consists of an identifier, which specifies the priority and content of the message and the data to be transferred. In

this study, there are three nodes as follows:

- Typhoon (HEV Model)
- Raspberry Pi (ECU-1, EM)
- Raspberry Pi (ECU-2, DF)

Data transmission in a CAN involves the dissemination of data from one node to the CAN bus, which can be accessed by all other nodes in the network. In this study, to establish a CAN network, Typhoon utilizes its own interface, employing CAN send and CAN receive blocks for data transmission. For targeted communication, a designated message-id is assigned to transmit data to specific ECUs such as ECU-1 (EM) and ECU-2 (DF). On the receiving end, the message-id is verified to ensure that the respective ECU receives the intended data. Similarly, in Raspberry Pis, Python code is written to facilitate data exchange through the CAN bus. This approach enables each of the aforementioned nodes to transmit and receive signals using specific message-ids, ensuring reliable communication while mitigating interference. The establishment of a communication system between different devices in RT-COOL is illustrated in Figure 6.2.

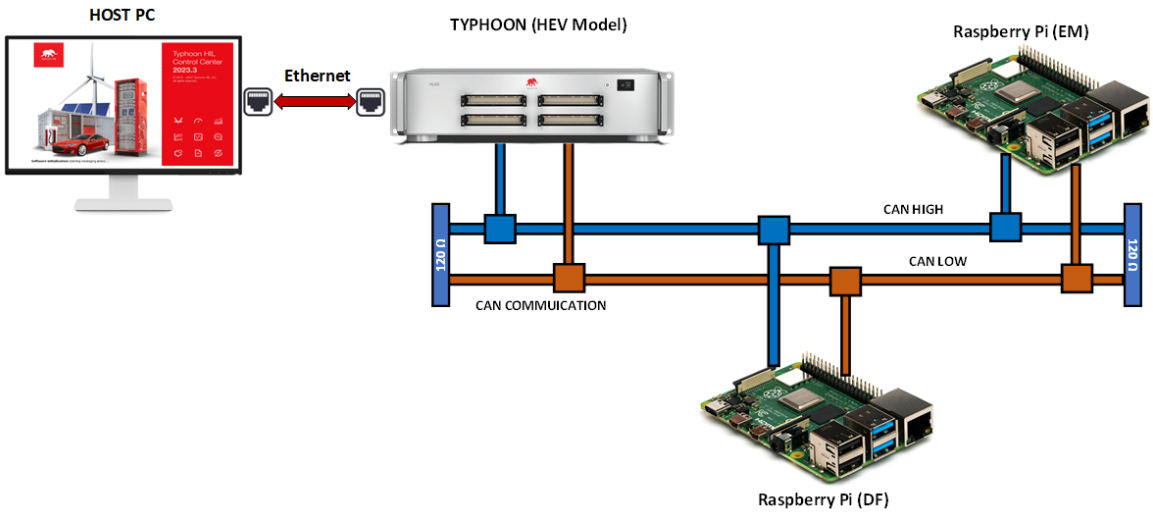

Figure 6.2: CHIL implementation of PBCF in real-time on actual components in RT-COOL.

6.4 Visualization

For the purpose of visualization, an interface called the human-machine interface (HMI) is developed. This interface is implemented through a HIL SCADA window in the Typhoon control center and a Python visualization environment. The Typhoon collects operational data from the host PC, the simulator, and all ECUs, including the EM and DF controllers, and presents them on the SCADA window. The HMI

consists of four primary screens: the control screen, HEV monitoring screen, energy management screen, and degradation forecasting screen.

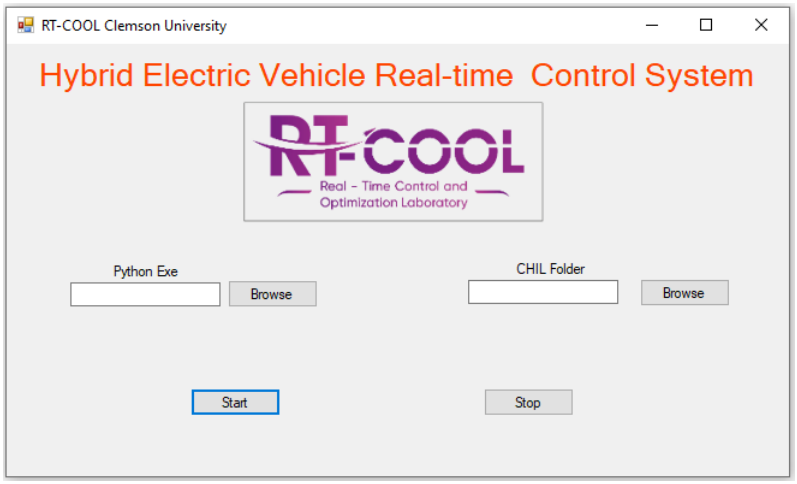

Figure 6.3: Real-Time implementation control screen.

The control screen provides a start/stop button that allows users to initiate or halt the real-time simulation. When the start button is pressed, a Python script associated with the control screen is triggered. This script contains all the required inputs for the CHIL system, including IP addresses for the various controllers (ECUs), simulators, and the host PC. Also, separate message IDs for the CAN communication to send the data between Typhoon, ECU-1 (EM), and ECU-2 (DF) are predefined in this script. Upon pressing the start button, the system performs several automated tasks. Firstly, it logs into the controllers and copies the necessary files to execute the EM and DF functions onto the designated Raspberry Pi. Additionally, the EM and degradation prediction processes are automatically initiated on both Raspberry Pis. As a result, data begins to flow through the CAN bus, enabling visualization of this data within the Typhoon SCADA window.

The HEV monitoring screen displays the loads demanded by the series HEV, the vehicle speed, and the SoC of the vehicle's battery. The loads like AC, DC, V2X connection load, and losses in the vehicle depend on the user. Hence the HEV model is developed in such a way that the users can control all the loads in real-time on the vehicle, except the propulsion load, as it follows a predefined drive cycle. The energy management screen shows the data transmitted by the EM controller to the Typhoon, which displays the power allocated by the EM to the battery and ICE to match the power demanded by the vehicle. Lastly, the degradation forecasting screen presents the battery's degradation path, remaining capacity received from the DF controller and also displays the degradation rate cost, fuel cost, and total savings achieved through the proposed control strategy. The main control implementation screen is displayed in Figure 6.3. After

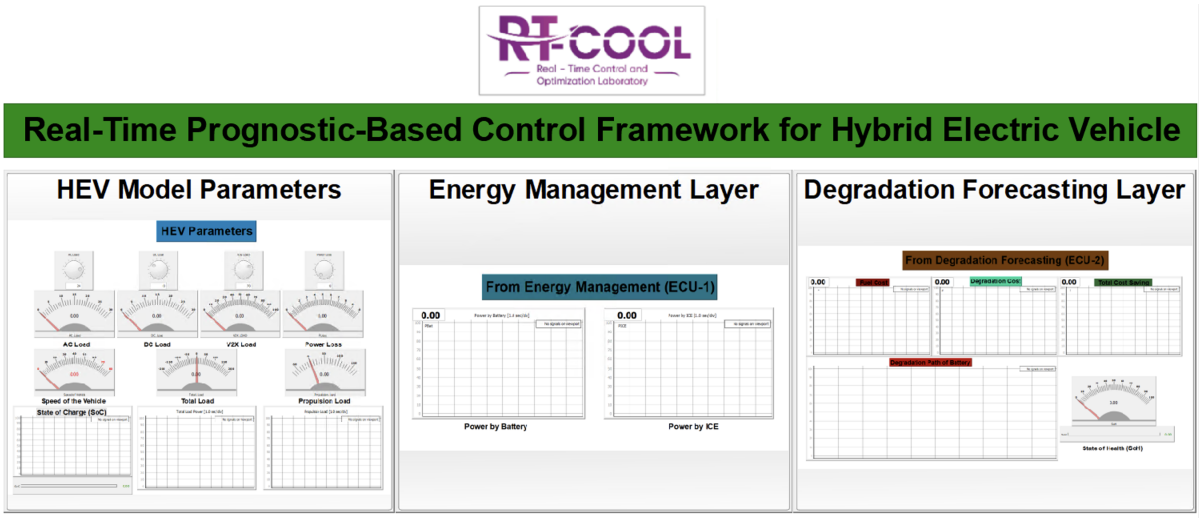

Figure 6.4: Visualization screen for CHIL experiment in SCADA window in Typhoon control center.

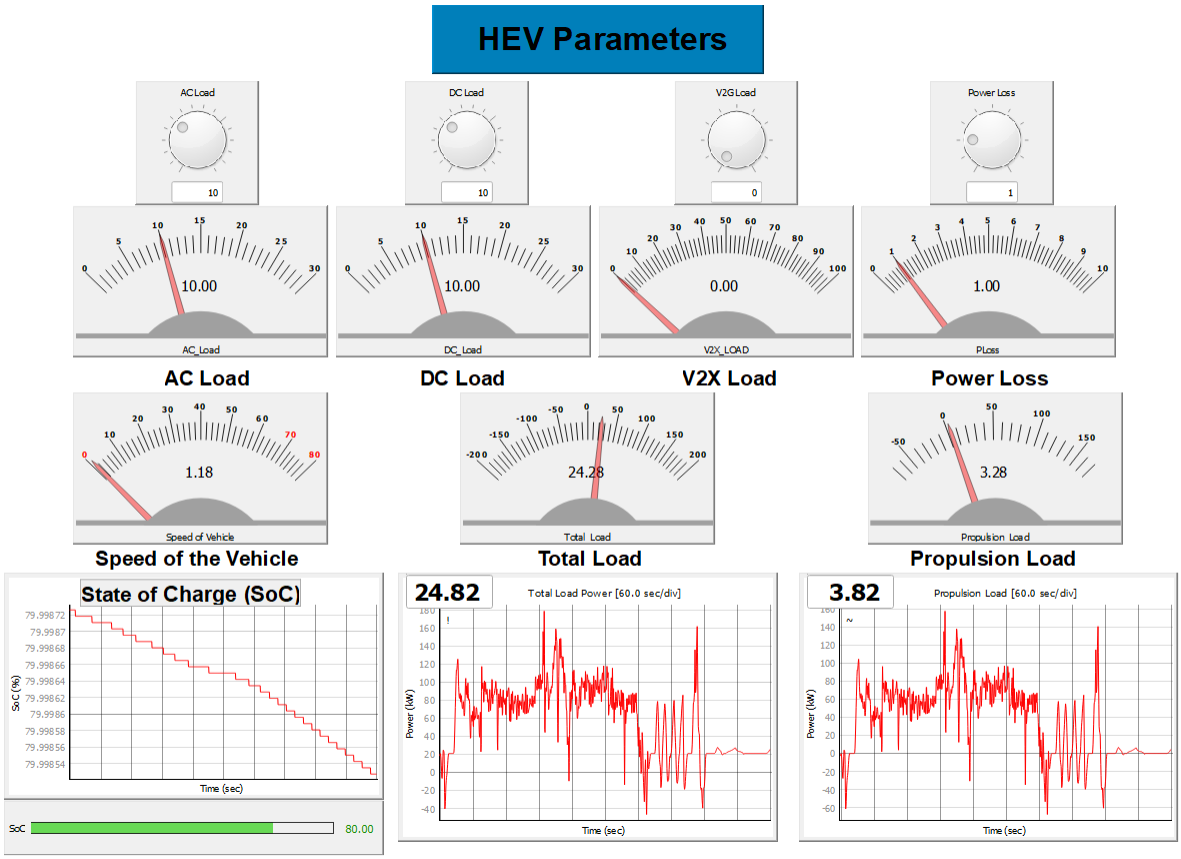

Figure 6.5: HMI display for HEV model parameters in real-time.

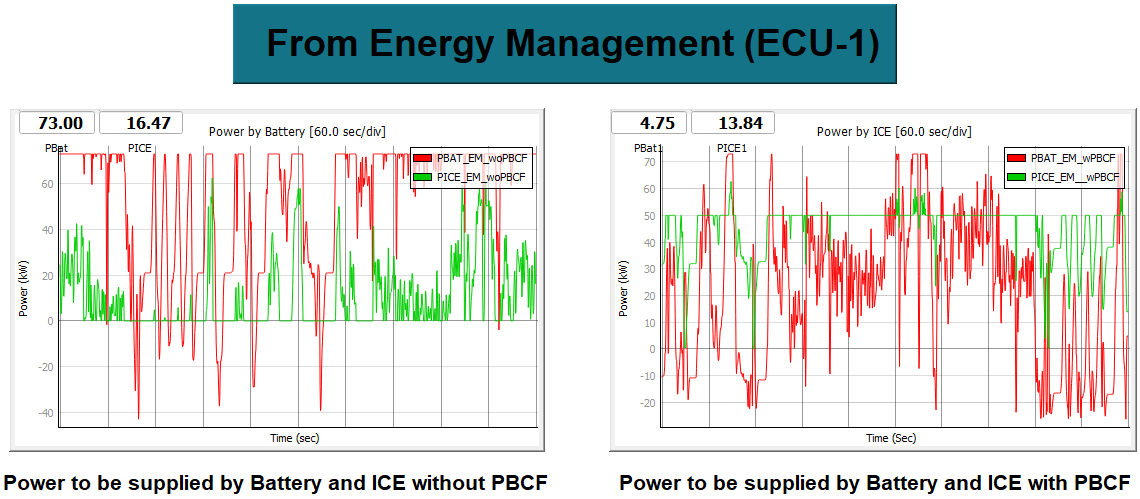

Figure 6.6: HMI display for EM layer in real-time.

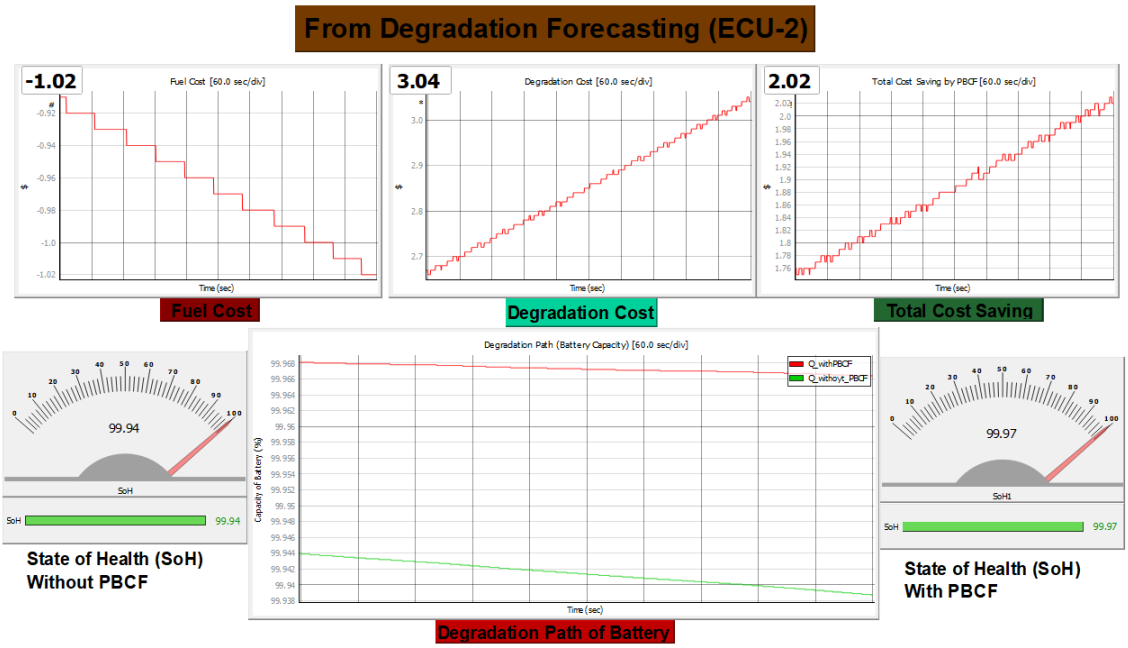

Figure 6.7: HMI display for DF layer in real-time.

pressing the start button, the CHIL experiment begins operating. Prior to pressing the start button, the user must select the Python executable file, as all the codes are written in Python, and choose the directory containing all the necessary codes for running the project in the CHIL folder shown in the figure. Figure 6.4 illustrates the main monitoring screen, which consists of three subsections: HEV monitoring, Energy

Management layer, and Degradation Forecasting Layer. Each subsection presents results from different controllers. Figure 6.5 displays the parameters of an HEV considered in this project. Figure 6.6 shows the optimized results sent from the EM layer to the Typhoon, while Figure 6.7 presents the results from the DF layer. As mentioned earlier, all data exchange between the ECUs and the DRTS is carried out using CAN communication.

6.5 Experimental Results

The constructed CHIL system described in Figures 6.1 and 6.2 is run, and the two layers, EM and DF, along with the HEV model, work synergically. Figure 6.6 shows that the proposed EM is running in real-time, and the ECU sends the data to Typhoon with the reference powers to be supplied by the ICE and battery to drive the power train. Also, in Figure 6.7, degradation signals are sent from the DF controller to HMI running in the Typhoon for displaying. It is noted that the fuel cost is increased after implementing the proposed strategy. However, the algebraic sum of degradation cost and fuel cost is positive, implying that the overall operating cost of the vehicle is reduced. Hence, the experimental results obtained from the CHIL experiment also conclude the same result obtained from the numerical simulations, as described in Chapter 5. The detailed discussion of the outcomes for each of the three scenarios outlined in Chapter 5 is presented below for the CHIL experiment.

6.5.1 Markov Chain-based Model

In line with the explanations provided in Chapter 5, the utilization of a Markov chain model for forecasting battery degradation is executed in real-time in this Chapter. Instead of running this model in MATLAB, it is deployed on a Raspberry Pi. This predictive model facilitates the computation of degradation rate cost, which is subsequently transmitted to the EM controller via CAN communication. Depending upon the received cost, the EM reallocates the power among the different sources. The comparison between the power allocations by the EM before and after the implementation of PBCF are depicted in Figures 6.8a and 6.8b.

These figures closely resemble the graphs in Figure 5.2a and 5.2b. Upon subjecting the simulation to 75 drive cycles, equivalent to 600 miles, the analysis shows a $8.2490 reduction in degradation costs. Notably, there is a $4.9216 rise in fuel costs; however, the net outcome remains a saving of $3.33. While this value slightly deviates from the findings in Chapter 5, Section 5.2. The recorded values from the real-time implementation are only slightly lower than those of the MATLAB implementation; nevertheless, both sets of results arrived at the same conclusion. It's important to highlight that the CHIL experiment effectively

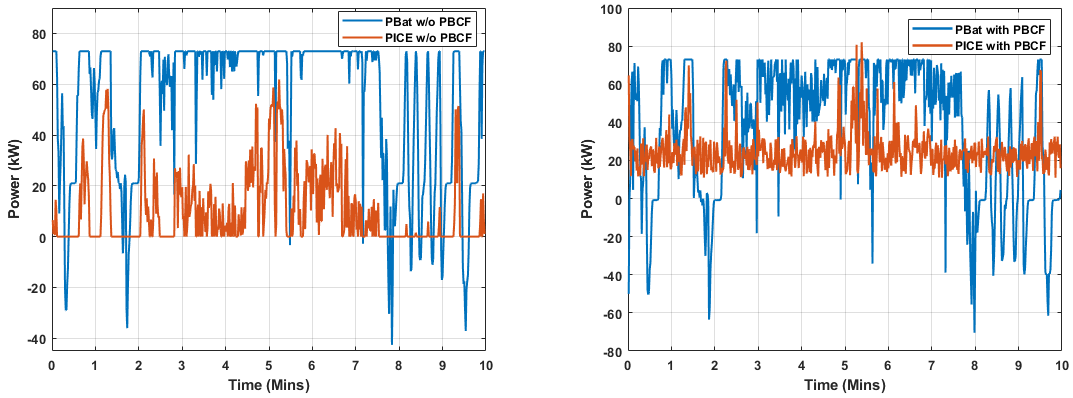

(a) (b)

Figure 6.8: Power allocation by EM: (a) without PBCF (b) With PBCF.

curtails the real-time battery degradation trajectory and concurrently decreases the overall operational expenses of the vehicle. The degradation path followed by the battery with and without PBCF is shown in Figure 6.9a, which clearly shows that after implementing the PBCF, the degradation of the battery is

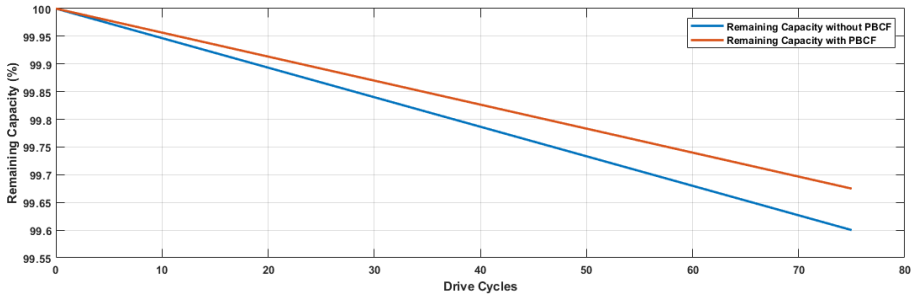

(a)

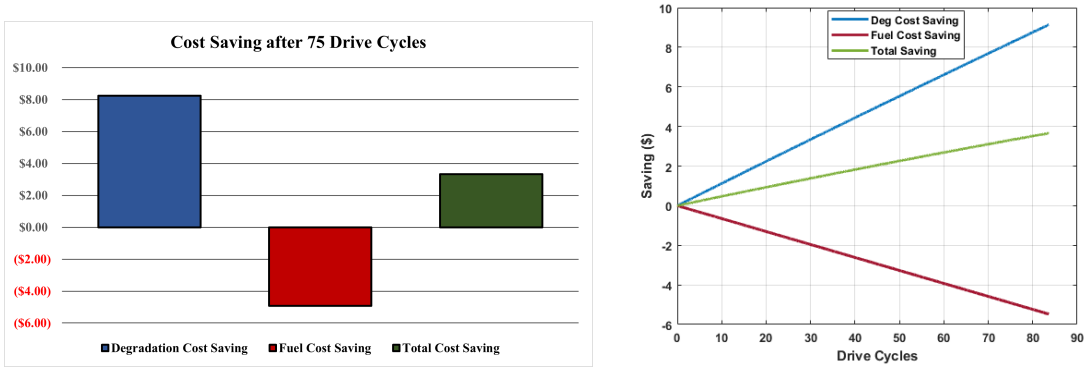

(b) (c)

Figure 6.9: (a) Degradation abatement of battery using PBCF (b)&(c) Cost saving using PBCF.

reduced. Figure 6.9b provides an overview of the cost savings achieved after implementing PBCF after 75 drive cycles. Additionally, Figure 6.9c depicts the cost savings corresponding to the number of drive cycles.

6.5.2 Neural Network based Model (Case-I)

In relation to the second scenario detailed in Chapter 5, this scenario involves utilizing a Neural Network model for predicting battery degradation paths. The real-time simulation process for this specific scenario closely parallels the methodology discussed in the previous case outlined in Section 6.5.1. The primary difference lies in the operation of ECU-2, i.e., Raspberry Pi operated as a DF layer, where the Neural Network model is employed instead of the previously used Markov chain model.

Graphs illustrating the power allocations performed by the EM before and after the incorporation of the PBCF are presented in Figures 6.10a and 6.10b. During the real-time implementation after applying PBCF, there are variations in power allocation compared to the allocations performed solely in MATLAB, as evident from Figures 5.5 and 6.10b, respectively. Nevertheless, the principle of engine load sharing is upheld, and there is consistency in the average power delivered by both the engine and the battery in both simulation scenarios.

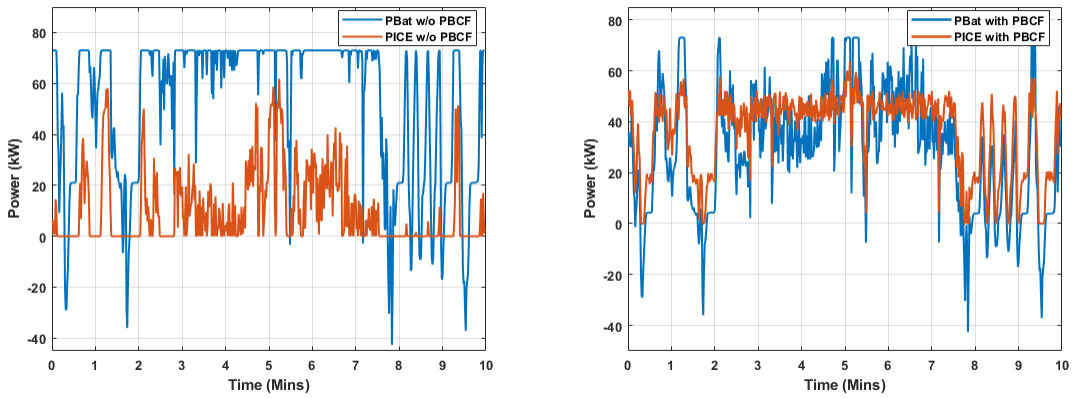

(a) (b)

Figure 6.10: Power allocation by EM: (a) without PBCF (b) With PBCF.

Upon subjecting the simulation to a total of 75 drive cycles, equivalent to covering a distance of 600 miles, the resulting battery degradation trajectory, as well as the overall implications for degradation and fuel costs, are visually depicted in Figures 6.11a and 6.11b. The real-time experiment predicts a reduction of $16.094 in degradation costs. Notably, there is a $6.7848 increase in fuel expenses due to the heightened contribution of power by the engine. Despite this, the net saving amounts to $9.3125. In comparison to the analysis done in Chapter 5, specifically in Section 5.3.1, these savings values demonstrate a consistent level

of similarity. Also, Figure 6.11c depicts the cost savings corresponding to the number of drive cycles.

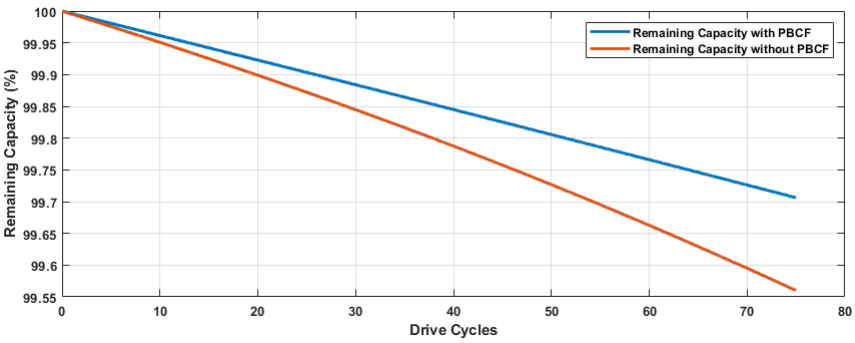

(a)

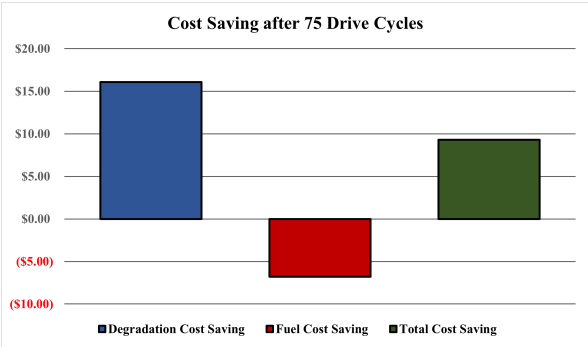

(b)

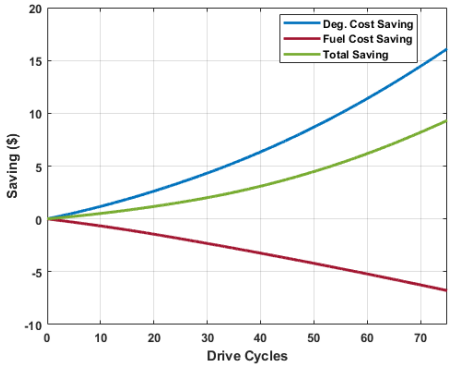

(c)

Figure 6.11: (a) Degradation abatement of battery using PBCF (b) & (c) Cost saving using PBCF.

6.5.3 Neural Network-based Model (Case-II)

Similarly, for the third scenario, as explained in Chapter 5, a new combined drive cycle is employed, using US06 and WLTP, which accentuates battery degradation. The real-time simulation for this particular scenario is similar; however, the drive cycle utilized in Typhoon to operate the HEV is modified, with everything else remaining consistent, as compared to Sections 6.5.1 and 6.5.2.

Graphs illustrating power allocations by the EM before and after the integration of the PBCF are presented in Figures 6.12a and 6.12b. While Figure 6.12a bears a resemblance to Figure 5.9a from chapter 5, there exists a disparity in the graph portrayed in Figure 5.9b, as it diverges from the real-time implementation depicted in Figure 6.12b. However, the concept of sharing the load by the engine is followed in both cases.

After subjecting the simulation to 27 drive cycles, corresponding to a distance of 606 miles, the analysis discloses a $19.63 reduction in degradation costs. Noteworthy is the $7.11 increase in fuel expenses as

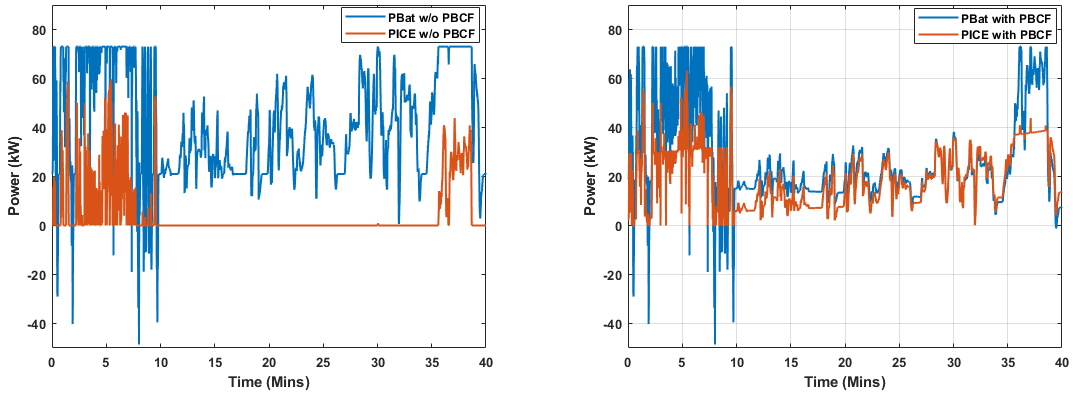

(a) (b)

Figure 6.12: Power allocation by EM: (a) without PBCF (b) With PBCF.

the engine supplies more power; nevertheless, the net saving is $12.52. While comparing these findings with those in Chapter 6, Section 5.3.2, the savings values exhibit a minor elevation while maintaining proximity. Also, Figure 6.13c depicts the cost savings corresponding to the number of drive cycles.

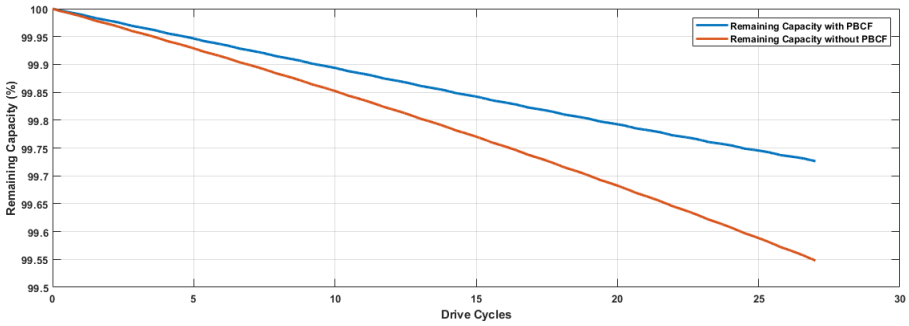

(a)

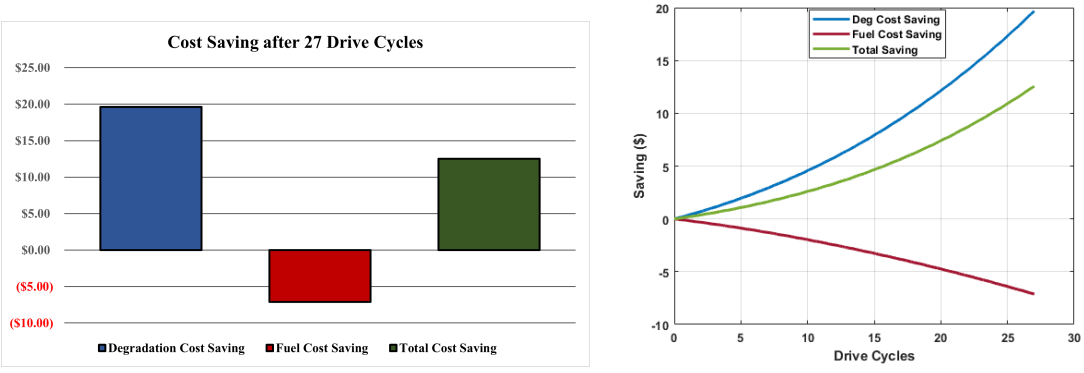

(b) (c)

Figure 6.13: (a) Degradation abatement of battery using PBCF (b)&(c) Cost saving using PBCF.

It is crucial to emphasize that this approach successfully addresses battery degradation trajectories in real-time, concurrently reducing the overall operational costs of the vehicle. Moreover, a consistent observation in all three real-time scenario simulations is that higher levels of battery degradation align with increased savings following the implementation of PBCF.

6.6 Comparison with Numerical Simulation Results

The collective outcomes derived from both the MATLAB/Simulink simulation and the CHIL experiment are presented in Table 6.1. For the Markov-chain based degradation model, there exist slight disparities in the results obtained from the NS and CHIL experiments. Nonetheless, these differences are minor, and the fundamental concept of the PBCF strategy is upheld: battery degradation is reduced in both simulation environments. Additionally, the results for Neural Network case I and case II exhibit remarkable similarity for the other two scenarios, with only marginal distinctions between NS and CHIL experiments.

Table 6.1: Comparison of Simulation Results from MATLAB and CHIL Experiment

Methods	**Markov Chain**	**Neural Network (Case-I)**	**Neural Network (Case-II)**
Capacity Loss Saving (NS)	0.0981%	0.1464%	0.1732%
Capacity Loss Saving (CHIL)	0.0749%	0.1460%	0.1787%
Degradation Cost (NS)	$10.8045	$15.82	$19.47
Degradation Cost (CHIL)	$8.2590	$16.094	$19.63
Fuel Cost (NS)	-$5.9808	-$6.7019	-$8.49
Fuel Cost (CHIL)	-$4.9216	-$6.7848	-$7.11
Total Saving (NS)	$4.8237	$9.1181	$10.98
Total Saving (CHIL)	$3.33	$9.3125	$12.52

Hence, we can deduce that the results from both simulations align, confirming that the implementation of the PBCF effectively mitigates battery degradation in HEVs, simultaneously reducing the overall operational costs of the vehicle. Furthermore, it's worth noting that the degree of battery degradation directly corresponds to the extent of savings achieved upon integrating the PBCF.

Chapter 7

Conclusion

The primary objective of this dissertation is to develop a control framework, named as the prognostic-based control framework (PBCF), for hybrid electric vehicles (HEVs). The framework aims to mitigate battery degradation in the vehicle and simultaneously minimize the vehicle's overall operating cost. To achieve this objective, several existing challenges need to be addressed. First and foremost, predicting the battery's degradation path, considering all contributing factors, remains a significant hurdle. Additionally, there is a notable absence of a degradation forecasting layer seamlessly integrated into the control architecture of HEVs. Another critical challenge involves finding a mechanism to incorporate insights from the degradation prediction into the objective function of the energy management (EM) system. This integration is essential for enabling real-time operation of the updated EM.

1. The prediction of the battery's degradation path, encompassing all the contributing factors, remains a significant issue.
2. The absence of a degradation forecasting framework that seamlessly integrates into the control architecture of HEVs is a notable gap.
3. A crucial challenge involves devising a mechanism to incorporate the findings from degradation prediction layer (obtained from point 2) into the objective function of the energy management (EM) system and enable real-time operation of the updated EM.

To address the identified gap, this dissertation make the following contributions:

- In Chapter 3, analytical and data-driven degradation modeling techniques are introduced to predict the battery's degradation path while considering four major factors that contribute to degradation. For the analytical method, a Markov chain-based model is employed to predict the battery's degradation

behaviors, utilizing a multi-state model. Additionally, for the data-driven method, three distinct neural networks are developed to forecast the battery's degradation path.

- In Chapter 4, a prognostic-based control framework (PBCF) is proposed. This framework includes a degradation forecasting layer that predicts the battery's degradation based on the vehicle's operating conditions. The degradation forecasting layer is integrated into the existing control architecture of the HEV as an upper layer of the energy management system (EM). By implementing this strategy, the battery degradation and overall operating cost of the vehicle are reduced, while maintaining the vehicle's performance.
- In Chapter 5 and 6 Simulations using MATLAB/Simulink and CHIL experiment are performed to validate the proposed strategy PBCF, respectively. To validate and assess the viability of the proposed framework, three distinct scenarios with varying levels of battery degradation and different drive cycles are employed.

By addressing these research challenges and presenting the proposed solutions, this dissertation makes a significant contribution to the advancement of PBCF for HEVs. It introduces capabilities for real-time degradation prediction and minimization, resulting in a reduction in the overall operating cost of the vehicle and an extension of the battery lifespan. Notably, the implementation of PBCF leads to higher savings on the overall vehicle operation, particularly as the battery degradation increases.

Bibliography

[1] C.C. Chan. The state of the art of electric and hybrid vehicles. *Proceedings of the IEEE*, 90(2):247–275, 2002.

[2] U.S. Energy Information Administration. Monthly energy review, table 2.1. `https://www.eia.gov/energyexplained/use-of-energy`. Accessed: 01/11/2022.

[3] U.S. Energy Information Administration. Monthly energy review. `https://www.eia.gov/todayinenergy/detail.php?id=48856`. Accessed: 01/11/2022.

[4] U.S. Environment Protection Agency. U.s. transportation sector greenhouse gas emissions 1990-2020. `https://www.epa.gov/greenvehicles/fast-facts-transportation-greenhouse-gas-emissions`. Accessed: 01/16/2022.

[5] Behnaz Papari, Payam Badr, Douglas Scruggs, Ali Arsalan, Phani Kumar Chamarthi, Ali Moghassemi, Laxman Timilsina, Gokan Ozkan, and Christopher S Edrington. An advanced meta metrics-based approach to assess an appropriate optimization method for wind/pv/battery based hybrid ac-dc microgrid. *Sustainability*, 2023.

[6] K Jorgensen. Technologies for electric, hybrid and hydrogen vehicles: Electricity from renewable energy sources in transport. *Utilities Policy*, 16(2):72–79, 2008.

[7] Irena. Global renewables outlook: Energy transformation 2050, 2020.

[8] Industry Steering Committee et al. Electric vehicle technology roadmap for canada: a strategic vision for highway-capable battery-electric, plug-in and other hybrid-electric vehicles. *Natural Resources Canada*, 2009.

[9] Anna Tomaszewska, Zhengyu Chu, Xuning Feng, Simon O'kane, Xinhua Liu, Jingyi Chen, Chenzhen Ji, Elizabeth Endler, Ruihe Li, Lishuo Liu, et al. Lithium-ion battery fast charging: A review. *ETransportation*, 1:100011, 2019.

[10] Zhengming John Zhang, Weifeng Fang, and Ruijun Ma. Brief review of batteries for xev applications. *eTransportation*, 2:100032, 2019.

[11] Phuong H Hoang, Gokhan Ozkan, Payam Badr, Laxman Timilsina, and Christopher Edrington. A prognostic based control framework for hybrid electric vehicles. Technical report, SAE Technical Paper, 2022.

[12] Mahammad A Hannan, FA Azidin, and Azah Mohamed. Hybrid electric vehicles and their challenges: A review. *Renewable and Sustainable Energy Reviews*, 29:135–150, 2014.

[13] Srdjan M Lukic, Jian Cao, Ramesh C Bansal, Fernando Rodriguez, and Ali Emadi. Energy storage systems for automotive applications. *IEEE Transactions on industrial electronics*, 55(6):2258–2267, 2008.

[14] Junye Wang, Hualin Wang, and Yi Fan. Techno-economic challenges of fuel cell commercialization. *Engineering*, 4(3):352–360, 2018.

[15] Laxman Timilsina, Payam R Badr, Phuong H Hoang, Gokhan Ozkan, Behnaz Papari, and Christopher S Edrington. Battery degradation in electric and hybrid electric vehicles: A survey study. *IEEE Access*, 2023.

[16] Patrick Lailler, Jean-François Sarrau, and Christian Sarrazin. Comparative study for "36 v" vehicle applications: advantages of lead-acid batteries. *Journal of power sources*, 95(1-2):58–67, 2001.

[17] Xiayue Fan, Bin Liu, Jie Liu, Jia Ding, Xiaopeng Han, Yida Deng, Xiaojun Lv, Ying Xie, Bing Chen, Wenbin Hu, et al. Battery technologies for grid-level large-scale electrical energy storage. *Transactions of Tianjin University*, 26(2):92–103, 2020.

[18] Katerina E Aifantis, Stephen A Hackney, and R Vasant Kumar. *High energy density lithium batteries*. Wiley Online Library, 2010.

[19] Ernest Henry Wakefield. *History of the electric automobile-hybrid electric vehicles*, volume 187. 1998.

[20] Siang Fui Tie and Chee Wei Tan. A review of energy sources and energy management system in electric vehicles. *Renewable and sustainable energy reviews*, 20:82–102, 2013.

[21] Ali Moghassemi, Laxman Timilsina, S M Imrat Rahman, Ali Arsalan, Phani Kumar Chamarthi, Gokhan Papari, Ozkan, Behnaz Papari, Christopher S Edrington, and Zhyeu Zhang. Nearest level control based modular multi-level converters for power electronics building blocks concept in electric ship system. *IEEE Transactions on Transportation Electrification*, 2023.

[22] Phani K Chamarthi, Ali Moghassemi, S M Imrat Rahman, Laxman Timilsina, Gokhan Ozkan, Behnaz Papari, and Christopher S Edrington. A novel four switch transformerless inverter with step up/down capability for pv fed grid connected systems. In *2024 IEEE Transportation Electrification Conference & Expo (ITEC)*. IEEE, 2024.

[23] Omonowo D Momoh and Michael O Omoigui. An overview of hybrid electric vehicle technology. In *2009 IEEE vehicle power and propulsion conference*, pages 1286–1292. Ieee, 2009.

[24] Oak Ridge National Laboratory U.S. Department of Energy, Energy Vehicle Technologies Office. Transportation energy data book. `https://tedb.ornl.gov/data/asofJun.21,2022.` Accessed: 05/18/2022.

[25] Bloomberg. Batteries for electric cars speed toward a tipping point. 134, 2020.

[26] Laxman Timilsina, Okan Ciftci, Ali Moghassemi, S M Imrat Rahman, Phani K Chamarthi, Gokhan Ozkan, Behnaz Papari, and Christopher S Edrington. A dual energy management for hybrid electric vehicle. In *2024 IEEE Transportation Electrification Conference & Expo (ITEC)*. IEEE, 2024.

[27] Ziyou Song, Heath Hofmann, Jianqiu Li, Jun Hou, Xuebing Han, and Minggao Ouyang. Energy management strategies comparison for electric vehicles with hybrid energy storage system. *Applied Energy*, 134:321–331, 2014.

[28] Siang Fui Tie and Chee Wei Tan. A review of energy sources and energy management system in electric vehicles. *Renewable and Sustainable Energy Reviews*, 20:82–102, 2013.

[29] A. Sciarretta, L. Serrao, P. C. Dewangan, P. Tona, E. N.D. Bergshoeff, C. Bordons, L. Charmpa, Ph Elbert, L. Eriksson, T. Hofman, M. Hubacher, P. Isenegger, F. Lacandia, A. Laveau, H. Li, D. Marcos, T. Nüesch, S. Onori, P. Pisu, J. Rios, E. Silvas, M. Sivertsson, L. Tribioli, A. J. van der Hoeven, and M. Wu. A control benchmark on the energy management of a plug-in hybrid electric vehicle. *Control Engineering Practice*, 29:287–298, 2014.

[30] Lorenzo Serrao, Simona Onori, and Giorgio Rizzoni. A comparative analysis of energy management strategies for hybrid electric vehicles. 2011.

[31] Emilia Silvas, Theo Hofman, Nikolce Murgovski, LF Pascal Etman, and Maarten Steinbuch. Review of optimization strategies for system-level design in hybrid electric vehicles. *IEEE Transactions on Vehicular Technology*, 66(1):57–70, 2016.

[32] Fei Ju, Nikolce Murgovski, Weichao Zhuang, Xiaosong Hu, Ziyou Song, and Liangmo Wang. Predictive energy management with engine switching control for hybrid electric vehicle via admm. *Energy*, 263:125971, 2023.

[33] Domenico Bianchi, Luciano Rolando, Lorenzo Serrao, Simona Onori, Giorgio Rizzoni, Nazar Al-Khayat, Tung-Ming Hsieh, and Pengju Kang. A rule-based strategy for a series/parallel hybrid electric vehicle: an approach based on dynamic programming. In *Dynamic Systems and Control Conference*, volume 44175, pages 507–514, 2010.

[34] Jianwei Li, Hongwen He, Zhongbao Wei, and Xudong Zhang. Hierarchical sizing and power distribution strategy for hybrid energy storage system. *Automotive Innovation*, 4:440–447, 2021.

[35] Li Tang, Giorgio Rizzoni, and Simona Onori. Energy management strategy for hevs including battery life optimization. *IEEE Transactions on Transportation Electrification*, 1(3):211–222, 2015.

[36] Chong Zhu, Fei Lu, Hua Zhang, Jing Sun, and Chunting Chris Mi. A real-time battery thermal management strategy for connected and automated hybrid electric vehicles (cahevs) based on iterative dynamic programming. *IEEE Transactions on Vehicular Technology*, 67(9):8077–8084, 2018.

[37] Xuebing Han, Minggao Ouyang, Languang Lu, Jianqiu Li, Yuejiu Zheng, and Zhe Li. A comparative study of commercial lithium ion battery cycle life in electrical vehicle: Aging mechanism identification. *Journal of Power Sources*, 251:38–54, 2014.

[38] Kandler Smith, Tony Markel, Gi-Heon Kim, and Ahmad Pesaran. Design of electric drive vehicle batteries for long life and low cost. In *Accelerated Stress Testing and Reliability (ASTR), IEE Workshop on*, pages 6–8, 2010.

[39] Ozan Erdinc, Bulent Vural, and Mehmet Uzunoglu. A dynamic lithium-ion battery model considering the effects of temperature and capacity fading. In *2009 International Conference on Clean Electrical Power*, pages 383–386. IEEE, 2009.

[40] Ira Boudway and B Hyperdrve. Batteries for electric cars speed toward a tipping point. *https://www. bloomberg. com/news/articles/2020-12-16/electric-cars-are-about-to-be-as-cheap-as-gas-powered-models. Checked on*, 2:2021, 2020.

[41] Pallavi Verma, Pascal Maire, and Petr Novák. A review of the features and analyses of the solid electrolyte interphase in li-ion batteries. *Electrochimica Acta*, 55(22):6332–6341, 2010.

[42] Naoki Nitta, Feixiang Wu, Jung Tae Lee, and Gleb Yushin. Li-ion battery materials: present and future. *Materials today*, 18(5):252–264, 2015.

[43] Poulomi Roy and Suneel Kumar Srivastava. Nanostructured anode materials for lithium ion batteries. *Journal of Materials Chemistry A*, 3(6):2454–2484, 2015.

[44] Xuebing Han, Languang Lu, Yuejiu Zheng, Xuning Feng, Zhe Li, Jianqiu Li, and Minggao Ouyang. A review on the key issues of the lithium ion battery degradation among the whole life cycle. *ETransportation*, 1:100005, 2019.

[45] Peter M Attia, Alexander Bills, Ferran Brosa Planella, Philipp Dechent, Goncalo Dos Reis, Matthieu Dubarry, Paul Gasper, Richard Gilchrist, Samuel Greenbank, David Howey, et al. "knees" in lithium-ion battery aging trajectories. *Journal of The Electrochemical Society*, 169(6):060517, 2022.

[46] Matthieu Dubarry, Cyril Truchot, and Bor Yann Liaw. Synthesize battery degradation modes via a diagnostic and prognostic model. *Journal of power sources*, 219:204–216, 2012.

[47] Matthieu Dubarry, George Baure, and Arnaud Devie. Durability and reliability of ev batteries under electric utility grid operations: path dependence of battery degradation. *Journal of The Electrochemical Society*, 165(5):A773, 2018.

[48] Phuong H Hoang, Gokhan Ozkan, Payam Ramezani Badr, Laxman Timilsina, Behnaz Papari, and Christopher S Edrington. Integrating degradation forecasting into distribution grids' advanced distribution management systems. *International Journal of Electrical Power & Energy Systems*, 150:109071, 2023.

[49] Peter M Attia, William C Chueh, and Stephen J Harris. Revisiting the t0. 5 dependence of sei growth. *Journal of the Electrochemical Society*, 167(9):090535, 2020.

[50] Xiaowei Ma, Jessie E Harlow, Jing Li, Lin Ma, David S Hall, Samuel Buteau, Matthew Genovese, Marc Cormier, and JR Dahn. Hindering rollover failure of li [ni0. 5mn0. 3co0. 2] o2/graphite pouch cells during long-term cycling. *Journal of The Electrochemical Society*, 166(4):A711, 2019.

[51] Paula Fermín-Cueto, Euan McTurk, Michael Allerhand, Encarni Medina-Lopez, Miguel F Anjos, Joel Sylvester, and Goncalo Dos Reis. Identification and machine learning prediction of knee-point and knee-onset in capacity degradation curves of lithium-ion cells. *Energy and AI*, 1:100006, 2020.

[52] Selcuk Atalay, Muhammad Sheikh, Alessandro Mariani, Yu Merla, Ed Bower, and W Dhammika Widanage. Theory of battery ageing in a lithium-ion battery: Capacity fade, nonlinear ageing and lifetime prediction. *Journal of Power Sources*, 478:229026, 2020.

[53] Daniel Müller, Thomas Dufaux, and Kai Peter Birke. Model-based investigation of porosity profiles in graphite anodes regarding sudden-death and second-life of lithium ion cells. *Batteries*, 5(2):49, 2019.

[54] Xianke Lin, Jonghyun Park, Lin Liu, Yoonkoo Lee, AM Sastry, and Wei Lu. A comprehensive capacity fade model and analysis for li-ion batteries. *Journal of The Electrochemical Society*, 160(10):A1701, 2013.

[55] Matthieu Dubarry, George Baure, and David Anseán. Perspective on state-of-health determination in lithium-ion batteries. *Journal of Electrochemical Energy Conversion and Storage*, 17(4), 2020.

[56] Ruqing Fang, Peng Dong, Hao Ge, Jiangtao Fu, Zhe Li, and Jianbo Zhang. Capacity plunge of lithium-ion batteries induced by electrolyte drying-out: Experimental and modeling study. *Journal of Energy Storage*, 42:103013, 2021.

[57] Jacqueline Sophie Edge, Simon O'Kane, Ryan Prosser, Niall D Kirkaldy, Anisha N Patel, Alastair Hales, Abir Ghosh, Weilong Ai, Jingyi Chen, Jason Jiang, et al. Lithium ion battery degradation: what you need to know. *Physical Chemistry Chemical Physics*, 2021.

[58] Christoph R Birkl, Matthew R Roberts, Euan McTurk, Peter G Bruce, and David A Howey. Degradation diagnostics for lithium ion cells. *Journal of Power Sources*, 341:373–386, 2017.

[59] Xiaosong Hu, Le Xu, Xianke Lin, and Michael Pecht. Battery lifetime prognostics. *Joule*, 4(2):310–346, 2020.

[60] Jens Vetter, Petr Novák, Markus Robert Wagner, Claudia Veit, K-C Möller, JO Besenhard, Martin Winter, Margret Wohlfahrt-Mehrens, Christoph Vogler, and Abderrezak Hammouche. Ageing mechanisms in lithium-ion batteries. *Journal of power sources*, 147(1-2):269–281, 2005.

[61] Ratnakumar V Bugga and Marshall C Smart. Lithium plating behavior in lithium-ion cells. *Ecs Transactions*, 25(36):241, 2010.

[62] Carlos Pastor-Fernández, Kotub Uddin, Gael H Chouchelamane, W Dhammika Widanage, and James Marco. A comparison between electrochemical impedance spectroscopy and incremental capacity-differential voltage as li-ion diagnostic techniques to identify and quantify the effects of degradation modes within battery management systems. *Journal of Power Sources*, 360:301–318, 2017.

[63] Shabbir Ahmed, Ira Bloom, Andrew N Jansen, Tanvir Tanim, Eric J Dufek, Ahmad Pesaran, Andrew Burnham, Richard B Carlson, Fernando Dias, Keith Hardy, et al. Enabling fast charging–a battery technology gap assessment. *Journal of Power Sources*, 367:250–262, 2017.

[64] F Grimsmann, F Brauchle, T Gerbert, A Gruhle, J Parisi, and M Knipper. Impact of different aging mechanisms on the thickness change and the quick-charge capability of lithium-ion cells. *Journal of Energy Storage*, 14:158–162, 2017.

[65] Tanvir R Tanim, Eric J Dufek, Michael Evans, Charles Dickerson, Andrew N Jansen, Bryant J Polzin, Alison R Dunlop, Stephen E Trask, Ryan Jackman, Ira Bloom, et al. Extreme fast charge challenges for lithium-ion battery: variability and positive electrode issues. *Journal of The Electrochemical Society*, 166(10):A1926, 2019.

[66] ER Logan and JR Dahn. Electrolyte design for fast-charging li-ion batteries. *Trends in Chemistry*, 2(4):354–366, 2020.

[67] Ping Liu, John Wang, Jocelyn Hicks-Garner, Elena Sherman, Souren Soukiazian, Mark Verbrugge, Harshad Tataria, James Musser, and Peter Finamore. Aging mechanisms of lifepo4 batteries deduced by electrochemical and structural analyses. *Journal of the Electrochemical Society*, 157(4):A499, 2010.

[68] Huanhuan Wang, Haisheng Wang, Shi Chen, Bowei Zhang, Guang Yang, Peng Gao, Jilei Liu, Xiaofeng Fan, Yizhong Huang, Jianyi Lin, et al. A depth-profiling study on the solid electrolyte interface: bis (fluorosulfuryl) imide anion toward improved k+ storage. *ACS Applied Energy Materials*, 2(11):7942–7951, 2019.

[69] Yuhang Shan, Libo Li, and Xueying Yang. Solid-state polymer electrolyte solves the transfer of lithium ions between the solid–solid interface of the electrode and the electrolyte in lithium–sulfur and lithium-ion batteries. *ACS Applied Energy Materials*, 4(5):5101–5112, 2021.

[70] Izaro Laresgoiti, Stefan Käbitz, Madeleine Ecker, and Dirk Uwe Sauer. Modeling mechanical degradation in lithium ion batteries during cycling: Solid electrolyte interphase fracture. *Journal of Power Sources*, 300:112–122, 2015.

[71] Bolun Xu, Alexandre Oudalov, Andreas Ulbig, Göran Andersson, and Daniel S Kirschen. Modeling of lithium-ion battery degradation for cell life assessment. *IEEE Transactions on Smart Grid*, 9(2):1131–1140, 2016.

[72] Michel Broussely, Ph Biensan, F Bonhomme, Ph Blanchard, S Herreyre, K Nechev, and RJ Staniewicz. Main aging mechanisms in li ion batteries. *Journal of power sources*, 146(1-2):90–96, 2005.

[73] Xianke Lin, Kavian Khosravinia, Xiaosong Hu, Ju Li, and Wei Lu. Lithium plating mechanism, detection, and mitigation in lithium-ion batteries. *Progress in Energy and Combustion Science*, 87:100953, 2021.

[74] Pankaj Arora, Marc Doyle, and Ralph E White. Mathematical modeling of the lithium deposition overcharge reaction in lithium-ion batteries using carbon-based negative electrodes. *Journal of The Electrochemical Society*, 146(10):3543, 1999.

[75] Nathalie Legrand, Bernard Knosp, Philippe Desprez, François Lapicque, and Stéphane Raël. Physical characterization of the charging process of a li-ion battery and prediction of li plating by electrochemical modelling. *Journal of Power Sources*, 245:208–216, 2014.

[76] Rajeswari Chandrasekaran. Quantification of bottlenecks to fast charging of lithium-ion-insertion cells for electric vehicles. *Journal of Power Sources*, 271:622–632, 2014.

[77] Simon Hein and Arnulf Latz. Influence of local lithium metal deposition in 3d microstructures on local and global behavior of lithium-ion batteries. *Electrochimica Acta*, 201:354–365, 2016.

[78] Hansen Wang, Yangying Zhu, Sang Cheol Kim, Allen Pei, Yanbin Li, David T Boyle, Hongxia Wang, Zewen Zhang, Yusheng Ye, William Huang, et al. Underpotential lithium plating on graphite anodes caused by temperature heterogeneity. *Proceedings of the National Academy of Sciences*, 117(47):29453–29461, 2020.

[79] Stephen J Harris, Adam Timmons, Daniel R Baker, and Charles Monroe. Direct in situ measurements of li transport in li-ion battery negative electrodes. *Chemical Physics Letters*, 485(4-6):265–274, 2010.

[80] Tao Gao, Yu Han, Dimitrios Fraggedakis, Supratim Das, Tingtao Zhou, Che-Ning Yeh, Shengming Xu, William C Chueh, Ju Li, and Martin Z Bazant. Interplay of lithium intercalation and plating on a single graphite particle. *Joule*, 5(2):393–414, 2021.

[81] Ting Guan, Shun Sun, Fengbin Yu, Yunzhi Gao, Peng Fan, Pengjian Zuo, Chunyu Du, and Geping Yin. The degradation of licoo2/graphite batteries at different rates. *Electrochimica Acta*, 279:204–212, 2018.

[82] Dongxu Ouyang, Yaping He, Jingwen Weng, Jiahao Liu, Mingyi Chen, and Jian Wang. Influence of low temperature conditions on lithium-ion batteries and the application of an insulation material. *RSC advances*, 9(16):9053–9066, 2019.

[83] Lu Zhang, Zhengcheng Zhang, Paul C Redfern, Larry A Curtiss, and Khalil Amine. Molecular engineering towards safer lithium-ion batteries: a highly stable and compatible redox shuttle for overcharge protection. *Energy & Environmental Science*, 5(8):8204–8207, 2012.

[84] Daniel Juarez-Robles, Anjul Arun Vyas, Conner Fear, Judith A Jeevarajan, and Partha P Mukherjee. Overcharge and aging analytics of li-ion cells. *Journal of The Electrochemical Society*, 167(9):090547, 2020.

[85] Madeleine Ecker, Pouyan Shafiei Sabet, and Dirk Uwe Sauer. Influence of operational condition on lithium plating for commercial lithium-ion batteries–electrochemical experiments and post-mortem-analysis. *Applied energy*, 206:934–946, 2017.

[86] Marie Kerlau, Marek Marcinek, Venkat Srinivasan, and Robert M Kostecki. Reprint of "studies of local degradation phenomena in composite cathodes for lithium-ion batteries". *Electrochimica Acta*, 53(3):1385–1392, 2007.

[87] Yongyao Xia, Yunhong Zhou, and Masaki Yoshio. Capacity fading on cycling of 4 v li/limn2 o 4 cells. *Journal of The Electrochemical Society*, 144(8):2593, 1997.

[88] Honghe Zheng, Qingna Sun, Gao Liu, Xiangyun Song, and Vincent S Battaglia. Correlation between dissolution behavior and electrochemical cycling performance for lini1/3co1/3mn1/3o2-based cells. *Journal of Power Sources*, 207:134–140, 2012.

[89] Neeraj Sharma, Vanessa K Peterson, Margaret M Elcombe, Maxim Avdeev, Andrew J Studer, Ned Blagojevic, Rozila Yusoff, and Norlida Kamarulzaman. Structural changes in a commercial lithium-ion battery during electrochemical cycling: An in situ neutron diffraction study. *Journal of Power Sources*, 195(24):8258–8266, 2010.

[90] Gholam-Abbas Nazri and Gianfranco Pistoia. *Lithium batteries: science and technology*. Springer Science & Business Media, 2008.

[91] Noshin Omar, Mohamed Abdel Monem, Yousef Firouz, Justin Salminen, Jelle Smekens, Omar Hegazy, Hamid Gaulous, Grietus Mulder, Peter Van den Bossche, Thierry Coosemans, et al. Lithium iron phosphate based battery–assessment of the aging parameters and development of cycle life model. *Applied Energy*, 113:1575–1585, 2014.

[92] Saurabh Saxena, Yinjiao Xing, Daeil Kwon, and Michael Pecht. Accelerated degradation model for c-rate loading of lithium-ion batteries. *International journal of electrical power & energy systems*, 107:438–445, 2019.

[93] Matthieu Dubarry, Nan Qin, and Paul Brooker. Calendar aging of commercial li-ion cells of different chemistries–a review. *Current Opinion in Electrochemistry*, 9:106–113, 2018.

[94] Madeleine Ecker, Nerea Nieto, Stefan Käbitz, Johannes Schmalstieg, Holger Blanke, Alexander Warnecke, and Dirk Uwe Sauer. Calendar and cycle life study of li (nimnco) o2-based 18650 lithium-ion batteries. *Journal of Power Sources*, 248:839–851, 2014.

[95] E Sarasketa-Zabala, I Gandiaga, LM Rodriguez-Martinez, and I Villarreal. Calendar ageing analysis of a lifepo4/graphite cell with dynamic model validations: Towards realistic lifetime predictions. *Journal of Power Sources*, 272:45–57, 2014.

[96] Samuel Pelletier, Ola Jabali, Gilbert Laporte, and Marco Veneroni. Battery degradation and behaviour for electric vehicles: Review and numerical analyses of several models. *Transportation Research Part B: Methodological*, 103:158–187, 2017.

[97] Elixabet Sarasketa-Zabala, I Laresgoiti, I Alava, M Rivas, Iogr Villarreal, and F Blanco. Validation of the methodology for lithium-ion batteries lifetime prognosis. In *2013 World Electric Vehicle Symposium and Exhibition (EVS27)*, pages 1–12. IEEE, 2013.

[98] Saeid Bashash, Scott J Moura, Joel C Forman, and Hosam K Fathy. Plug-in hybrid electric vehicle charge pattern optimization for energy cost and battery longevity. *Journal of power sources*, 196(1):541–549, 2011.

[99] J Belt, V Utgikar, and I Bloom. Calendar and phev cycle life aging of high-energy, lithium-ion cells containing blended spinel and layered-oxide cathodes. *Journal of Power Sources*, 196(23):10213–10221, 2011.

[100] Maik Naumann, Michael Schimpe, Peter Keil, Holger C Hesse, and Andreas Jossen. Analysis and modeling of calendar aging of a commercial lifepo4/graphite cell. *Journal of Energy Storage*, 17:153–169, 2018.

[101] Eric Prada, D Di Domenico, Y Creff, J Bernard, Valérie Sauvant-Moynot, and François Huet. A simplified electrochemical and thermal aging model of lifepo4-graphite li-ion batteries: power and capacity fade simulations. *Journal of The Electrochemical Society*, 160(4):A616, 2013.

[102] Sébastien Grolleau, Arnaud Delaille, Hamid Gualous, Philippe Gyan, Renaud Revel, Julien Bernard, Eduardo Redondo-Iglesias, Jérémy Peter, and SIMCAL Network. Calendar aging of commercial graphite/lifepo4 cell–predicting capacity fade under time dependent storage conditions. *Journal of Power Sources*, 255:450–458, 2014.

[103] M Safari and C Delacourt. Aging of a commercial graphite/lifepo4 cell. *Journal of The Electrochemical Society*, 158(10):A1123, 2011.

[104] Nobuhiro Ogihara, Yuichi Itou, Tsuyoshi Sasaki, and Yoji Takeuchi. Impedance spectroscopy characterization of porous electrodes under different electrode thickness using a symmetric cell for high-performance lithium-ion batteries. *The Journal of Physical Chemistry C*, 119(9):4612–4619, 2015.

[105] Xuezhe Wei, Bing Zhu, and Wei Xu. Internal resistance identification in vehicle power lithium-ion battery and application in lifetime evaluation. In *2009 International Conference on Measuring Technology and Mechatronics Automation*, volume 3, pages 388–392. IEEE, 2009.

[106] Matthieu Dubarry, Vojtech Svoboda, Ruey Hwu, and Bor Yann Liaw. Capacity and power fading mechanism identification from a commercial cell evaluation. *Journal of Power Sources*, 165(2):566–572, 2007.

[107] Daniel J Noelle, Meng Wang, Anh V Le, Yang Shi, and Yu Qiao. Internal resistance and polarization dynamics of lithium-ion batteries upon internal shorting. *Applied energy*, 212:796–808, 2018.

[108] Eric Wood, Marcus Alexander, and Thomas H Bradley. Investigation of battery end-of-life conditions for plug-in hybrid electric vehicles. *Journal of Power Sources*, 196(11):5147–5154, 2011.

[109] Feng Leng, Cher Ming Tan, and Michael Pecht. Effect of temperature on the aging rate of li ion battery operating above room temperature. *Scientific reports*, 5(1):1–12, 2015.

[110] K Amine, J Liu, and I Belharouak. High-temperature storage and cycling of c-lifepo4/graphite li-ion cells. *Electrochemistry communications*, 7(7):669–673, 2005.

[111] Benjamin Ng, Paul T Coman, Ehsan Faegh, Xiong Peng, Stavros G Karakalos, Xinfang Jin, William E Mustain, and Ralph E White. Low-temperature lithium plating/corrosion hazard in lithium-ion batteries: electrode rippling, variable states of charge, and thermal and nonthermal runaway. *ACS Applied Energy Materials*, 3(4):3653–3664, 2020.

[112] Lucille Bodenes, Romain Naturel, Hervé Martinez, Rémi Dedryvère, Michel Menetrier, Laurence Croguennec, Jean-Paul Pérès, Cécile Tessier, and Florent Fischer. Lithium secondary batteries working at very high temperature: Capacity fade and understanding of aging mechanisms. *Journal of Power Sources*, 236:265–275, 2013.

[113] Li Tan, Li Zhang, Qingna Sun, Ming Shen, Qunting Qu, and Honghe Zheng. Capacity loss induced by lithium deposition at graphite anode for lifepo4/graphite cell cycling at different temperatures. *Electrochimica Acta*, 111:802–808, 2013.

[114] Matthieu Dubarry, Bor Yann Liaw, Mao-Sung Chen, Sain-Syan Chyan, Kuo-Chang Han, Wun-Tong Sie, and She-Huang Wu. Identifying battery aging mechanisms in large format li ion cells. *Journal of Power Sources*, 196(7):3420–3425, 2011.

[115] Yancheng Zhang, Chao-Yang Wang, and Xidong Tang. Cycling degradation of an automotive lifepo4 lithium-ion battery. *Journal of power sources*, 196(3):1513–1520, 2011.

[116] M Rosa Palacín. Understanding ageing in li-ion batteries: a chemical issue. *Chemical Society Reviews*, 47(13):4924–4933, 2018.

[117] Ang Yang, Yu Wang, Fangfang Yang, Dong Wang, Yanyang Zi, Kwok Leung Tsui, and Bin Zhang. A comprehensive investigation of lithium-ion battery degradation performance at different discharge rates. *Journal of Power Sources*, 443:227108, 2019.

[118] Marijn R Jongerden and Boudewijn R Haverkort. Battery aging, battery charging and the kinetic battery model: A first exploration. In *International Conference on Quantitative Evaluation of Systems*, pages 88–103. Springer, 2017.

[119] Xin Xu, Zhiguo Li, and Nan Chen. A hierarchical model for lithium-ion battery degradation prediction. *IEEE Transactions on Reliability*, 65(1):310–325, 2015.

[120] Fangfang Yang, Dong Wang, Yang Zhao, Kwok-Leung Tsui, and Suk Joo Bae. A study of the relationship between coulombic efficiency and capacity degradation of commercial lithium-ion batteries. *Energy*, 145:486–495, 2018.

[121] Aramis Perez, Vanessa Quintero, Francisco Jaramillo, Heraldo Rozas, Diego Jimenez, Marcos Orchard, and Rodrigo Moreno. Characterization of the degradation process of lithium-ion batteries when discharged at different current rates. *Proceedings of the Institution of Mechanical Engineers, Part I: Journal of Systems and Control Engineering*, 232(8):1075–1089, 2018.

[122] Gang Ning, Bala Haran, and Branko N Popov. Capacity fade study of lithium-ion batteries cycled at high discharge rates. *Journal of power sources*, 117(1-2):160–169, 2003.

[123] Fengchun Sun, Rui Xiong, Hongwen He, Weiqing Li, and Johan Eric Emmanuel Aussems. Model-based dynamic multi-parameter method for peak power estimation of lithium–ion batteries. *Applied Energy*, 96:378–386, 2012.

[124] D Anseán, M Dubarry, A Devie, BY Liaw, VM García, JC Viera, and M González. Operando lithium plating quantification and early detection of a commercial lifepo4 cell cycled under dynamic driving schedule. *Journal of Power Sources*, 356:36–46, 2017.

[125] Shrikant C Nagpure, Bharat Bhushan, Suresh Babu, and Giorgio Rizzoni. Scanning spreading resistance characterization of aged li-ion batteries using atomic force microscopy. *Scripta Materialia*, 60(11):933–936, 2009.

[126] Mohammad Kassem, Julien Bernard, Renaud Revel, Serge Pelissier, François Duclaud, and C Delacourt. Calendar aging of a graphite/lifepo4 cell. *Journal of Power Sources*, 208:296–305, 2012.

[127] Camilo Suarez and Wilmar Martinez. Fast and ultra-fast charging for battery electric vehicles–a review. In *2019 IEEE Energy Conversion Congress and Exposition (ECCE)*, pages 569–575. IEEE, 2019.

[128] André Hackbarth and Reinhard Madlener. Consumer preferences for alternative fuel vehicles: A discrete choice analysis. *Transportation Research Part D: Transport and Environment*, 25:5–17, 2013.

[129] Sanya Carley, Rachel M Krause, Bradley W Lane, and John D Graham. Intent to purchase a plug-in electric vehicle: A survey of early impressions in large us cites. *Transportation Research Part D: Transport and Environment*, 18:39–45, 2013.

[130] Ryan Collin, Yu Miao, Alex Yokochi, Prasad Enjeti, and Annette Von Jouanne. Advanced electric vehicle fast-charging technologies. *Energies*, 12(10):1839, 2019.

[131] C Dericioglu, E Yirik, E Unal, MU Cuma, B Onur, and M Tumay. A review of charging technologies for commercial electric vehicles. *International Journal of Advances on Automotive and Technology*, 2(1):61–70, 2018.

[132] Charles Botsford and Adam Szczepanek. Fast charging vs. slow charging: Pros and cons for the new age of electric vehicles. In *International Battery Hybrid Fuel Cell Electric Vehicle Symposium*, pages 1–9. Citeseer, 2009.

[133] Justine Sears, David Roberts, and Karen Glitman. A comparison of electric vehicle level 1 and level 2 charging efficiency. In *2014 IEEE Conference on Technologies for Sustainability (SusTech)*, pages 255–258. IEEE, 2014.

[134] Tanvir R Tanim, Matthew G Shirk, Randy L Bewley, Eric J Dufek, and Bor Yann Liaw. Fast charge implications: Pack and cell analysis and comparison. *Journal of Power Sources*, 381:56–65, 2018.

[135] Alexis Laforgue, Xiao-Zi Yuan, Alison Platt, Shawn Brueckner, Florence Perrin-Sarazin, Mathieu Toupin, Jean-Yves Huot, and Asmae Mokrini. Effects of fast charging at low temperature on a high energy li-ion battery. *Journal of the Electrochemical Society*, 167(14):140521, 2020.

[136] Dipesh D Patel, Frank P Tredeau, and Ziyad M Salameh. Temperature effects on fast charging large format prismatic lithium iron phosphate cells. In *2010 IEEE Vehicle Power and Propulsion Conference*, pages 1–4. IEEE, 2010.

[137] Romain Mathieu, Olivier Briat, Philippe Gyan, and Jean-Michel Vinassa. Comparison of the impact of fast charging on the cycle life of three lithium-ion cells under several parameters of charge protocol and temperatures. *Applied Energy*, 283:116344, 2021.

[138] Sivapriya Mothilal Bhagavathy, Hannah Budnitz, Tim Schwanen, and Malcolm McCulloch. Impact of charging rates on electric vehicle battery life. *Findings*, 2021(March), 2021.

[139] Alexis Laforgue, Xiao-Zi Yuan, Alison Platt, Shawn Brueckner, Florence Perrin-Sarazin, Mathieu Toupin, Jean-Yves Huot, and Asmae Mokrini. Comparative investigation of the impact of fast charging at low temperature on commercial li-ion cells. *Journal of Power Sources*, 524:231071, 2022.

[140] Ganesan Nagasubramanian. Electrical characteristics of 18650 li-ion cells at low temperatures. *Journal of applied electrochemistry*, 31(1):99–104, 2001.

[141] Marco-Tulio Fonseca Rodrigues, Victor A Maroni, David J Gosztola, Koffi PC Yao, Kaushik Kalaga, Ilya A Shkrob, and Daniel P Abraham. Lithium acetylide: A spectroscopic marker for lithium deposition during fast charging of li-ion cells. *ACS Applied Energy Materials*, 2(1):873–881, 2018.

[142] Abdilbari Shifa Mussa, Anti Liivat, Fernanda Marzano, Matilda Klett, Bertrand Philippe, Carl Tengstedt, Göran Lindbergh, Kristina Edström, Rakel Wreland Lindström, and Pontus Svens. Fast-charging effects on ageing for energy-optimized automotive lini1/3mn1/3co1/3o2/graphite prismatic lithium-ion cells. *Journal of Power Sources*, 422:175–184, 2019.

[143] Vivek Agarwal, Kasemsak Uthaichana, Raymond A DeCarlo, and Lefteri H Tsoukalas. Development and validation of a battery model useful for discharging and charging power control and lifetime estimation. *IEEE Transactions on Energy Conversion*, 25(3):821–835, 2010.

[144] J Li, E Murphy, J Winnick, and PA Kohl. Studies on the cycle life of commercial lithium ion batteries during rapid charge–discharge cycling. *Journal of Power Sources*, 102(1-2):294–301, 2001.

[145] Minggao Ouyang, Dongsheng Ren, Languang Lu, Jianqiu Li, Xuning Feng, Xuebing Han, and Guangming Liu. Overcharge-induced capacity fading analysis for large format lithium-ion batteries with liyni1/3co1/3mn1/3o2+ liymn2o4 composite cathode. *Journal of power sources*, 279:626–635, 2015.

[146] Matthieu Dubarry, Cyril Truchot, and Bor Yann Liaw. Cell degradation in commercial lifepo4 cells with high-power and high-energy designs. *Journal of Power Sources*, 258:408–419, 2014.

[147] Alan Millner. Modeling lithium ion battery degradation in electric vehicles. In *2010 IEEE Conference on Innovative Technologies for an Efficient and Reliable Electricity Supply*, pages 349–356. IEEE, 2010.

[148] Shaobo Xie, Shanwei Qi, and Kun Lang. A data-driven power management strategy for plug-in hybrid electric vehicles including optimal battery depth of discharging. *IEEE Transactions on Industrial Informatics*, 16(5):3387–3396, 2019.

[149] Justin DK Bishop, Colin J Axon, David Bonilla, Martino Tran, David Banister, and Malcolm D McCulloch. Evaluating the impact of v2g services on the degradation of batteries in phev and ev. *Applied energy*, 111:206–218, 2013.

[150] Jeffrey R Belt, Chinh D Ho, Chester G Motloch, Ted J Miller, and Tien Q Duong. A capacity and power fade study of li-ion cells during life cycle testing. *Journal of Power Sources*, 123(2):241–246, 2003.

[151] CH Chen, J Liu, and K Amine. Symmetric cell approach and impedance spectroscopy of high power lithium-ion batteries. *Journal of Power Sources*, 96(2):321–328, 2001.

[152] DP Abraham, JL Knuth, DW Dees, I Bloom, and JP Christophersen. Performance degradation of high-power lithium-ion cells—electrochemistry of harvested electrodes. *Journal of Power Sources*, 170(2):465–475, 2007.

[153] Yancheng Zhang and Chao-Yang Wang. Cycle-life characterization of automotive lithium-ion batteries with linio2 cathode. *Journal of the Electrochemical Society*, 156(7):A527, 2009.

[154] YongZhi Zhang, Rui Xiong, HongWen He, Xiaobo Qu, and Michael Pecht. Aging characteristics-based health diagnosis and remaining useful life prognostics for lithium-ion batteries. *ETransportation*, 1:100004, 2019.

[155] Seyed Mohammad Rezvanizaniani, Zongchang Liu, Yan Chen, and Jay Lee. Review and recent advances in battery health monitoring and prognostics technologies for electric vehicle (ev) safety and mobility. *Journal of power sources*, 256:110–124, 2014.

[156] Lifeng Wu, Xiaohui Fu, and Yong Guan. Review of the remaining useful life prognostics of vehicle lithium-ion batteries using data-driven methodologies. *Applied Sciences*, 6(6):166, 2016.

[157] Andrew T Stamps, Charles E Holland, Ralph E White, and Edward P Gatzke. Analysis of capacity fade in a lithium ion battery. *Journal of Power Sources*, 150:229–239, 2005.

[158] Kai Goebel, Bhaskar Saha, Abhinav Saxena, Jose R Celaya, and Jon P Christophersen. Prognostics in battery health management. *IEEE instrumentation & measurement magazine*, 11(4):33–40, 2008.

[159] Elutunji Buraimoh, Gokhan Ozkan, Laxman Timilsina, Ali Arsalan, Behnaz Papari, Phani Kumar Chamarthi, and Christopher Edrington. Model free time delay compensation for damped impedance method interfaced power system co-simulation testing. Technical report, SAE Technical Paper, 2023.

[160] Zhonghua Yun and Wenhu Qin. Remaining useful life estimation of lithium-ion batteries based on optimal time series health indicator. *Ieee Access*, 8:55447–55461, 2020.

[161] Jufeng Yang, Bing Xia, Wenxin Huang, Yuhong Fu, and Chris Mi. Online state-of-health estimation for lithium-ion batteries using constant-voltage charging current analysis. *Applied energy*, 212:1589–1600, 2018.

[162] Benvolence Chinomona, Chunhui Chung, Lien-Kai Chang, Wei-Chih Su, and Mi-Ching Tsai. Long short-term memory approach to estimate battery remaining useful life using partial data. *Ieee Access*, 8:165419–165431, 2020.

[163] Matthieu Dubarry and David Beck. Big data training data for artificial intelligence-based li-ion diagnosis and prognosis. *Journal of Power Sources*, 479:228806, 2020.

[164] Dong Zhang, Satadru Dey, Hector E Perez, and Scott J Moura. Remaining useful life estimation of lithium-ion batteries based on thermal dynamics. In *2017 American Control Conference (ACC)*, pages 4042–4047. IEEE, 2017.

[165] Muratahan Aykol, Chirranjeevi Balaji Gopal, Abraham Anapolsky, Patrick K Herring, Bruis van Vlijmen, Marc D Berliner, Martin Z Bazant, Richard D Braatz, William C Chueh, and Brian D Storey. Perspective—combining physics and machine learning to predict battery lifetime. *Journal of The Electrochemical Society*, 168(3):030525, 2021.

[166] Daniel J Tait, F Brosa Planella, Theodoros Damoulas, and W Dhammika Widanage. Scalable multitask latent force models with applications to predicting lithium-ion concentration. *NeurIPS*, 2020.

[167] Valentin Sulzer, Peyman Mohtat, Antti Aitio, Suhak Lee, Yen T Yeh, Frank Steinbacher, Muhammad Umer Khan, Jang Woo Lee, Jason B Siegel, Anna G Stefanopoulou, et al. The challenge and opportunity of battery lifetime prediction from field data. *Joule*, 5(8):1934–1955, 2021.

[168] Ziyou Song, Heath Hofmann, Jianqiu Li, Jun Hou, Xuebing Han, and Minggao Ouyang. Energy management strategies comparison for electric vehicles with hybrid energy storage system. *Applied Energy*, 134:321–331, 2014.

[169] John Wang, Ping Liu, Jocelyn Hicks-Garner, Elena Sherman, Souren Soukiazian, Mark Verbrugge, Harshad Tataria, James Musser, and Peter Finamore. Cycle-life model for graphite-lifepo4 cells. *Journal of power sources*, 196(8):3942–3948, 2011.

[170] Li Chen, Yuqi Tong, and Zuomin Dong. Li-ion battery performance degradation modeling for the optimal design and energy management of electrified propulsion systems. *Energies*, 13(7):1629, 2020.

[171] Mohammadhosein Safari, Mathieu Morcrette, A Teyssot, and C Delacourt. Life-prediction methods for lithium-ion batteries derived from a fatigue approach: I. introduction: Capacity-loss prediction based on damage accumulation. *Journal of The Electrochemical Society*, 157(6):A713, 2010.

[172] Jiageng Ruan, Bin Zhang, Bendong Liu, and Shuo Wang. The multi-objective optimization of cost, energy consumption and battery degradation for fuel cell-battery hybrid electric vehicle. In *2021 11th International Conference on Power, Energy and Electrical Engineering (CPEEE)*, pages 50–55. IEEE, 2021.

[173] Yuliya Preger, Heather M Barkholtz, Armando Fresquez, Daniel L Campbell, Benjamin W Juba, Jessica Romàn-Kustas, Summer R Ferreira, and Babu Chalamala. Degradation of commercial lithium-ion cells as a function of chemistry and cycling conditions. *Journal of The Electrochemical Society*, 167(12):120532, 2020.

[174] Sandia National Lab. Data for degradation of commercial lithium-ion cells as a function of chemistry and cycling conditions. `https://www.batteryarchive.org/snl_study.html`. Accessed: 06/11/2022.

[175] Kollmeyer P. Panasonic 18650pf li-ion battery data. `https://data.mendeley.com/datasets/cp3473x7xv/3`, note = Accessed: 06/11/2022.

[176] Zhiqiang Li, Tingxue Xu, Junyuan Gu, Qi Dong, and Linyu Fu. Reliability modelling and analysis of a multi-state element based on a dynamic bayesian network. *Royal Society open science*, 5(4):171438, 2018.

[177] Quynh Thi Tu Tran, Kevin Davies, Leon Roose, Binh V Doan, and Ninh Q Nguyen. Online distribution service transformer health assessment using real-time grid energy monitor. In *2020 IEEE Kansas power and energy conference (KPEC)*, pages 1–6. IEEE, 2020.

[178] Erik Möllerström, Fredric Ottermo, Anders Goude, Sandra Eriksson, Jonny Hylander, and Hans Bernhoff. Turbulence influence on wind energy extraction for a medium size vertical axis wind turbine. *Wind Energy*, 19(11):1963–1973, 2016.

[179] Laxman Timilsina, Phuong H. Hoang, Ali Moghassemi, Elutunji Buraimoh, Phani Kumar Chamarthi, Gokhan Ozkan, Behnaz Papari, and Christopher S. Edrington. A real-time prognostic-based control framework for hybrid electric vehicles. *IEEE Access*, 11:127589–127607, 2023.

[180] R. Billinton and R. N. Allan. Reliability evaluation of power systems (second edition). *Plenum Press, New York and London*, 1996.

[181] Phuong H. Hoang, Payam R. Badr, Gokhan Ozkan, Christopher S. Edrington, and Behnaz Papari. Integrating degradation forecasting into control and management system of dc microgrids. In *2021 IEEE Fourth International Conference on DC Microgrids (ICDCM)*, pages 1–6, 2021.

[182] N Mo, ZY Zou, Ka Wing Chan, and TYG Pong. Transient stability constrained optimal power flow using particle swarm optimisation. *IET Generation, Transmission & Distribution*, 1(3):476–483, 2007.

[183] AM Emsley and GC Stevens. Review of chemical indicators of degradation of cellulosic electrical paper insulation in oil-filled transformers. *IEE Proceedings-Science, Measurement and Technology*, 141(5):324–334, 1994.

[184] Laxman Timilsina, Phuong H Hoang, Ali Arsalan, Bill R Badr, Gokhan Ozkan, Behnaz Papari, and Christopher S Edrington. Degradation abatement in hybrid electric vehicles using data-driven technique. *Transportation Research Procedia*, 70:52–60, 2023.

[185] Laxman Timilsina, Phuong H Hoang, Ali Moghassemi, Elutunji Buraimoh, Ali Arsalan, Gokhan Ozkan, Behnaz Papari, and Christopher S Edrington. A real-time degradation abatement technique in hybrid electric vehicle using data-driven methods. *IEEE Transactions on Vehicular Technology*, 2024.

[186] Robert Hecht-Nielsen. Theory of the backpropagation neural network. In *Neural networks for perception*, pages 65–93. Elsevier, 1992.

[187] Ali Arsalan, Laxman Timilsina, Behnaz Papari, Grace Muriithi, Gokhan Ozkan, Phani Kumar, and Christopher S Edrington. Cyber attack detection and classification for integrated on-board electric vehicle chargers subject to stochastic charging coordination. *Transportation Research Procedia*, 70:44–51, 2023.

[188] Ali Arsalan, Behnaz Papari, S M Imrat RAHMAN, Laxman Timilsina, Gokhan Ozkan, and Christopher S Edrington. Enhanced capability of atm-based fcs-mpc for ev powertrain in terms of disturbance detection and localization. *IEEE Transactions on Transportation Electrification*, 2024.

[189] Ali Arsalan, Behnaz Papari, SM Imrat Rahman, Laxman Timilsina, Ali Moghassemi, Grace Muriithi, Gokhan Ozkan, and Christopher S Edrington. Machine learning approach for open circuit fault localization in ev motor drive systems. Technical report, SAE Technical Paper, 2024.

[190] Martin Sundermeyer, Ralf Schlüter, and Hermann Ney. Lstm neural networks for language modeling. In *Thirteenth annual conference of the international speech communication association*, 2012.

[191] Vivienne Sze, Yu-Hsin Chen, Tien-Ju Yang, and Joel S Emer. Efficient processing of deep neural networks: A tutorial and survey. *Proceedings of the IEEE*, 105(12):2295–2329, 2017.

[192] Encyclopaedia Britannica et al. *Encyclopædia britannica*. Chicago: University of Chicago, 1993.

[193] Diederik P Kingma and Jimmy Ba. Adam: A method for stochastic optimization. *arXiv preprint arXiv:1412.6980*, 2014.

[194] Weichao Zhuang, Shengbo Li, Xiaowu Zhang, Dongsuk Kum, Ziyou Song, Guodong Yin, and Fei Ju. A survey of powertrain configuration studies on hybrid electric vehicles. *Applied Energy*, 262:114553, 2020.

[195] Payam Badr, Gokhan Ozkan, Behnaz Papari, Christopher S Edrington, Valarie Phillips, and Laxman Timilsina. Evolutionary multi-objective current magnitude optimization for traction ipmsm in electric/hybrid-electric vehicles. *IEEE Transactions on Transportation Electrification*, 2023.

[196] Laxman Timilsina, Payam R. Badr, Ali Arsalan, Gokhan Ozkan, Behnaz Papari, and Christopher S Edrington. Reliable fault-tolerant distributed control for traction ipmsm in electric vehcile/hybrid electric vehicle. In *2024 IEEE Transportation Electrification Conference & Expo (ITEC)*. IEEE, 2024.

[197] Ali Moghassemi, Laxman Timilsina, S M Imrat Rahman, Ali Arsalan, Phani K Chamarthi, Gokhan Ozkan, Behnaz Papari, Christopher S Edrington, and Zhyeu Zhang. Nearest level control based modular multi-level converters for power electronics building blocks concept in electric ship system. In *2024 IEEE Transportation Electrification Conference & Expo (ITEC)*. IEEE, 2024.

[198] Phani K Chamarthi, S M Imrat Rahman, Laxman Timilsina, Ali Moghassemi, Gokhan Ozkan, Behnaz Papari, and Christopher S Edrington. A proposed cuk converter based dual input hybrid converter topology as ev charging station. In *2024 IEEE Transportation Electrification Conference & Expo (ITEC)*. IEEE, 2024.

[199] Phani Kumar Chamarthi, Christopher Edrington, Ali Arsalan, Laxman Timilsina, Behnaz Papari, Gokhan Ozkan, and Ali Moghassemi. A novel 1-ϕ cuk based on-board electric vehicle charger with minimal number of power components. Technical report, SAE Technical Paper, 2023.

[200] S M Imrat Rahman, Ali Moghassemi, Ali Arsalan, Laxman Timilsina, Phani Kumar Chamarthi, Behnaz Papari, Gokhan Ozkan, and Christopher S Edrington. Emerging trends and challenges in thermal management of power electronic converters: A state of the art review. *IEEE Access*, 2023.

[201] S M Imrat Rahman, Ali Moghassemi, Laxman Timilsina, Payam R. Badr, Qilun Zhu, Robert Prucka, Gokhan Ozkan, Phuong H. Rahman, Hoang, Christopher S Edrington, Qilun Zhu, and Robert Prucka. Model-based active thermal management for neutral-point clamped power converter with adaptive weight,. In *2024 IEEE Transportation Electrification Conference & Expo (ITEC)*. IEEE, 2024.

[202] Laxman Timilsina, Ali Moghassemi, Phuong H Hoang, Ali Arsalan, Elutunji Buraimoh, Gokhan Ozkan, Behnaz Papari, and Christopher S Edrington. Impact of vehicle-to-grid (v2g) on battery degradation in a plug-in hybrid electric vehicle. Technical report, SAE Technical Paper, 2024.

[203] Qilun Zhu, Asit Kumar, Anirudh Sundar, Daniel Egan, Hamidreza Mirzaei, Da Chang, Matthias Schmid, Robert Prucka, Benjamin Lawler, and Chris Paredis. Development of a series hybrid electrified powertrain for a high speed tracked vehicle based on driving cycle simulation. *SAE International Journal of Advances and Current Practices in Mobility*, 4(2022-01-0367):1403–1412, 2022.

[204] Simona Onori, Lorenzo Serrao, and Giorgio Rizzoni. Hybrid electric vehicles: Energy management strategies. 2016.

[205] Elutunji Buraimoh, Gokhan Ozkan, Laxman Timilsina, Ali Arsalan, Grace Muruthi, Behnaz Papari, and Christopher S Edrington. Distributed deep deterministic policy gradient algorithm for real-time energy management of dc microgrid. In *2024 IEEE Sixth International Conference on DC Microgrids (ICDCM)*, 2024.

[206] Laxman Timilsina, Ali Moghassemi, Elutunji Buraimoh, Ali Arsalan, SM Imrat Rahman, Gokhan Ozkan, Behnaz Papari, and Christopher S Edrington. Degradation and state of health prediction of a battery used in a microgrid in real-time. In *2024 IEEE Sixth International Conference on DC Microgrids (ICDCM)*, 2024.

[207] Phuong H Hoang, Gokhan Ozkan, Payam R Badr, Behnaz Papari, Christopher S Edrington, Mustafa Alparslan Zehir, Barry Hayes, Laura Mehigan, Dlzar Al Kez, and Aoife M Foley. A dual distributed optimal energy management method for distribution grids with electric vehicles. *IEEE Transactions on Intelligent Transportation Systems*, 23(8):13666–13677, 2021.

[208] The Economist. Lithium battery costs have fallen by 98% in three decades. 134, 2021.

[209] Elutunji Buraimoh, Gokhan Ozkan, Laxman Timilsina, Phani Kumar Chamarthi, Behnaz Papari, and Christopher S Edrington. Overview of interface algorithms, interface signals, communication and delay in real-time co-simulation of distributed power systems. *IEEE Access*, 2023.

[210] Elutunji Buraimoh, Gokhan Ozkan, Laxman Timilsina, Ali Arsalan, Christopher S Edrington, Behnaz Papari, and Mustafa Ozden. Adaptive multi-parameter model free delay compensation in real-time co-simulation. *IEEE Transactions on Industrial Informatics*, 2024.

[211] Elutunji Buraimoh, Gokhan Ozkan, Laxman Timilsina, Ali Arsalan, Christopher S Edrington, Behnaz Papari, and Mustafa Ozden. Advanced power management in military-based vehicle-to-grid and vehicle-to-vehicle microgrid— distributed real-time co-simulation. *IEEE Transactions on Transportation Electrification*, 2024.